Study on PyrzA with a different scaffold from known prolyl hydroxylase domain protein inhibitors: integrated analysis of hypoxic protective function and selection of higher HIF activity of PyrzA derivatives

既存プロリン水酸化酵素阻害剤と骨格を異にする PyrzA に関する研究：低酸素防御機能の統合的解析と高活性誘導体の選抜

Kento Sonoda

2023

Contents

Abbreviations

ADME: Absorption, distribution, metabolism, excretion

AQ: Adaptaquin

ATP: Adenosine triphosphate

BCA: Bicinchoninate

CCK-8: Cell counting kit-8

CETSA: Cellular thermal shift assay

CKD: Chronic kidney disease

ClogP: Calculated logarithm of the octanol/water partition coefficient

CBP/p300: cAMP response element binding protein-binding protein/the adenovirus E1A-associated 300 kDa protein

DFO: Defeoxamin mesylate

D-MEM: Dulbecco's modified eagle medium

DMOG: Dimethyloxallyl glycine

DMSO: Dimethyl sulfoxide

DTT: Dithiothreitol

EC_{50}: Half maximal (50%) effective concentration

EPO: Erythropoietin

FIH: Factor inhibiting hypoxia-inducible factor

GLUT1: Glucose transporter 1

HIF: Hypoxia-inducible factor

HRE: Hypoxia response element

HTS: High-throughput screening

JMJD family: Jumonji C domain-containing family

LogP: Logarithm of the octanol/water partition coefficient

MCL buffer: Mammalian cell lysis buffer

NLuc: Nanoluciferase

ODDs: Oxygen-dependent degradation domains

OPD: *o*-Phenylenediamine

PDB: Protein data bank

PHDs: Prolyl hydroxylase domain-containing proteins

PHIs: PHD inhibitors

pVHL: von Hippel−Lindau protein

PyrzA: 5-(1-acetyl-5-phenylpyrazolidin-3-ylidene)-1,3-dimethylbarbituric acid

RIPA: Radioimmunoprecipitation assay

RPMI: Roswell park memorial institute

SEM: Standard error of the mean

VEGF: Vascular endothelial growth factor

2-OG: 2-Oxoglutarate

Chapter 1
General Introduction

A sufficient amount of molecular oxygen (O_2) must be delivered to the peripheral tissues to create adenosine triphosphate (ATP) through the cellular respiration pathway. In live cells and/or organisms, lowering the O_2 concentration leads to severe stress. To date, the formation of microclots in capillary vessels has been reported to induce hypoxic stress, which becomes to an initial event for stroke, heart failure, and kidney diseases[1–3].

Transactivation with hypoxia-inducible factors (HIFs) is an indispensable event in protecting against hypoxic stress through the hypoxia-protective proteins[4–6]. HIFs are divided into two major subfamilies: those with the unstable alpha subunit (HIF-α) and those with the stable beta subunit (HIF-β)[7,8]. After forming the HIF α/β heterodimer, HIF has the potential to bind the hypoxia response element (HRE) ([A/G]CGTC) and transactivate the hypoxia target genes[9,10] such as *VEGF* (*vascular endothelial growth factor*), *EPO* (*erythropoietin*), and *GLUT1* (*glucose transporter 1*)[11–15].

The regulation of HIF-α plays an important role in the response to changes in oxygen availability. Under normoxic conditions, HIF-α is continuously hydroxylated by prolyl hydroxylase domain-containing proteins (PHDs)[15–17]. PHDs require oxygen and ferrous ions (Fe^{2+}), the cofactor 2-oxoglutarate (2-OG), and oxygen molecules (Figure 1-1)[18–20]. Fe^{2+} promotes proline hydroxylation of HIF-α by binding 2-OG, PHDs, and oxygen molecules to the catalytic site. This event leads to the polyubiquitylation of hydroxylated HIF-α, which leads to its degradation via the ubiquitin−proteasome system. Conversely, under hypoxic conditions, HIF-α hydroxylation is suppressed due to a reduction in oxygen molecules. Then, HIF-α stabilizes and translocalizes to the nucleus. As a result,

PHDs lead to HIF inactivation via the hydroxylation of a specific proline residue of HIF-α (Figure 1-2).

Continuous HIF-α stabilization has at least two benefits: in the treatment of ischemic injury and the treatment of renal anemia associated with chronic kidney disease (CKD)[21–23], via the upregulation of *EPO*. For these reasons, academic researchers, and pharmaceutical companies have been working on exploring small molecular compounds that can activate the hypoxia sensing system without exposing the low oxygen condition. Almost HIF activators have been derived from the 2-OG structure to inhibit PHDs[21,23–25].

However, the broad-spectrum 2OG dioxygenase inhibitors affect broad tissues and cause unfavorable side effects such as neovascularization, plethora, and tumorigenesis[26–28]. As examples of side effects due to the non-specificity of the PHD isoforms, first, only PHD2 knockout mice, but not PHD1 or PHD3 knockout mice, died during the embryonic period[27,29]. Second, the frequency of polycythemia in adult liver-specific PHD2 knockout mice was higher than that in PHD1 or PHD3 knockout mice[30,31]. Third, each PHD1-3 isoform interacts with more than 20 potential non-HIF proteins[32–41].

HIF activators have been required to have high specificities, although almost HIF activators are known as 2-OG analogs to inhibit PHDs. Currently, five 2-OG analogs (Roxadustat, Vadadustat, Enarodustat, Daprodustat, and Molidustat) have been approved as therapeutic compounds for anemia (Figure 1-3)[22,23,42–48]. However, a major concern, these small molecules may have side effects because more than 60 human proteins besides PHDs require 2-OG as a cofactor[24,25,49]. Instead of 2-OG analogs, VHL inhibitor[50,51] and FIH (Factor inhibiting hypoxia-inducible factor) inhibitor[52–56] have been developed as inhibitors targeting compounds other than PHDs without mimicking 2-OG; however, they have not yet been approved. Therefore, in a previous study, to identify a novel structure-

type HIF activator, a classic HRE-reporter system, which included a hypoxia response output event HIF activation reporter assay was generated (Figure 1-4)[57], potential compounds were found from a broad range of chemical libraries using high-throughput screening (HTS). Potential compounds were categorized among known PHD inhibitors, and finally an unlisted compound, 5-(1-acetyl-5-phenylpyrazolidin-3-ylidene)-1,3-dimethylbarbituric acid (PyrzA) (Figure 1-5)[58,59] was identified. However, PyrzA is a novel chemical compound that has only been reported for its chemical structure, and there have been no official reports on its use.

In this thesis, in Chapter 2, the stabilization of both HIF-α proteins and upregulation of HIF target genes treated with PyrzA in several cells showed that PyrzA activated the HIF signal cascade. PyrzA also upregulated HIF target genes in mice. Moreover, the stabilization of both prolyl-hydroxylated HIF-α and the docking simulation revealed that PyrzA was involved in the inhibition of PHDs. In Chapter 3, 5-(1-*n*-Butyryl-5-phenylpyrazolidin-3-ylidene)-1,3-dicyclohexyl-pyrimidine-2,4,6(1*H*,3*H*,5*H*)-trione (**2c**) was selected by evaluation of PyrzA derivatives using HRE-reporter cell. In addition, **2c** stabilized HIF-α proteins and up-regulated HIF target genes compared to roxadustat, a commercially available HIF activator. In Chapter 4, to determine the mechanism of inhibition PHDs by PyrzA, PHDs recombinant proteins produced by using the insect cells (SF21 cells) or silkworms as host organisms, and 2-OG oxygenases assay was performed.

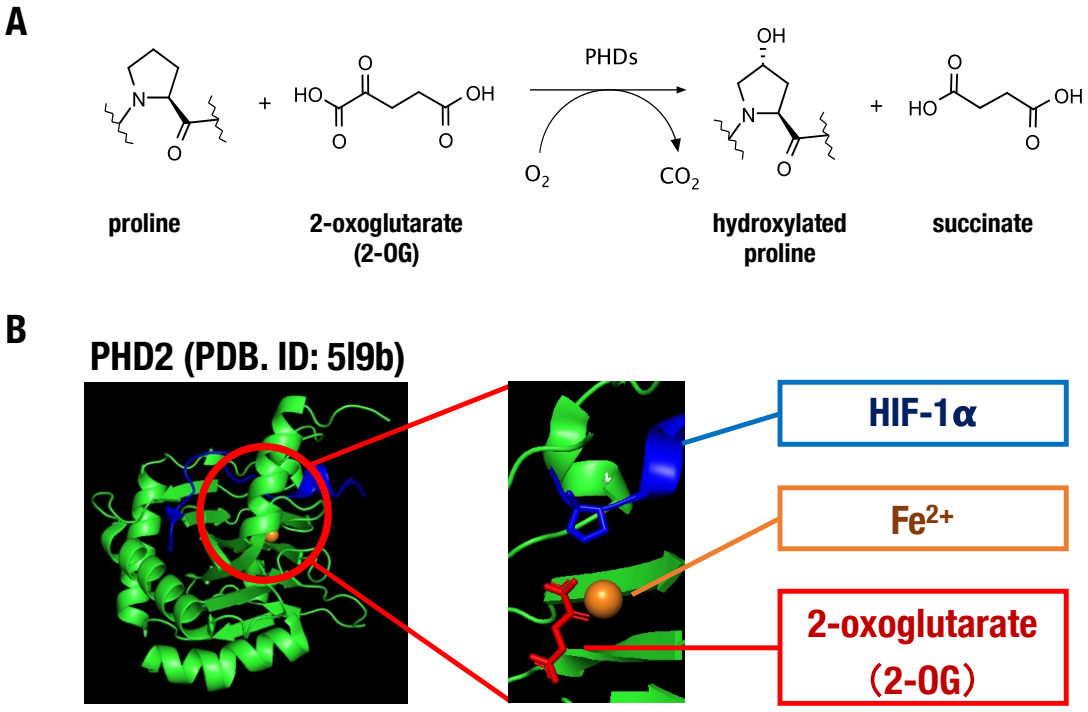

Figure 1-1. PHDs require 2-oxoglutarate (2-OG). (A) The reaction of HIF-α hydroxylation: PHD catalyzed prolyl-hydroxylation. (B) Views from crystal structures 2-OG complexed with PHD2. Mn^{2+} was substituted for Fe^{2+}. The human PHD2:Mn^{2+}:2-OG:HIF-α substrate complex (PDB ID: 5l9b[60]) was selected as a template structure using the PyMOL Molecular Graphics System.

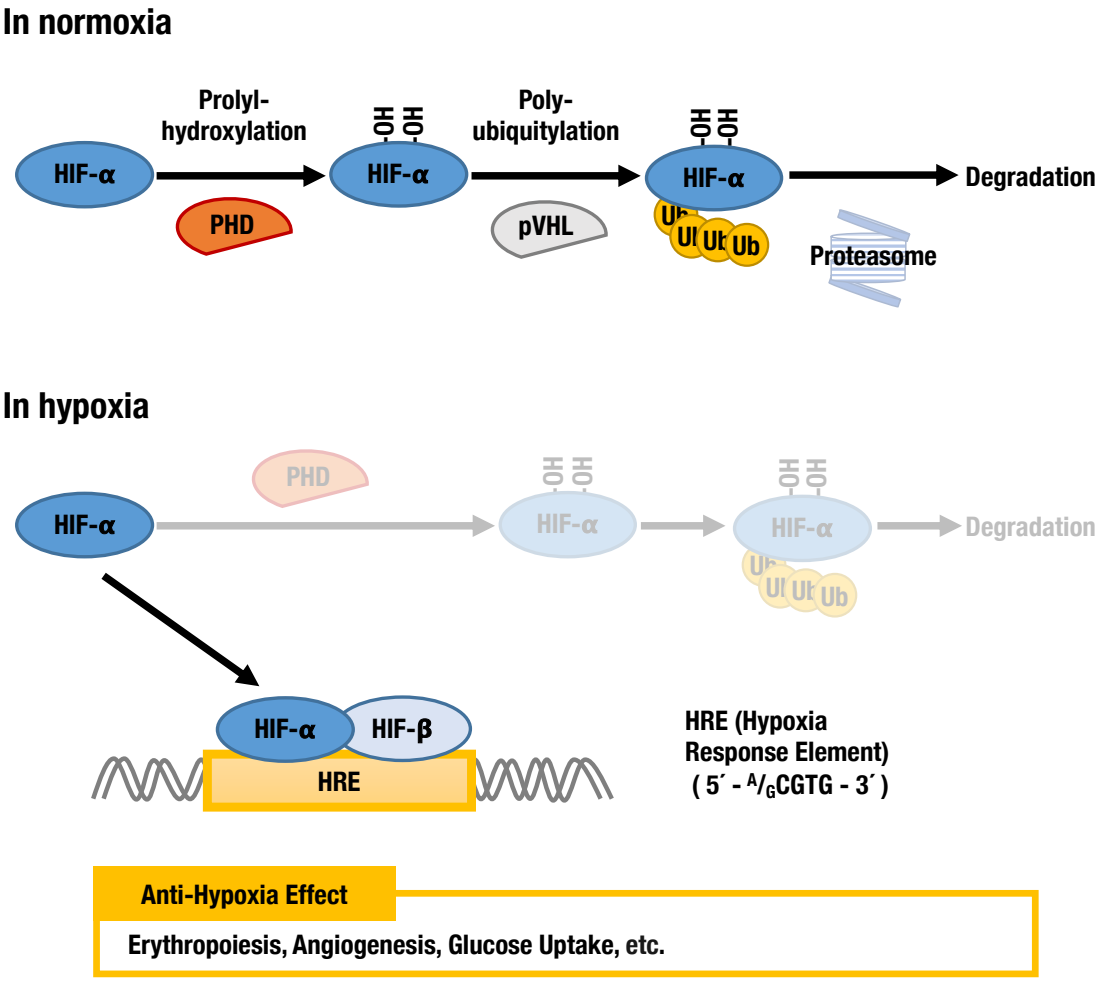

Figure 1-2. Regulation and role of HIF-α protein. Under normoxic conditions, HIF-α is hydroxylated by prolyl hydroxylase domain-containing proteins (PHDs). Hydroxylated HIF-α is polyubiquitylated by von Hippel−Lindau protein. Polyubiquitylated HIF-α is degraded by proteasome. Under hypoxic conditions, HIF-α hydroxylation is suppressed, stabilizes, and translocalizes to the nucleus. Then, HIF-α heterodimerize with HIF-β and they bind to hypoxia response element (HRE) ([A/G]CGTC) and transactivate hypoxia target genes.

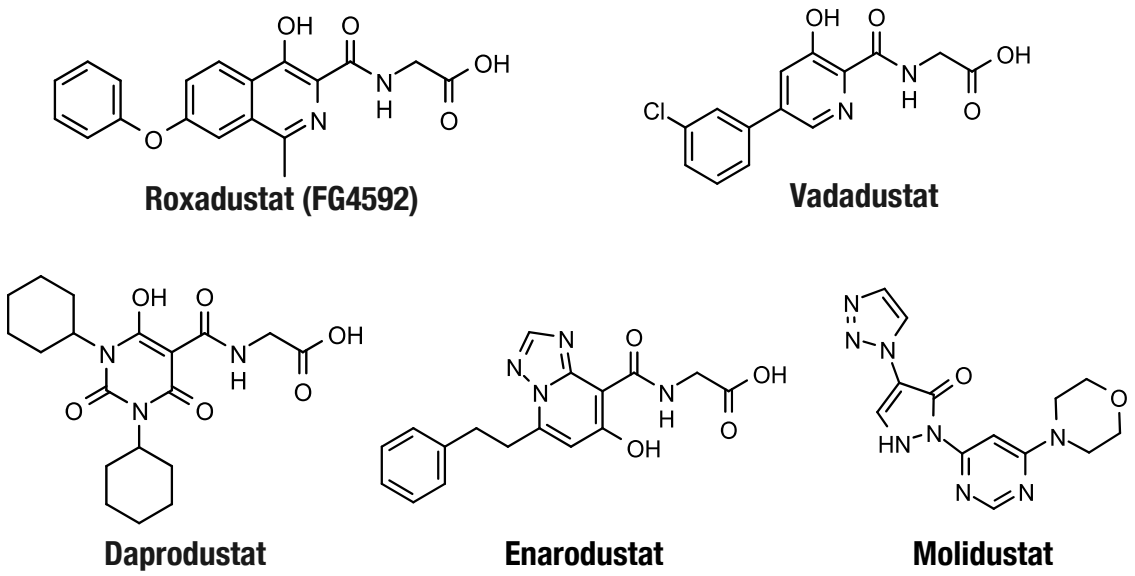

Figure 1-3. The chemical structure of five 2-OG analogs which have been approved as therapeutic compounds for anemia.

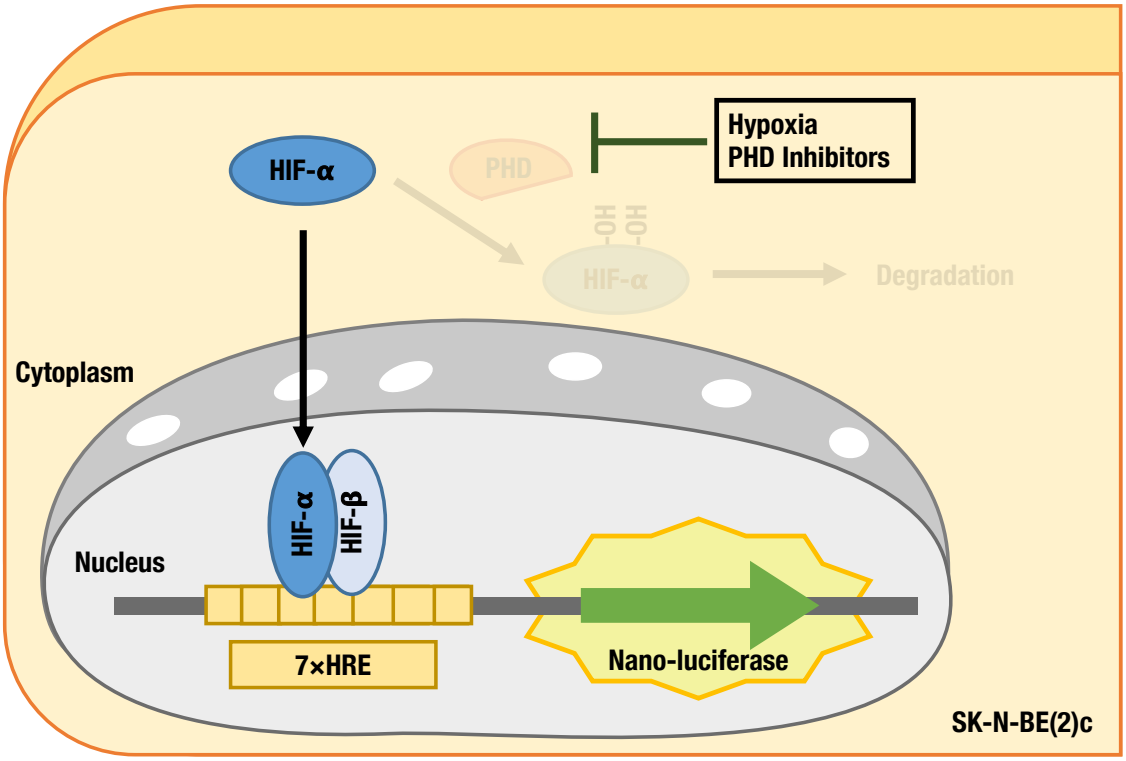

Figure 1-4. HIF-α transcriptional activity was evaluated using SKN:HRE-NLuc reporter system. Constructs that consist of a Nano luciferase (NLuc) under the transcriptional regulation of an enhancer containing 7 copies of *VEFG* 40-bp HRE upstream of a mini-TATA promoter was generated. This construct was stably into the human neuroblastoma cell line (SK-N-BE(2)c). Finally, stable transformation was named SKN:HRE-NLuc.

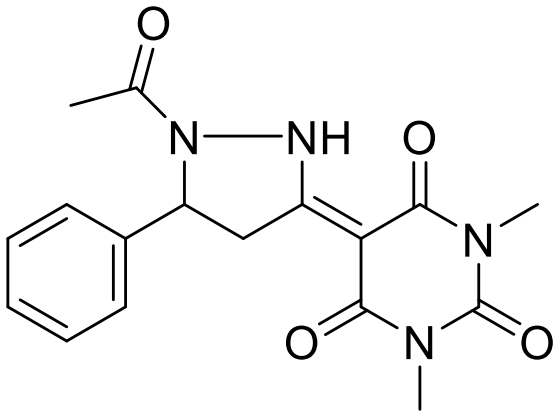

5-(1-acetyl-5-phenylpyrazolidin-3-ylidene)-1,3-dimethylbarbituric acid

Figure 1-5. The chemical structure of PyrzA: 5-(1-acetyl-5-phenylpyrazolidin-3-ylidene)-1,3-dimethylbarbituric acid.

Chapter 2

Biochemical Characterization of PyrzA

2-1. Introduction

In previous study, due to monitoring the endpoint HIF-α transcriptional activity, a nanoluciferase (NLuc) reporter system under control with seven tandem repeats of human VEGF HRE elements attached to a mini-TATA promoter was generated. The human neuroblastoma cell line SK-N-BE(2)c stably harbored the construct named SKN:HRE-NLuc (Figure 1-5)[57]. To identify a novel structure-type HIF activator, SKN:HRE-NLuc was stimulated with the core 9600 chemical library (final dose in 20 μM) obtained from the Drug Discovery Initiative, University of Tokyo. 24 h after stimulation, nano-Glo luciferase reagent was added directly, and 40 compounds of high HIF-α transcriptional activity were selected as the first hit compounds (Figure 2-1). Known HIF activators such as dihydroxybenzene[61,62] and oxyquinoline[63,64], and PAINS (pan-assay interference compounds)[65,66] were excluded from the first hit compounds (Figure 2-2). 2-OG scaffold compounds also were removed from the candidate list. Eventually, 5-(1-acetyl-5-phenylpyrazolidin-3-ylidene)-1,3-dimethylbarbituric acid (PyrzA) was selected as a novel HIF activator without 2-OG scaffold (Figure 1-5). However, PyrzA was a novel chemical compound that had only been reported for its chemical structure, and there have been no official reports on its usage.

In the first half of this chapter, PyrzA activates the HIF cascade not only in several culture cells but also in mice tissue. In the second half of this chapter, PyrzA activates HIF-α by inhibiting PHDs, mainly by detecting prolyl-hydroxylated HIF-1α and docking simulations between PHD2 and PyrzA.

2-2. Experimental section

2-2-1. Reagents

Dimethyl sulfoxide (DMSO) was purchased from Fujifilm Wako (Osaka, Japan). FG4592 (roxadustat) was purchased from Cayman Chemical Company (Ann Arbor, MI, USA). Dimethyloxallyl glycine (DMOG) was purchased from Sigma-Aldrich (St. Louis, MO, USA). Adaptaquin (AQ), Defeoxamin mesylate (DFO) were purchased from Tocris Bioscience (Bristol, UK). Ciclopirox olamine (CPO) was purchased from Tokyo Chemical Industry (Tokyo, Japan). MG132 was obtained from Peptide Institution (Osaka, Japan). Heparin was purchased from Mochida Pharmaceutical (Tokyo, Japan). The following antibodies were used. HIF-1α: Hif1a (PAB12138) rabbit pAb (Abnova, Taipei, Taiwan), human HIF-2α: HIF-2 alpha (D6T8V) rabbit mAb (Cell Signaling Technology, Danvers, MA, USA), mouse HIF-2α: HIF-2alpha antibody (GT125) mouse mAb (Gene Tex, Irvine, CA, USA), Hydroxy-HIF-1α (Pro402): Anti-HIF-1-alpha, hydroxyproline (Pro402) (2972081) rabbit pAb (Millipore, Burlington, MA, USA), Hydroxy-HIF-1α (Pro564): Hydroxy-HIF (Pro564) (D43B5) rabbit mAb, PHD1: anti-HIF Prolyl Hydroxylase 1 (NB100-310) rabbit pAb (Novus Biologicals, Centennial, CO, USA), PHD2: anti-HIF Prolyl Hydroxylase 2 (NB100-2219) rabbit pAb (Novus Biologicals) PHD3: Rb pAb to PHD3 (ab30782) (Abcam, Cambridge, UK), and β-Actin: Anti β-Actin (PTG9395) mouse mAb (Fujifilm Wako).

2-2-2. Chemical Synthesis of PyrzA

All starting materials, except (*E*)-1,3-dimethyl-5-(3-phenylacryloyl)barbituric acid, were obtained from commercial suppliers and used without additional purification. General pathway for the synthesis of PyrzA is shown in Scheme 2-1. ^{1}H and ^{13}C NMR

spectra were recorded using an NMR 400 MHz system (Agilent, Santa Clara, CA, USA). The chemical shift (δ) was assigned relative to $SiMe_4$ as an internal control at δ 0 ppm. High-resolution mass spectra were obtained using an Agilent G6224AA TOF-MS system (Agilent).

(*E*)-1,3-Dimethyl-5-(3-phenylacryloyl)barbituric acid[67] was synthesized as described in the literature.

Synthesis of 1,3-Dimethyl-5-(5-phenylpyrazolidin-3-ylidene)barbituric acid. Under a nitrogen atmosphere, (*E*)-1,3-dimethyl-5-(3-phenylacryloyl)barbituric acid (1 mmol), hydrazine monohydrate (2 mmol), and ethanol (30 mL) were placed in a 50 mL two-necked flask. The mixture was stirred under reflux for 1 h. After the reaction, a white precipitate was formed. After the precipitate was filtered, washed with ethanol, and dried, 1,3-Dimethyl-5-(5-phenylpyrazolidin-3-ylidene)barbituric acid was obtained in 84% yield. 1,3-dimethyl-5-(5-phenylpyrazolidin-3-ylidene)barbituric acid: white solid; ^{1}H NMR (400 MHz, $CDCl_3$) δ 3.28 (s, 3H), 3.31 (s, 3H), 3.74 (dd, J = 7.7, 18.9 Hz, 1H), 4.10 (dd, J = 9.2, 18.9 Hz, 1H), 4.80－4.88 (dd, J = 7.7, 9.2 Hz, 1H), 5.20 (d, J = 7.4 Hz, 1H), 7.29－7.40 (m, 5H), 12.02 (s, 1H); ^{13}C NMR (100 MHz, $CDCl_3$) δ 27.6, 27.7, 42.9, 59.5, 86.2, 126.2, 128.4, 129.0, 139.2, 151.8, 162.2, 164.9, 165.8. HRMS (TOF) calculated for $C_{15}H_{17}N_4O_3$ $[M + H]^+$: 301.1301; found: 301.1302.

Synthesis of 5-(1-Acetyl-5-phenylpyrazolidin-3-ylidene)-1,3-dimethylbarbituric acid (PyrzA). Under a nitrogen atmosphere, 1,3-Dimethyl-5-(5-phenylpyrazolidin-3-ylidene)barbituric acid (0.5 mmol), acetic acid (0.5 mL, 8.7 mmol), and acetic anhydride (0.5 mL, 5.3 mmol) were placed in a 25 mL two-necked flask. The mixture was stirred at 125°C (bath temperature) for 2 h. After the reaction, the mixture was concentrated and dried under a vacuum. Purification was performed by recycling preparative HPLC using

GPC column with $CHCl_3$ as the eluent. After purification, compound PyrzA was obtained in 74% yield. 5-(1-acetyl-5-phenylpyrazolidin-3-ylidene)-1,3-dimethyl-barbituric acid: white solid; melting point was 273－274°C. ^{1}H NMR (400 MHz, $CDCl_3$) δ 1.94 (s, 3H), 3.27 (s, 3H), 3.37 (s, 3H), 3.99 (dd, J = 2.5, 19.5 Hz, 1H), 4.30 (dd, J = 10.9, 19.5 Hz, 1H), 5.40 (d, J = 8.2 Hz, 1H), 7.23－7.28 (m, 2H), 7.31－7.47 (m, 3H), 13.19 (br, 1H); ^{13}C NMR (100 MHz, $CDCl_3$) δ 20.6, 27.7, 45.1, 58.6, 86.3, 125.0, 129.0, 129.7, 139.3, 151.6, 157.7, 162.1, 163.6, 164.3. HRMS (TOF) calculated for $C_{17}H_{19}N_4O_4$ $[M + H]^+$: 343.1406; found: 343.1437. PyrzA has two racemic structures, we have not established the separation strategy; therefore, we used this mixture PyrzA in the subsequent experiments.

2-2-3. Cell culture

The human neuroblastoma cell line, SK-N-BE(2)c and the human hepatocellular carcinoma cell line, Hep3B were obtained from the American Type Culture Collection (ATCC; Manassas, VA, USA). HeLa, the human cervical epithelioid carcinoma cell line was obtained from the RIKEN Bio Resource Center (Tsukuba, Ibaraki, Japan). SK-N-BE(2)c was cultured in Roswell Park Memorial Institute (RPMI) 1640 medium with L-Glutamine and Phenol Red (Fujifilm Wako) then supplemented with 5% fetal bovine serum (EQUITEC-BIO, Kerrville, TX, USA) and 1% penicillin-streptomycin (Nacalai Tesque, Kyoto, Japan). HeLa and Hep3B cells were cultured in high-glucose Dulbecco's Modified Eagle Medium (D-MEM) with L-Glutamine and Phenol Red (Fujifilm Wako). All cell lines were cultured in a humidified atmosphere containing 5% CO_2 at 37°C.

2-2-4. Evaluation of HIF activity and cellular viability

SKN:HRE-NLuc cells, stable transformants of SK-N-BE(2)c with a reporter vector possessing secretion-type NLuc, were developed as previously described[57]. SKN:HRE-NLuc was cultured in RPMI1640 (Fujifilm Wako) then supplemented with 5% charcoal/resin absorbed heat-inactivated fetal bovine serum (EQUITEC-BIO) and 1% penicillin-streptomycin (Nacalai Tesque). The SKN:HRE-NLuc cells (7.0×10^3 cells/well) were then seeded into a 384-well plate (Corning, Corning, NY, USA) and incubated for 16 h. The medium was replaced with fresh medium containing the target compounds, PyrzA or PHD inhibitors, sequentially diluted from 100 μM to 98 nM. The cells were stimulated for 24 h. After incubation, the nano luciferase activity was measured using the Nano-Glo Luciferase Assay System (Promega, Madison, WI, USA) by SpectraMax i3x equipped with luminescence glow 384 SpectraMax detection cartridge (Molecular Devices, Sunnyvale, CA, USA). HIF activity was calculated as the intensity of luciferase activity based on the vehicle treatments (1% DMSO). To analyze cellular viability, the medium of chemically stimulated SKN:HRE-NLuc was replaced with new medium containing 1/10 (v/v) of CCK-8 assay reagents (Cell Counting Kit-8, Dojindo, Kumamoto, Japan) and incubated for 90 min. CCK-8 assay regents are using WST-8 (2-(2-methoxy-4-nitrophenyl)-3-(4-nitrophenyl)-5-(2,4-disulfophenyl)-2H-tetrazolium). After incubation, the OD_{450} of CCK-8 reagents was measured using the SpectraMax i3x. Cell viability was presented as a percentage based on the cells stimulated with 1% DMSO and used as a positive control.

2-2-5. Animals

All procedures for the mouse experiments were approved by the Animal Care Committee of Saga University and conformed with the Guide for the Care and Use of Laboratory Animals issued by the National Institute of Health. Six-week-old female or male C57B6 mice were housed in environments with a 12 h light/12 h dark cycle and constant temperature. PyrzA dissolved corn oil or vehicle control corn oil was administrated intraperitoneally. Sex, PyrzA concentrations, injection time, and sacrificed time are changed for each experiments listing Table 2-1. After being sacrificed, blood and tissues were harvested from all the mice. In addition, for each mouse blood containing heparin, one hematocrit tube (Paul Marienfeld, Lauda-Königshofen, Germany) of blood was collected and centrifuged at 10,000 rpm for 5 min using KUBOTA 3200 (Tokyo, Japan) equipped with hematocrit rotor (Kubota). The hematocrit values were calculated with hematocrit meter (Kubota).

2-2-6. Estimating for protein concentration

Mice liver or kidney tissue was homogenized in radioimmunoprecipitation assay (RIPA) buffer (50 mM Tris-HCl, pH 7.5, 150 mM NaCl, 1% [v/v] NP-40, 0.5% [w/v] sodium deoxycholate, 0.1% [v/v] SDS) supplemented 1× protease inhibitor cocktail (Nacalai Tesque) and 20 μM MG132. The suspension was centrifuged at 13,000 rpm at 4°C for 10 min. The supernatant was transferred to a new tube and measured for protein concentrations using the Protein Assay Bicinchoninate (BCA) Kit (Nacalai Tesque).

2-2-7. Immunoblot assay

The cells were solubilized with 4 × SDS sample buffer (0.25 M Tris-HCl, pH 6.8, 20% [w/v] Dithiothreitol (DTT), 8% [w/v] SDS, 20% [w/v] sucrose, 0.008% [w/v] bromophenol blue). Mice samples were lysed in RIPA buffer and measured for protein concentration using BCA assay. After finishing BCA assay, mice samples were mixed with 4 × SDS sample buffer to a final concentration of 1×. Those samples were boiled at 90°C or 60°C for 10 min and subjected to SDS-PAGE electrophoresis and transferred to polyvinylidene fluoride membranes (Fujifilm Wako). The blots were incubated with primary antibodies against HIF-1α, human HIF-2α, mice HIF-2α, Hydroxy-HIF-1α (Pro402), Hydroxy-HIF-1α (Pro564), PHD1, PHD2, PHD3 or β-Actin, and subsequently treated with immunogen-matched horseradish peroxidase-conjugated secondary antibodies. The proteins were visualized with ImmunoStar LD (Fujifilm Wako) using Lumino Graph I (ATTO, Tokyo, Japan).

2-2-8. RNA isolation and quantitative PCR

Cellular total RNA from the cells was prepared using the Blood/Cultured Cell Total RNA Mini Kit (FAVORGEN, Pingtung, Taiwan) following the manufacturer's instructions. Total RNA from the mouse liver and kidney tissues were extracted using Sepasol RNA I Super G (Nacalai Tesque) according to the manufacturer's instructions. The total RNA was reverse transcribed to cDNA using the Transcriptor Universal cDNA Master (Roche, Basel, Switzerland) or the FastGene cDNA Synthesis Reagent (Nippon Genetics, Tokyo, JAPAN). The resulting cDNA was used as a template for quantitative PCR (qPCR) using the KAPA SYBR FAST qPCR Master Mix (2×) Kit (KAPA Bioscience, Potters Bar, UK) with a LightCycler 96 system (Roche) or Mx3005P qPCR

system (Agilent). β-Actin or 18S rRNA expression levels were used as internal controls. The primer sequences used were as follows: *human carbonic anhydrase 9* (*CA9*): (forward) 5′–CCT TTG CCA GAG TTG ACG AG–3′ and (reverse) 5′–GAC AGC AAC TGC TCA TAG GC–3′; human *PHD3*: (forward) 5′–CAC GAA GTG CAG CCC TCT TA–3′ and (reverse) 5′–TTG GCT TCT GCC CTT TCT TCA–3′; human erythropoietin (*EPO*): (forward) 5′–TCA TCT GTG ACA GCC GAG TC–3′ and (reverse) 5′–CAA GCT GCA GTG TTC AGC AC–3′; human *β-Actin*: (forward) 5′– CCT CGC CTT TGC CGA TCC–3′ and (reverse) 5′–CAT GCC GGA GCC GTT GT–3′; mouse BCL2/adenovirus E1B interacting protein 3 (*Bnip3*): (forward) 5′–GTT ACC CAC GAA CCC CAC TTT–3′ and (reverse) 5′–GTG GAC AGC AAG GCG AGA AT–3′; mouse carbonic anhydrase 9 (*Car9*): (forward) 5′–TGC TCC AAG TGT CTG CTC AG–3′ and (reverse) 5′–CAG GTG CAT CCT CTT CAC TGG–3′; and mouse *18S rRNA* (forward): 5′–GTA ACC CGT TGA ACC CCA TT–3′ and (reverse) 5′–CCA TCC AAT CGG TAG TAG C–3′.

2-2-9. Erythropoietin ELISA

Mice whole blood administrated with PyrzA, or the vehicle control were collected in a 1.5 mL tube containing heparin. Samples were spun at 5,000 rpm for 5 min at 4°C. The concentration of mice plasma was measured using an enzyme-linked immunosorbent assay (ELISA). The erythropoietin analysis was performed using the mouse erythropoietin ELISA kit (Proteintech, Rosemont, IL, USA) following the manufacturer's instructions. The detection and quantification of plasma EPO were performed using SpectraMax i3x with SoftMax Pro 7 (Molecular Devices). The detection limits of the samples were calculated as half of the detection limit.

2-2-10. Cellular thermal shift assay (CETSA)

SK-N-BE(2)c cells were washed with PBS twice, harvested with trypsin, centrifuged at 800 rpm, for 3 min, and lysed in mammalian cell lysis (MCL) buffer (20 mM Tris-HCl, pH7.4, 200 mM Sodium Chloride, 2.5 mM Magnesium Chloride, 0.05% [w/v] NP-40) supplemented 1× protease inhibitor cocktail (Nacalai Tesque) for 10 min on ice. The lysate was centrifuged at 20,000 × g for 20 min at 4°C. The supernatant was measured for total protein concentrations using the BCA Kit (Nacalai Tesque) and diluted to 2.0 mg/mL total protein. The lysate was used for three reactions, for (1) 100 μM FG4592, (2) 100 μM PyrzA, and (3) vehicle (1% DMSO). 15 min after incubation at room temperature, smaller aliquots (50 μL) and heated at various temperatures (45-65°C) for 3 min using T100 Thermal Cycler (Bio-rad). The incubated lysates were centrifuged at 20,000 × g for 15 min at 4°C. PHD1, PHD2, PHD3, and β-Actin levels were analyzed in those soluble fractions by immunoblot.

2-2-11. Docking simulation

Docking simulation for PHD2 and PyrzA was performed using Molegro Virtual Docker 7.0.0. (Molexus, Odder, Denmark). The crystal structure data for PHD2 (PDB ID: 3hqr[20]) was obtained from the Protein Data Bank (PDB; https://pdbj.org). The docking simulations were performed using the Molegro Virtual Docker 7.0.0[68]. To select a favorable binding mode, the MolDock score was used. The number of trial runs for calculations was 20. The chemical structures of the ligands were drawn using ChemBioDraw Ultra 20.0 and optimized by MM2 calculations in Chem3D Pro 20.0.

2-2-12. Statistical analysis

The quantification of every immunoblot intensity was performed using ImageJ. All data were expressed as mean ± standard error of the mean (SEM). All data were analyzed using one-way ANOVA or two-tailed, unpaired Student's *t* tests. For multiple comparisons, the Dunnett's test was used.

2-3. Result

2.3.1 Activation of HIF signal cascade by PyrzA

2-3-1-1. HIF reporter activities and cellular toxicities

HIF reporter activities and cellular toxicities of PyrzA compared with other PHD inhibitors (PHIs) were evaluated using SKN:HRE-NLuc. FG4592, DMOG, AQ, DFO, and CPO were used as PHIs (2-OG analogs: FG4592 and DMOG, inhibition of PHDs catalytic site: AQ, Fe^{2+} chelate: DFO and CPO). Especially, FG4592 has been approved as a PHD inhibitor for the treatment of renal anemia[47]. First, SKN:HRE-NLuc cells were treated with a serial diluted PyrzA or PHIs for 24 h. The HIF transcriptional activity and cellular viability were measured using NLuc activity and the cell counting kit-8 (CCK-8), respectively (Figure 2-3A-F). The HIF activity for PyrzA or PHIs was shown with a NLuc ratio of a 1% DMSO value as 1.0. The cell viability for these three chemicals was also indicated as the percentile ratio for 1% DMSO value as 100%. All chemicals activated the HRE NLuc reporter in a dose-dependent manner. PyrzA and PHIs concentrations for 5-fold HRE NLuc activity and cellular toxicity were shown in Figure 2-3G. Those results indicated that PyrzA had a similar HIF activation potential to that of DMOG. In addition, PyrzA and PHIs without AQ showed no cellular toxicity, even at the highest concentration (100 μM).

Next, the time-dependent HIF reporter activities of PyrzA and FG4592 were evaluated comparatively. SKN:HRE-NLuc cells were treated with three concentrations (25, 50, and 100 μM) PyrzA or FG4592 several times (1, 2, 4, 6, 12, and 24 h). The HIF-α transcriptional activity and cellular viability were measured using NLuc activity and the cell counting kit-8 (CCK-8), respectively (Figure 2-4). The HIF activity for PyrzA or PHIs was shown with a NLuc ratio of chemicals treatment for 0 h value as 1.0. The cell viability for these three chemicals was also indicated as the percentile ratio for chemicals treatment for 0 h value as 100%. Both PyrzA and FG4592 activated the HRE NLuc reporter in a time-dependent manner at high and middle concentrations. The 5-fold HRE NLuc activity was exceeded at 4 h treatment with FG4592 and 6 h stimulation with PyrzA at all concentrations. These results indicated that while the HIF-α transcriptional activity of PyrzA started 2 h later than that of FG4592, PyrzA and FG4592 maintained high HIF-α transcriptional activity even after 24 h.

2-3-1-2. Stabilization of HIF-α proteins under normoxic conditions

HIF-α consists two isoforms, HIF-1α and HIF-2α, with strictly different roles[69,70]. To confirm the stabilization of these proteins, immunoblot analysis was conducted in several cell lines. SKN-BE-2(c), HeLa, and Hep3B cells have already reported HIF stabilization with several HIF activators, including a PHD inhibitor containing a 2-OG structure. Before chemical challenging, 5.0×10^5 cells were seeded into each well of 12-well plates and preincubated for 16 h. After incubation, the cells were challenged with PyrzA or FG4592 at concentrations up to 100 μM for 24 h and the negative control vehicle, DMSO. The results showed that treatment with PyrzA or FG4592 led to dose-dependent stabilization of HIF-1α in SK-N-BE(2)c, HeLa, and Hep3B cells (Figure 2-5). Since the

seeding of 2.5 × 10^5 cells resulted in faint HIF-α proteins, the number of cells was increased to 5.0 × 10^5 cells. The amount of HIF-α protein levels when treated with PyrzA compared to FG4592 was the same in all three cells. These results suggest that PyrzA has the potential to stabilize HIF-α proteins, similar to the approved PHD inhibitor, FG4592.

2-3-1-3. Effects of HIF target genes

To investigate HIF-α transcriptional activity, the mRNA expression profiles of HIF target genes were measured. To do this, the *carbonic anhydrase 9* (*CA9*), *PHD3*, and *erythropoietin* (*EPO*) genes were selected. Hep3B cells (5.0 × 10^5) were seeded into 3 cm dishes and preincubated for 16 h. After preincubation, the cells were challenged with PyrzA or FG4592 (10, 30, and 100 μM) for 24 h and the negative control vehicle, DMSO. PyrzA induced all selected genes and FG4592 at 100 μM. The expression of the HIF target genes after treatment with PyrzA responded significantly at 100 μM (Figure 2-6). Therefore, PyrzA can stabilize the HIF-α protein and stimulate the HIF signaling cascade.

2-3-1-4. Confirmation of PyrzA activity in mouse model with intraperitoneal injection

To examine whether PyrzA promoted HIF signaling cascade in wild-type C57BL6 mice, 6-week-old mice were intraperitoneally administered with PyrzA dissolved corn oil or vehicle control corn oil. For the first time, PyrzA dissolved corn oil or vehicle control corn oil was administrated intraperitoneal at 50 mg/kg body weight every day. Five injections were administered in total. On the day following the final PyrzA injection, blood and tissues were harvested from all mice (Table 2-1, condition **1** and **2**). These results showed that female mice were more effective than male mice. Maximum plasma

Epo concentrations were observed after 6 h injection[71–73]; blood and tissue harvest time was changed from 24 h to 6 h. To explain each experiment, conditions such as sex, PyrzA concentrations, and injection frequency are shown in Table 2-1 as condition **3**-**7**. Under those conditions, the following were measured: (1) body weight, (2) spleen weight, (3) hematocrit, (4) plasma EPO protein concentration, (5) the mRNA level of HIF target genes in the kidney and liver, (6) the HIF-α protein levels in the kidneys and liver. Among those conditions, condition **4** was chosen following experiments.

Body weight, spleen weight, and blood analysis (hematocrit and plasma EPO protein concentration) among 7 conditions were shown in Table 2-2. Regarding body and spleen weight, no change was observed while under condition **5**, mice significantly increased the spleen / body weight ratio. Regarding blood analysis, the concentration of plasma Epo protein was significantly increased under condition **6**. The hematocrit level was also significantly increased under condition **4** and **6**. Considering that the upregulation of *Epo* causes increasing plasma Epo concentration and producing red blood cells, PyrzA activated HIF cascade *in vivo* as well as reported HIF activators.

Regarding the mRNA levels of the principal target genes of HIF-α, including BCL2/ adenovirus E1B interacting protein 3 (*Bnip3*), carbonic anhydrase 9 (*Car9*) and *Epo*, PyrzA significantly upregulated HIF target genes in the liver under condition **2**. PyrzA also significantly upregulated HIF target genes in the kidney under condition **4** (Figure 2-7). Those results also confirmed PyrzA activated HIF cascade *in vivo*. However, the HIF-α protein levels in kidney and liver were the same in the PyrzA-treated group (Figure 2-8). These experiments suggest that because PyrzA can upregulate HIF target genes, PyrzA effectively drives the HIF-α pathway, even *in vivo*.

2.3.2 Inhibition of PHDs by PyrzA

2-3-2-1. Evaluation of the combinational treatment effect of FG4592 and PyrzA using HIF reporter assay

Simultaneous stimulation with two chemicals is common in many experimental designs aimed at a studying mechanism. When two chemicals are present at the same time, it is important to determine whether the effects are additive or synergistic. In the case of an additive effect, it is a competitive inhibition. In the case of a synergistic effect, it becomes a non-competitive allosteric inhibition. FG4592 and PyrzA, which have similar HIF-α transcriptional effects, were examined to determine whether their effects are additive or synergistic.

To predict this additive or synergistic effect when two chemicals using SKN:HRE-NLuc, the evaluation strategy was designated as in Figure 2-9A. (1) Serial diluted chemical solution was made for 100 to 0.195 μM and the other chemical was added indicated concentrations. At the same time, serial diluted only chemical solution was also made. (2) 24 h after stimulation, luciferase activity was measured and plotted as experimental value and calculated as expected values (the sum of HIF-α transcriptional activity values when two compounds are stimulated alone at the same concentrations as the experimental values for each compound). (3) Comparing the Experimental and Expected values on same graph. (4) Calculate the 50-fold luciferase activities on expected values and experimental values. (5) Calculate a ratio of expected values / experimental values to evaluate additive or synergistic effect.

First, the effects of simultaneous addition were compared for the combination of FG4592 and PyrzA with both 2-OG analogs (FG4592 and IOX2). IOX2 is also a PHD inhibitor which harbors a 2-OG scaffold (Figure 2-9B). SKN:HRE-NLuc cells were

treated with (1) serial diluted PyrzA or IOX2 and fixed FG4592 (5 μM) or (2) serial diluted FG4592 and fixed PyrzA or IOX2 (15 or 20 μM respectively) for 24 h. Fixed chemical concentrations are predicted 5-fold concentrations. The HIF transcriptional activity was measured using NLuc activity. The HIF activity for PyrzA or PHIs was shown with a NLuc ratio of a 1% DMSO value as 1.0. As a result, experimental HIF transcriptional activity was higher than expected HIF transcriptional activity, and the ratio of 50-fold luciferase activity of fixed FG4592-diluted IOX2, fixed FG4592-diluted PyrzA, fixed IOX2-diluted FG4592, and fixed PyrzA-diluted PyrzA were 1.50, 1.79, 2.08, and 7.62 respectively (Figure 2-9B). In addition, the ratio of luciferase activity of FG4592 and PyrzA when added simultaneously at several concentrations was examined. SKN:HRE-NLuc cells were treated with (1) serial diluted PyrzA and three fixed FG4592 (6.25, 12.5, and 25 μM) or (2) serial diluted FG4592 and three fixed PyrzA (12.5, 25 and 50 μM) for 24 h. These results were shown in Figure 2-9C. In the case of fixed FG4592 or PyrzA at medium or high concentrations because all concentrations were more than 50-fold luciferase activity, a ratio of 100-fold luciferase activity was measured at middle concentration and a ratio of 300-fold luciferase activity was measured at high concentration. The resulting 50-fold ratio of luciferase activity for fixed FG4592 and fixed PyrzA at low concentrations were 6.29 and 8.48. The resulting 100-fold ratio of luciferase activity for fixed FG4592 and fixed PyrzA at middle concentrations were 8.83 and 49.1. The resulting 300-fold ratio of luciferase activity for fixed FG4592 and fixed PyrzA at high concentrations were 8.61 and 9.74. Those results showed that the luciferase activity ratio of simultaneous effect for FG4592 and PyrzA were higher than that of FG4592 and IOX2 (Figure 2-9B). In conclusion, the ratio of luciferase activity became to more than 5-fold under all conditions. Those indicated that since FG4592 and PyrzA

might bind to different sites on the PHDs. These results support PyrzA inhibit PHDs protein with non-competition with 2-OG chemicals.

2-3-2-2. PyrzA inhibits HIF-1α prolyl hydroxylation

On HIF-α, PHDs recognize two proline residues called oxygen-dependent degradation domains (ODDs): in the case of HIF-1α, one on the N-terminal side (NODD Pro402) and the other on the C-terminal side (CODD, Pro564)[60,74]. Two prolyl residues were hydroxylated by PHD activity. The hydroxylated form of HIF-1α was ubiquitinated by the VHL complex. The ubiquitinated HIF-1α was degraded via the ubiquitin－proteasome system.

Because most of the known HIF activators target the 2-OG HIF-α prolyl hydroxylation epicenter in PHDs, the changes in PHDs activity by PyrzA were observed using immunoblot. To confirm PHDs activity, the protein levels of hydroxylated HIF-1α are measured. However, under normoxia, hydroxylated HIF-1α was degraded immediately by ubiquitin－proteasome system in VHL deficient cells[24,75,76]. In this study, to stabilize the hydroxylated HIF-α protein, the proteasome inhibitor, MG132 was used instead of VHL-deficient cells. Before this experiment, the toxic effects of MG132 were examined in SK-N-Be(2)c, HeLa, and Hep3B cells. The three cell types were treated with serial dilutions of MG132 for 24 h, and the cell viability was analyzed using CCK-8. The LD_{50} of MG132 in all three cell lines was over 10 μM (Figure 2-10A-C). However, the majority of the Hep3B cells showed ballooning features during treatment with high concentrations of MG132 (Figure 2-10D); therefore, we decided not to use Hep3B to check the inhibitory activity of HIF-α prolyl hydroxylation by PyrzA and FG4592 (Figure 2-11). To stabilize the HIF-1α protein, we set the MG132 concentration at 10 μM to partially inhibit the

proteasomal activity. As shown in Figure 2-5, 5.0×10^5 SK-N-Be(2)c and HeLa cells were challenged with various doses of PyrzA or FG4592 (1, 5, 25, and 100 μM). The cells were treated with 10 μM MG132 for 24 h to investigate the hydroxylation of HIF-1α before degradation. Two hydroxylation sites on HIF-1α, including Pro402 and Pro564, were detected with hydroxylation-specific antibodies. In SK-N-Be(2)c and HeLa cells, single treatment with PyrzA or FG4592 treatment stabilized the HIF-1α protein. MG132 treatment also stabilized the HIF-1α protein in SK-N-Be(2)c and HeLa cells. PyrzA or FG4592 treatment blocked the Pro402 and Pro564 hydroxylation of HIF-1α in SK-N-Be(2)c and HeLa cells in a dose-dependent manner (Figure 2-11). Notably, PyrzA inhibited the hydroxylation of Pro402 and Pro564 on HIF-1α when compared with FG4592 activity. Furthermore, PyrzA inhibited both Pro402 and Pro564 in HIF-1α hydroxylation.

2-3-2-3. Effect of cellular thermal shift assay (CETSA)

To investigate whether PyrzA could interact with PHD proteins directory or not, the cellular thermal shift assay (CETSA) was performed. The CETSA detects the shift in protein thermal stability altered by a compound binding the target protein via immunoblot[77]. Recently, it has been reported that chemical binding for a set of important clinical targets was observed using this assay[51,77,78]. CETSA can confirm protein-ligand interactions in cultured cells without the use of specialized equipment or recombinant proteins. This assay also has the advantage of validating whether PyrzA specifically inhibits PHDs. SK-N-BE(2)c cells were lysed in MCL buffer and diluted into 2.0 mg/mL total protein. Multiple aliquots of cell lysates were treated with FG4592, PyrzA, and 1% DMSO, and incubated in various temperatures (PHD1: 45.0–56.9ºC), (PHD2 and PHD3:

50.0–61.2ºC). After centrifugation, the target PHD proteins in the supernatant were analyzed by immunoblot. In the presence of PyrzA or FG4592, the thermal stabilization shift of PHD1-3 cannot observe in our study condition (Figure 2-12A and B). The result of the quantification of band intensity of PHD1-3 was the same (Figure 2-12C-E). These results showed that the shift in protein thermal stability of PHD1-3 by PyrzA or FG4592 should be improved using purified recombinant proteins in further study.

2-3-2-3. Docking simulation using PyrzA and PHD2

To predict the binding sites of PHD and PyrzA, the docking simulation using PyrzA and PHD2. The human PHD2:Mn^{2+}:*N*-oxalylglycine:HIF-α substrate complex (PDB ID: 3hqr[20]) was selected as a template structure using the Molegro Virtual Docker 7.0.0 (Figure 2-13)[68]. The coordinates of the five-membered ring structure of PyrzA were found to overlap the coordinates of Pro564 in HIF-1α CODD. Additionally, both of the racemic PyrzA, including (*S*)- or (*R*)-PyrzA, could bind to the PHD protein. Their docking (MolDoc) scores were -99.6763 and -89.3412 (kcal/mol), respectively (Figure 2-13J). PyrzA had the potential to interrupt the PHD2 and HIF-1α CODD binding. The docking results indicate that PyrzA potentially has increased selectivity for enzymes with 2-OG as a cofactor over inhibitors of 2-OG analogs.

2-4. Discussion

PyrzA which does not harbor a 2-OG scaffold had high HIF-α transcriptional activity. PyrzA was also relatively higher HIF-α transcriptional activity compound in the first hit compounds excluding dihydroxybenzene, oxyquinoline, or PAINS scaffold (Figure 2-2). Dihydroxybenzene and oxyquinoline analogs, including AQ, inhibit by binding to Fe^{2+} in

the PHD catalytic site[61,63]. PAINS appear to activate in multiple assays such as curcumin, toxoflavin, isothiazolones and hydroxyphenyl hydrozones[65,66]. For example, curcumin has the following PAINS properties: covalent labeling of proteins, metal chelation, redox reactivity, aggregation, membrane disruption, fluorescence interference, and structural decomposition[79].However, in this assay, only hydroxyphenyl hydrazone analogs had high HIF-α transcriptional activities. This structure called salicylaldimine chelates metal ions[80] and has been made for a variety of applications such as catalysts, antibacterial and anticancer drugs[81,82].

The efficacy of PyrzA was comparable to that of the known PHD inhibitor DMOG in a dose-dependent manner. For cytotoxicity, LC_{50} values of PyrzA and PHIs were greater than 100 μM except for AQ. Since chelate agents such as DFO and CPO work on a variety of metal ions, including ferrous ions, it affects broad tissues and causes more side effects. 2-OG analogs also act on several 2-oxygenases. Remarkably, DMOG: a broad-spectrum 2-OG analog inhibits other 2-oxygenases such as FIH and JMJD (jumonji C domain-containing) family histone demethylases[25,70,83]. Under normoxic condition, HIF-α is also asparaginyl-hydroxylated by FIH and asparaginyl-hydroxylated HIF-α blocks the interaction with the cAMP response element binding protein-binding protein/p300 (CBP/p300) transcriptional coactivator. Under hypoxic condition, HIF-α hydroxylation is suppressed due to a reduction in oxygen molecules. Then, HIF-α can interact with CBP/p300 and transactivate the hypoxia target genes[84–87]. JMJD family histone demethylases are 2-OG oxygenases which histone N^{ε}-methyl lysine demethylases and alter the regulation of many gene expressions[49,88,89]. Importantly, PyrzA has HIF transcriptional activities which might be a novel mechanism with no cytotoxicity effect. Therefore, the efficacy of PyrzA was comparable to that of FG4592 in a time-dependent

manner. This result indicated that intracellular absorption and degradation of PyrzA was similar to that of FG4592 under 1% DMSO solvent. Still, further study will be required for ADME (absorption, distribution, metabolism, excretion) in living organisms.

PyrzA stabilizes the HIF protein in three types of cells and accumulates both the HIF-α isoforms (HIF-1α and HIF-2α). PyrzA is also capable of upregulating HIF target genes including *EPO*. Those results show that PyrzA triggers the HIF signaling cascade. In particular, HIF-1α and HIF-2α have shown changes in the tissues where they are expressed[90–92], expression time[93,94], and downstream target genes[69,70,95,96]. For example, HIF-1α suppresses tumorigenesis by inhibiting c-Myc transcriptional activity. Conversely, HIF-2α promotes tumorigenesis by enhancing c-Myc function[93,97–99]. Therefore, the stabilization strategies of the specificity of HIF-α isoform using chemical compounds have become attractive. One of the future goals of this study is to develop PyrzA derivatives that distinguish the specificity for HIF-α isoforms.

PyrzA also activates HIF cascade *in vivo*. HIF activators upregulate *Epo* and increase plasma Epo concentration and hematocrit values and then, the spleen weight gain. So, HIF activators upregulate *EPO*, and increase plasma EPO concentration, and promote erythropoiesis. Finally, the spleen and bone marrow are contributed for stress erythropoiesis[30,31,100]. PyrzA also significantly upregulates several HIF target genes including *Epo* and increases plasma Epo concentration under several conditions. In addition, PyrzA tends to increase plasma Epo concentration and hematocrit values under all conditions. PyrzA also appears to significantly hematocrit values under several conditions. While it takes a few days to increase red blood cells or enlarge the spleen[101], the hematocrit levels were significantly increased under conditions harvested 6 h after the first injection of PyrzA. Hence, increasing hematocrit value and spleen weights under

some conditions must be considered for other reasons (dehydration or inactivation due to injection of PyrzA).

Regarding kidney and liver tissue, PyrzA upregulated HIF target genes under some conditions, however, the stabilization of both HIF-α proteins cannot be observed. In this experiment, PyrzA dissolved corn oil or vehicle control corn oil was intraperitoneally administered. Corn oil was used as the solvent instead of DMSO because PyrzA was difficult to dissolve in PBS and DMSO was toxic to mice. However, PyrzA was difficult to dissolve in corn oil either. This could be attributed to the low lipophilicity of PyrzA[58]. The logP (logarithm of the octanol/water partition coefficient) value of PyrzA was 1.10 ± 0.09. As a result, most PyrzA molecules are likely not to be absorbed and to be excreted through urine. In the future, this pharmacological feature will be improved by synthesizing more efficient derivatives.

Since most HIF activators target the treatment of renal anemia, the focus was on increasing Epo protein levels. Epo protein produces mainly in kidney and liver[102]. In addition, several papers have been reported that the HIF activation *in vivo* is demonstrated only by increased plasma EPO protein concentration[102,103], not by upregulation of HIF target genes or stabilization of HIF-α protein. In addition, HIF activators also need to target the treatment of ischemic injury of heart or brain[105–107]. Because excessive upregulated *Epo* also leads problems including polycythemia, the treatment of ischemic injury requires the use of other HIF target genes to protect the tissue[30]. In the future, the examination of HIF target gene expression in other tissues is needed.

As a result of the expression of mRNA levels, HIF target genes were significantly upregulated in the kidneys or liver on PyrzA-treated mice considering the reduced absorption due to the low solubility of PyrzA. These results were similar to the experiment

of a functional comparison of PyrzA with 2-OG analogs. In this experiment, while PyrzA upregulated HIF target genes and increased plasma Epo protein levels, the effects were weaker than other 2-OG analogs. However, the change of mRNA levels of HIF target genes of the mice treated with high concentration PyrzA (200 mg/kg) did not observe. This result indicated that HIF-α was negative feedback control in several manners[108–110].

The HIF-α protein levels *in vivo* were the same in the PyrzA-treated group in the experiments conducted. In terms of the time-dependent HIF reporter activities of PyrzA, the metabolism and degradation of PyrzA are similar for FG4592. Therefore, PyrzA may not be metabolized or excreted immediately after absorption. This suggests that detecting HIF-α protein was difficult from the absence of papers that HIF activators have not demonstrated the stabilization of the HIF-α protein.

In conclusion, PyrzA can activate HIF signaling cascade in mice, but the elevation of HIF activity is weaker than FG4592. As the next step, optimizing the current PyrzA molecule to improve its bioavailability should be primarily research focus. Furthermore, changing harvesting time or harvesting other tissues will be examined.

Next, to investigate that what protein PyrzA interacts with, the focus was on changes in PHD activity, which is the target of many HIF activation events. For this purpose, measuring PHDs activity include detecting the prolyl-hydroxylated HIF-α and performing PHDs enzyme assay. Among them, detecting the prolyl-hydroxylated HIF-1α using immunoblot in VHL deficient cells is a common method to check PHDs activity. However, inspired using MG132 to stabilize other transcription factors, and it was used instead of VHL deficient cells. As a result, when treating with MG132 to prevent the degradation of hydroxylated HIF-1α, PyrzA remarkably suppressed the hydroxylated HIF-1α at both prolines. This result suggests that PyrzA effectively inhibits PHDs. In

addition, since the time when HIF-α transcriptional activity began to increase PyrzA is the same as that of FG4592, PyrzA suggests that PyrzA interacts somewhere into PHDs.

To determine whether PyrzA interacts with the catalytic site or other sites of PHDs, FG4592 and PyrzA were added simultaneously and examined whether additive or synergistic effects. In the case of an additive effect, FG4592 and PyrzA are competitive inhibition and PyrzA might interact with the catalytic site of PHDs. In the case of a synergistic effect, FG4592 and PyrzA are a non-competitive inhibition and PyrzA might interact with the other site into PHDs. Evaluation of two chemical interactions is mainly used isobologram analysis[111,112]. However, this reporter assay is not appropriate strategy to get maximum induction because the chemical cytotoxicity may be observed[113] before to reach the value, therefore hardly calculate EC_{50} (half maximal (50%) effective concentration) value. In this time, instead of using isobologram analysis with EC_{50} value, a ratio of activity concentration of SKN:HRE-NLuc reporter cell line was used for to indicate the effect for simultaneous addition of FG4592 and PyrzA. Determination of the effect during FG4592 and IOX2 was added simultaneously as a control experiment. FG4592 and IOX2 are both 2-OG analogs and act as the catalytic site of PHDs, and therefore, the simultaneous addition of FG4592 and IOX2 might have an additive effect. As a result, the ratio of 50-fold luciferase activity values using PyrzA was higher than using IOX2. Therefore, PyrzA might interact with the other site in PHDs. However, Beyett T. S. *et al* reported that during the adjacency of two binding sites, certain combinations of chemicals exhibit not only synergistic effects but also antagonistic effects[114]. Therefore, PyrzA may not interfere with the binding FG4592 and PHDs. As a next step, it is necessary to verify the interaction of PyrzA with PHDs in other experiments.

The CETSA can validate the interaction of a cellular protein with a ligand without using a purification protein. In addition, Frost J. *et al* reported FG4592 interacted with cellular PHD2 protein using a CETSA[51]. Cell lysis and CETSA were performed as described in Nagasawa *et al*[78]. As a result, in the presence of not only PyrzA but also FG4592, the thermal stabilization shift of PHD1-3 was not observed. When the difference in the thermal shift was smaller, the alteration of the shift in protein thermal stability was not observed. Changing cell lines, chemical concentrations, or methods of cell lysis need to be considered additionally. Especially, the cell extraction method that preserves PHDs activity is important. Furthermore, the interaction of PyrzA with PHDs requires other experiments such as docking simulation, PHDs enzyme assay, or X-ray crystallography.

To predict the binding sites of PHD and PyrzA, the docking simulation using PyrzA and PHD2 protein crystallography structure. Among three PHD isoforms, PHD2 was selected due to almost all crystal structure information comes from PHD2. As a result, PyrzA might interrupt the PHD2 and HIF-1α CODD binding site. To the best of our knowledge, PHD inhibitors with HIF-1α CODD analogs have not been reported, and this is the first study. If the binding site of an inhibitor does not have a 2-OG vacancy, it may potentially have increased selectivity for enzymes with 2-OG as a cofactor over inhibitors of 2-OG analogs.

The docking simulation using PyrzA and PHD2 showed that PyrzA mimics HIF-1α CODD. Therefore, PyrzA has the potential not to interact with other 2-oxygenases which do not react with proline resides such as FIH and JMJD family histone demethylases. Moreover, PyrzA also has the potential not to interact with VHL because VHL inhibitors including VH298 mimic 4-hydroxyproline resides but PyrzA does not mimic

them[50,51,115,116]. However, PyrzA should be noted for its interaction with recognizing proline resides including collagen hydroxylases[25,117,118].

Comparing the results of the luciferase activity simultaneously and the docking simulation, PyrzA, and 2-OG analogs have the potential to inhibit in another manner. To examine between the binding site of HIF-α CODD and 2-OG site in the catalytic site of PHDs, the two sites were compared using X-ray crystallography data (Figure 2-14)[20,24,119,120]. IOX4 is a PHD inhibitor without a 2-OG scaffold. However, because the triazole scaffold of IOX4 mimics a carboxylate of 2-OG, IOX4 is a competitive inhibitor of 2-OG as well as 2-OG analogs[120]. The results show that the catalytic site of PHDs may interact with a different site than the binding HIF-α CODD site. Those results also indicated that PyrzA inhibits PHDs non-competitively allosterically and it is important to investigate the synergistic effect of PyrzA.

In conclusion, this section reveals that PyrzA activates HIF-α *in vitro* and *in vivo* by inhibiting PHDs in several manners. On the other hand, the next issues such as the synthesis of PyrzA derivatives to improve lipophilicity, the clarification of ADME of PyrzA or its derivatives, and the validation of the mechanism of PHDs inhibition of PyrzA are also clarified.

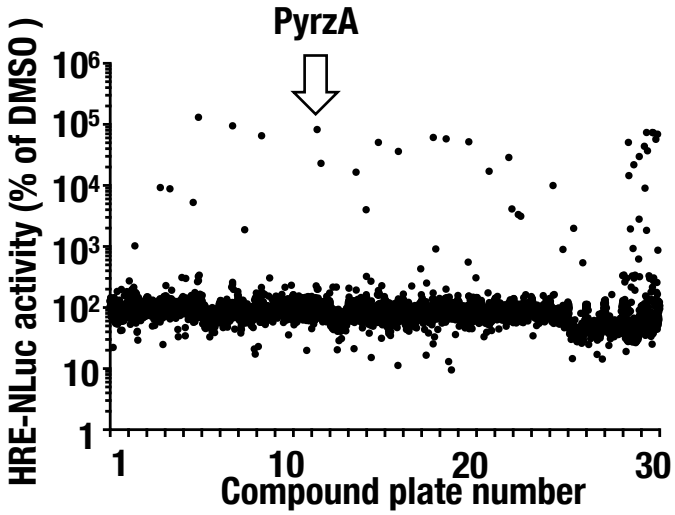

Figure 2-1. Identification of the unique HIF inducer, PyrzA, from a large chemical library. The initial screening result from the core 9600 chemical library from the Drug Discovery Initiative, The University of Tokyo using with SKN:HRE-NLuc reporter cell line. SKN:HRE-NLuc cells (7.0×10^3 cells) were seeded into a 384-well plate and treated with the chemical compound library (20 μM each) for 24 h. The nano luciferase activity in each well was measured. The HIF reporter activity of each compound was calculated with the indicated with % of nano luciferase activity of positive controls (100 μM $CoCl_2$) and indicated as an individual dot. The Hit compound, PyrzA, is indicated with an open arrow.

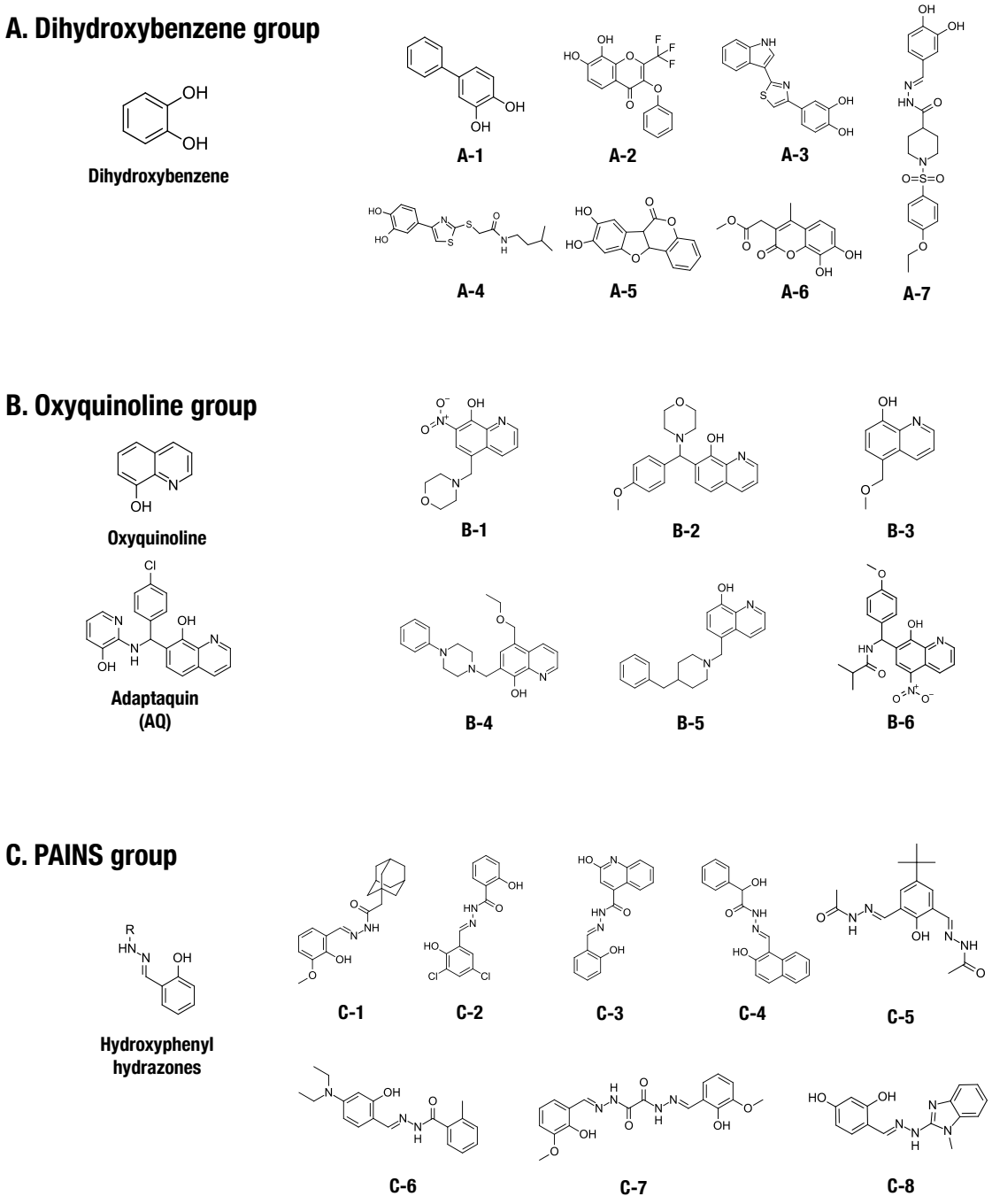

Figure 2-2. The chemical structure of several first-hit compounds which have high HIF-α transcriptional activity. Since several first-hit compounds contain the dihydroxybenzene (A) or oxyquinoline (B) scaffold which is known as HIF activators or PAINS scaffold, they were excluded.

Scheme 2-1. General pathway for the synthesis of 1,3-Dimethyl-5-(5-phenylpyrazolidin-3-ylidene)barbituric acid and PyrzA

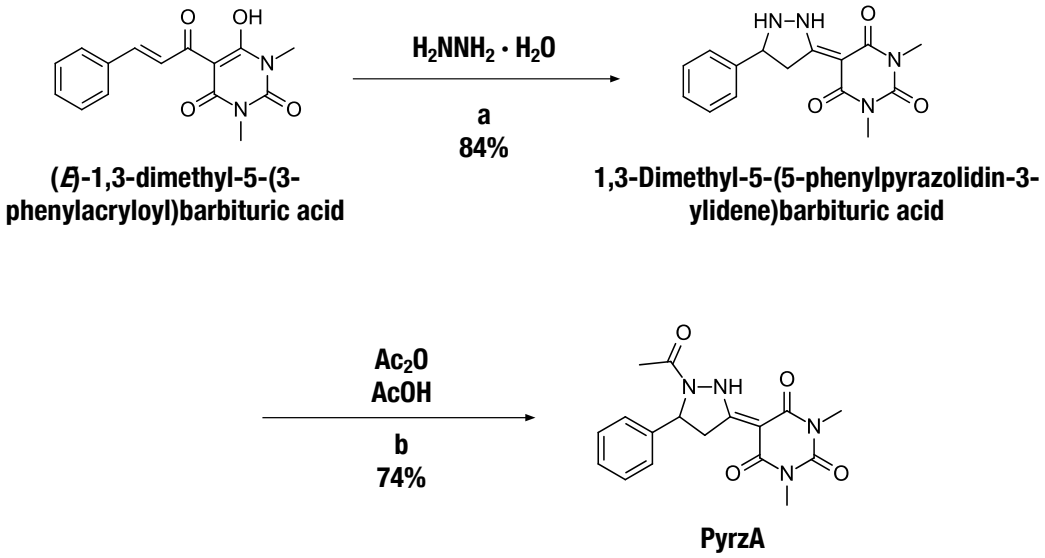

[a]Synthesis of 1,3-Dimethyl-5-(5-phenylpyrazolidin-3-ylidene)barbituric acid: (*E*)-1,3-dimethyl-5-(3-phenylacryloyl)barbituric acid, hydrazine monohydrate, ethanol, reflux, 1 h (84%).

[b]Synthesis of PyrzA: 1,3-Dimethyl-5-(5-phenylpyrazolidin-3-ylidene)barbituric acid, acetic acid, acetic anhydride 125°C, 2 h (74%).

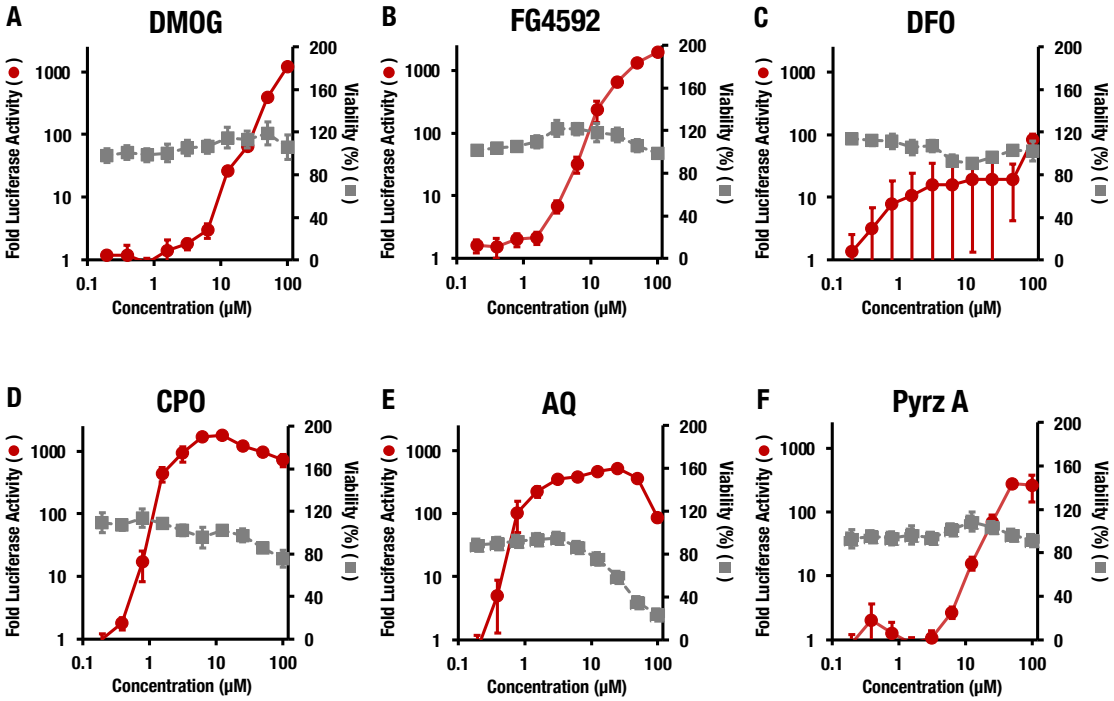

G

Chemical	5-Fold concentration (μM)	LC_{50} (μM)
DMOG	6.78	>100
FG4592	2.52	>100
DFO	0.545	>100
CPO	0.473	>100
AQ	0.390	33.9
PyrzA	7.34	>100

Figure 2-3. PyrzA can activate HRE reporter cells in a dose-dependent manner without exhibiting toxicity. (A-F) HIF-α transcriptional activity and cellular viability results for DMOG (A), FG4592 (B), DFO (C), CPO (D), AQ (E), or PyrzA (F) using SKN:HRE-NLuc for 24 h. The HRE reporter activities are indicated as fold luciferase activity, based on the value from 1% DMSO treated cells (filled red circle and red solid line). The cell viability percentile is represented on the value from 1% DMSO treated cells as 100% viability (filled gray square and gray dashed line). Error bars represent SEM (n= 4). (G) 5-fold concentration (μM) and the lethal concentration 50% (LC_{50}) values of PyrzA and PHIs.

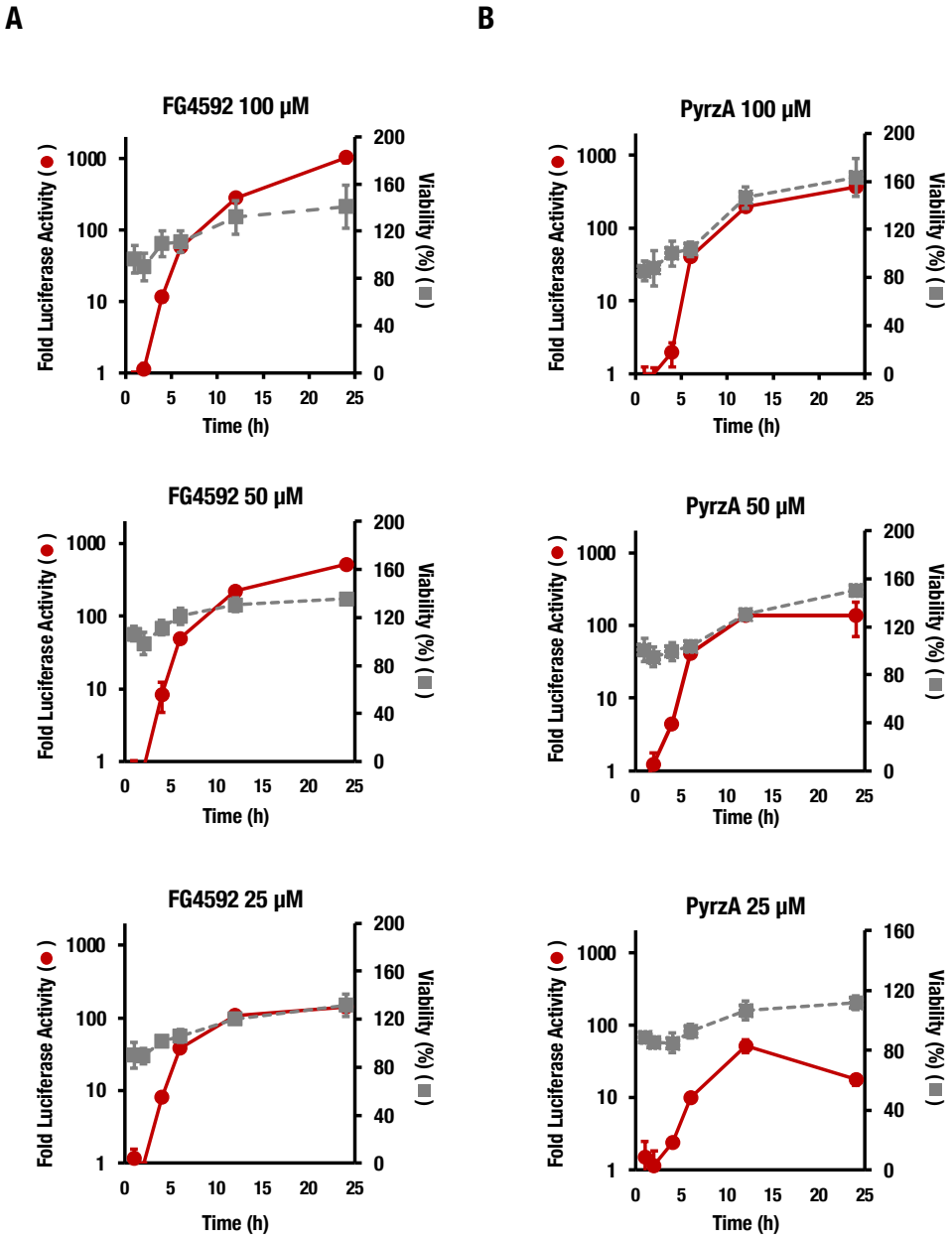

Figure 2-4. PyrzA can activate HRE reporter cells in a time-dependent manner without exhibiting toxicity. HIF-α transcriptional activity and cellular viability results for FG4592 (A) or PyrzA (B) using SKN:HRE-NLuc for 1-24 h. The HRE reporter activities are indicated as fold luciferase activity, based on the value from 0 h treated cells. (filled red circle and red solid line). The cell viability percentile is represented on the value from 0 h treated cells as 100% viability (filled gray square and gray dashed line). Error bars represent SEM (n= 4).

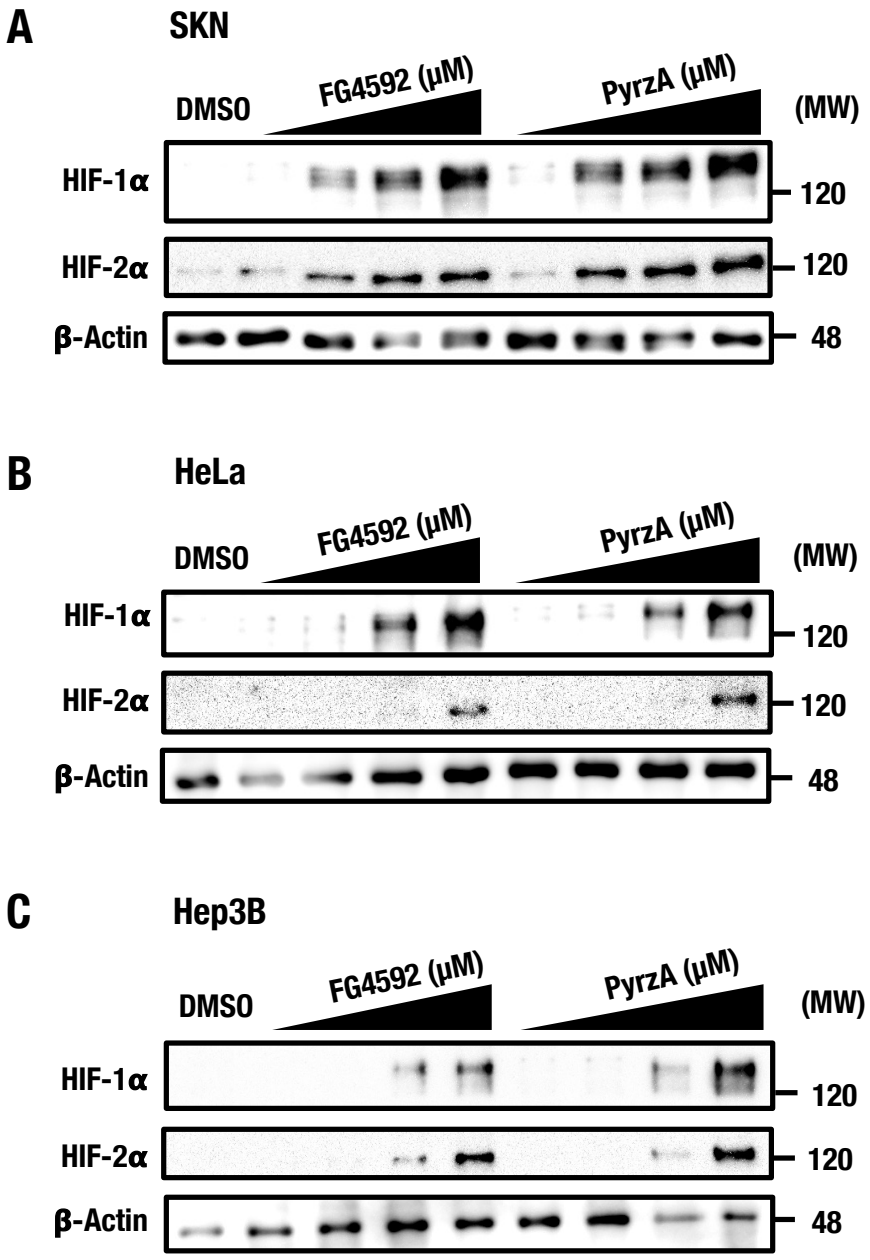

Figure 2-5. PyrzA stabilizes HIF-α protein in various cell lines. (A−C) Immunoblot analyses of HIF-α during various concentrations (1.0, 5.0, 25, and 100 μM) of PyrzA and target positive control, FG4592. in SK-N-BE(2)c (A), HeLa (B), and Hep3B (C) cells. Lane 1 shows a negative DMSO vehicle control. Equal loading was assessed by probing the blots with antibodies against β-Actin. All experiments were performed in triplicate, representative data are shown.

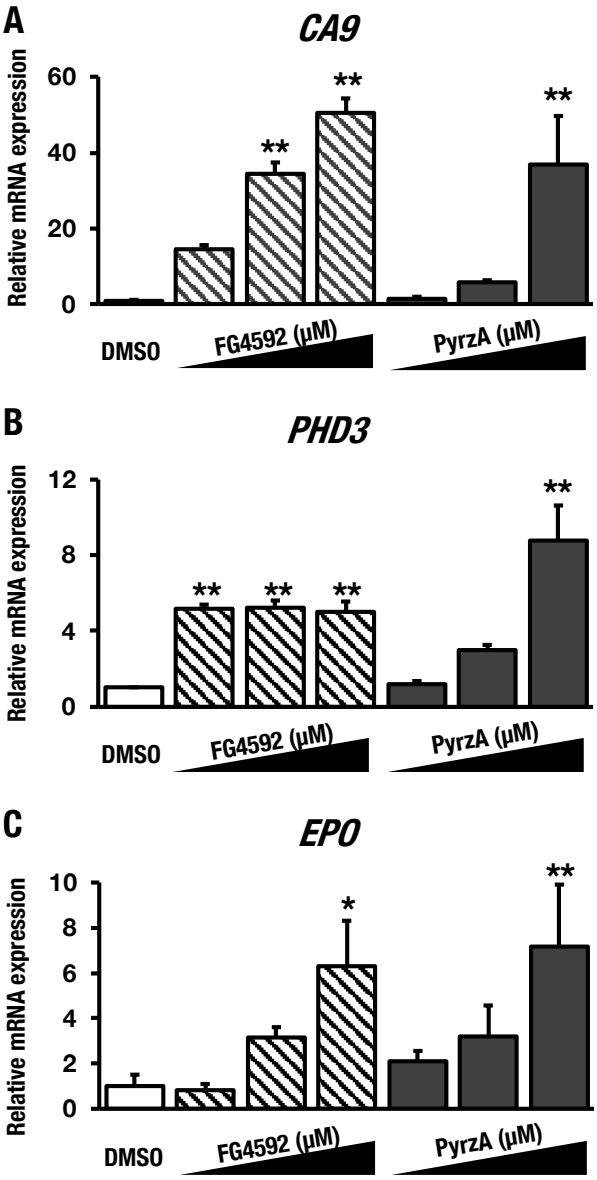

Figure 2-6. Effect of PyrzA on HIF-α target gene regulation. (A-C) The expression levels of carbonic anhydrase 9 (*CA9*), *PHD3*, and erythropoietin (*EPO*) were measured using RT-qPCR after treatment with FG4592 or PyrzA (10, 30, and 100 μM) for 24 h and Hep3B. Experiments were performed in triplicates. Each date is mean ± SE (n = 3) and based on the value from 1% DMSO-treated cells set as 1. **P* < 0.05, ***P* < 0.01 compared with 1% DMSO (one-way ANOVA with Dunnett's test). All data are expressed as mean ± SEM.

Table 2-1. Several conditions in experiments with PyrzA in wild-type C57BL6 mice

Condition No.	Sex	PyrzA treatment (mg/kg)	Mouse vehicle group	Mouse PyrzA group	Injection days (Days)	Harvest time (h)
1	male	50	5	4	5	24
2	female	50	7	6	5	24
3	male	50	1	2	1	6
4	female	50	7	8	1	6
5	female	50	7	7	3	6
6	male	200	4	5	1	6
7	female	200	3	5	1	6

Table 2-2. The results of body weight, spleen weight, hematocrit, and plasma EPO concentration, in multiple conditions

Condition No.	injection	Treatment (mg/kg)	Weight (g)	Spleen (mg)	Percentage of spleen (%)	Hematocrit (%)	EPO conc. (pg/mL)
1	vehicle	0	n.d.	73.8±5.77	n.d.	n.d.	298±293
1	PyrzA	50	n.d.	74.2±2.55	n.d.	n.d.	541±82.5
2	vehicle	0	n.d.	66.1±12.3	n.d.	n.d.	134±120
2	PyrzA	50	n.d.	66.7±12.3	n.d.	n.d.	319±225
3	vehicle	0	n.d.	62.5	n.d.	n.d.	n.d.
3	PyrzA	50	n.d.	56.6±3.32	n.d.	n.d.	n.d.
4	vehicle	0	18.7±0.91	52.1±7.19	0.279±0.043	47.2±0.84[b]	105±44.0
4	PyrzA	50	17.8±0.93	52.0±1.92	0.292±0.016	50.0±1.10[b]	151±174
5	vehicle	0	19.2±1.31	67.7±10.3	0.352±0.036[a]	39.3±4.19	220±78.0
5	PyrzA	50	17.4±2.04	70.4±10.9	0.404±0.033[a]	43.0±5.32	249±52.6
6	vehicle	0	20.1±3.68	51.7±9.79	0.259±0.029	46.5±3.70[b]	111±56.6[a]
6	PyrzA	200	19.0±1.82	44.0±2.90	0.223±0.033	54.4±2.51[b]	976±472[a]
7	vehicle	0	13.6±2.29	46.4±1.38	0.347±0.054	39.7±9.07	155±109
7	PyrzA	200	13.7±3.07	42.0±6.39	0.314±0.046	42.0±13.8	682±481

Statistical analysis: Each date is mean ± SD. [a] $P < 0.05$, [b] $P < 0.01$ compared with vehicle (two-tailed, unpaired Student's *t* test).

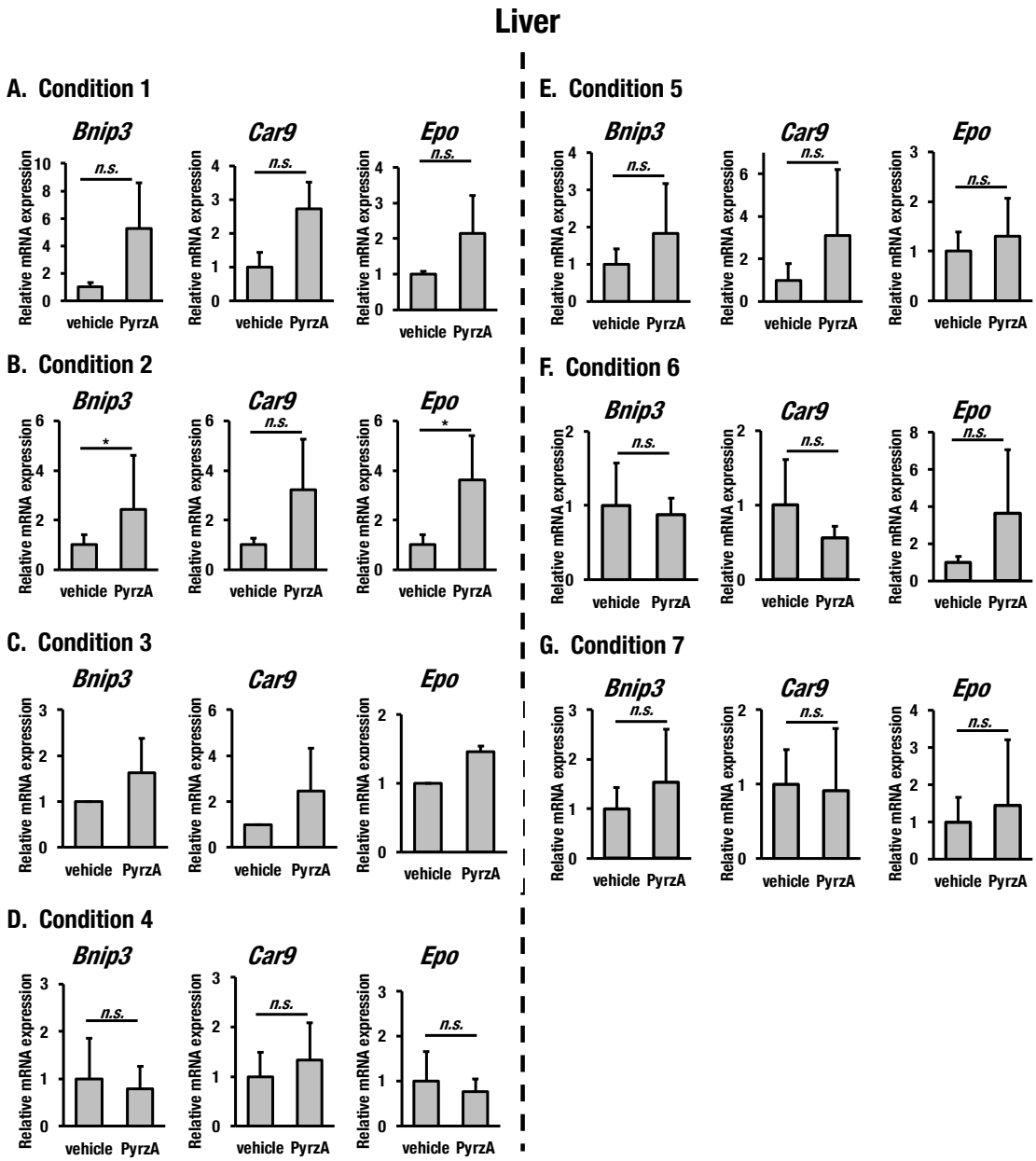
Liver
A. Condition 1
B. Condition 2
C. Condition 3
D. Condition 4
E. Condition 5
F. Condition 6
G. Condition 7
Bnip3
Car9
Epo
Relative mRNA expression
n.s.
*
vehicle
PyrzA

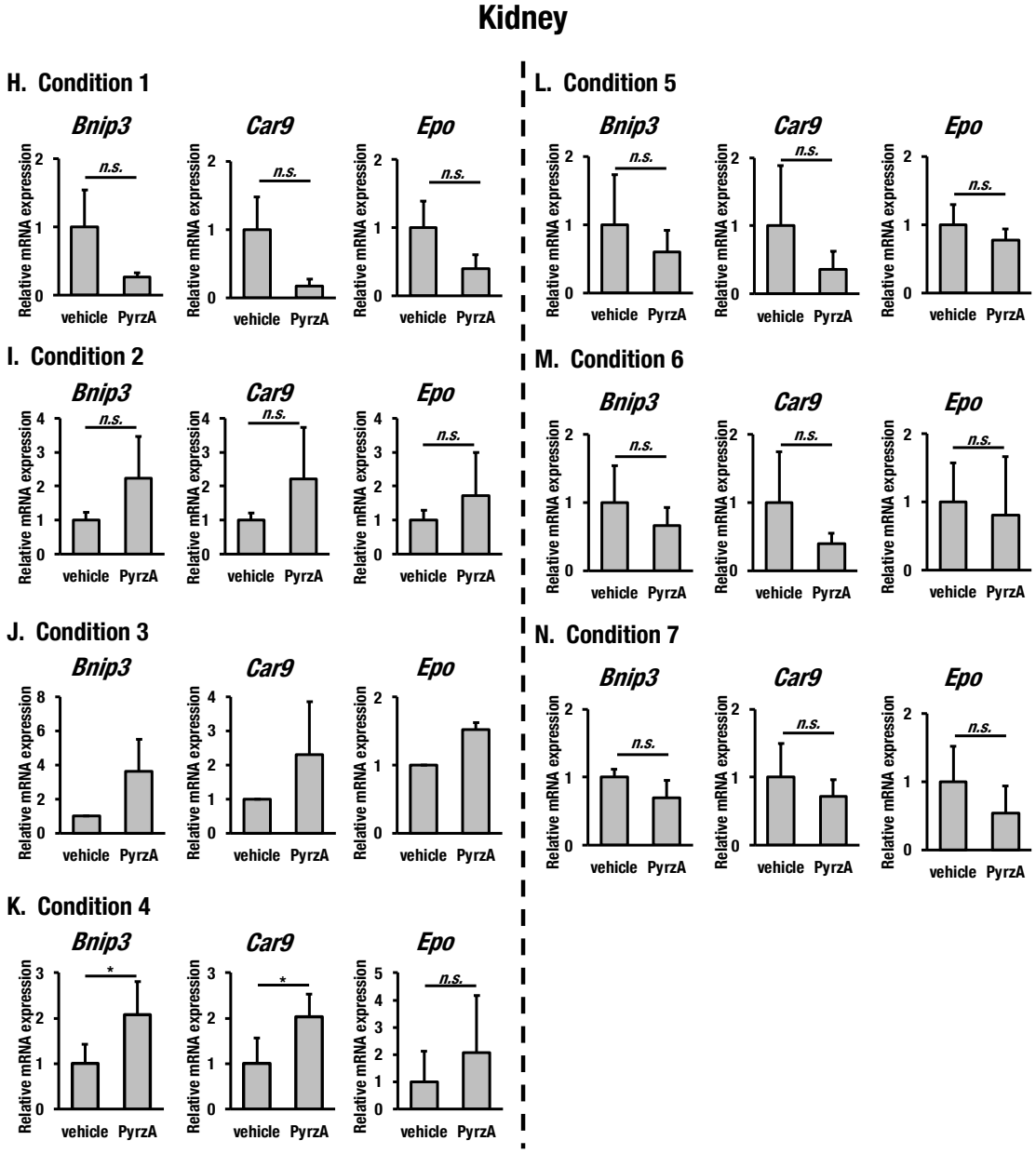

Figure 2-7. Effect of PyrzA on HIF-α target gene regulation in mice under condition **1-7**. The expression of BCL2/adenovirus E1B interacting protein 3 (*Bnip3*), carbonic anhydrase 9 (*Car9*), and *Epo* was measured using RT-qPCR in the liver (A-G) or kidney (H-N). **P* < 0.05 compared with vehicle (two-tailed, unpaired Student's *t* test). All data are expressed as mean ± SEM.

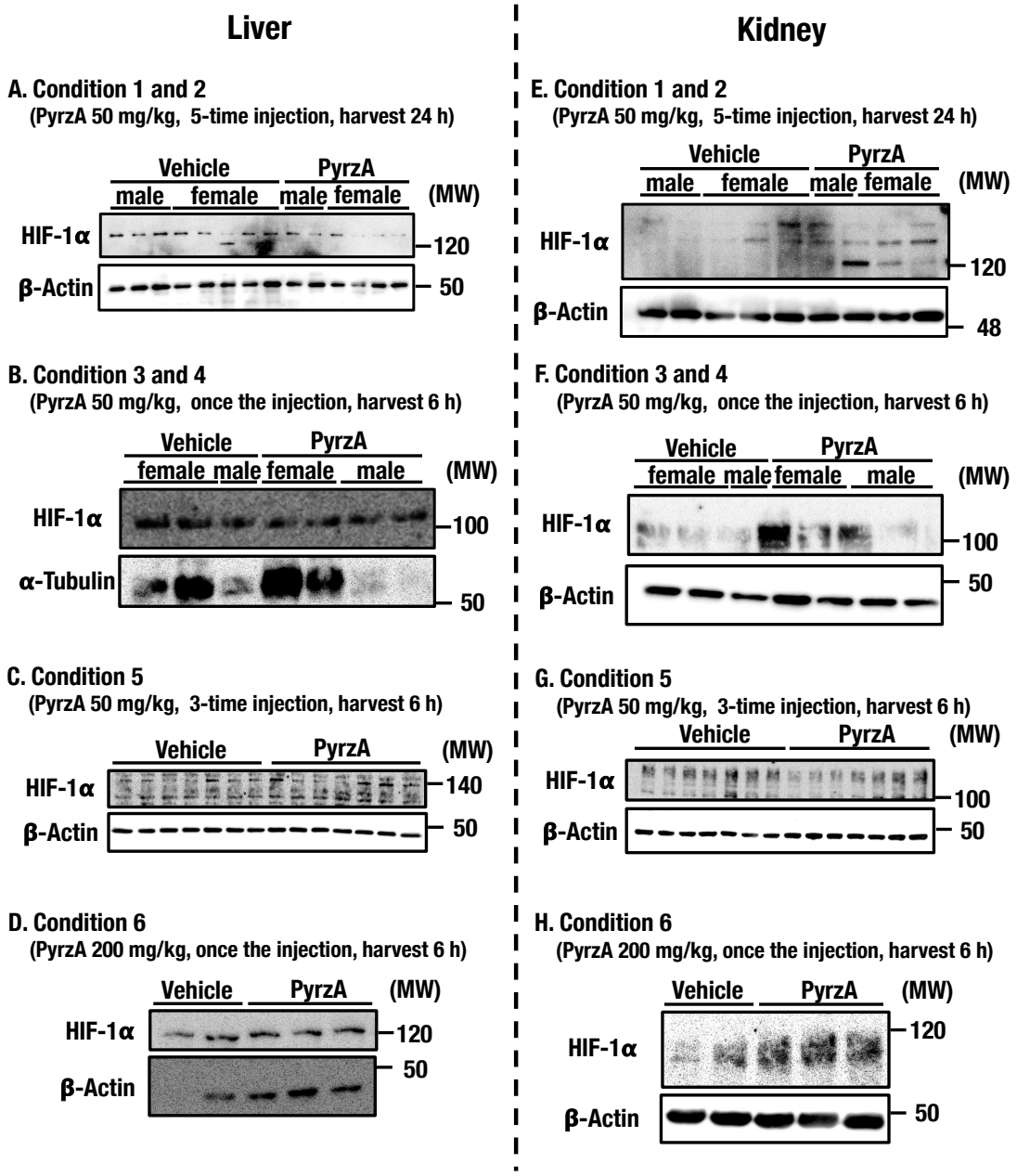

Figure 2-8. Stabilization of HIF-α proteins administrated with PyrzA, or the vehicle control in mice was compared under condition **1**-**6**. Immunoblot analyses of HIF-α in mice kidney and liver under various conditions. These tissues were homogenized, and sample protein concentrations were measured using BCA assay. Samples of 20 μg of total protein were loaded and subjected to immunoblot assay. Equal loading was assessed by probing the blots with antibodies against β-Actin or α-Tubulin.

A

Evaluation of 2 chemicals interaction (additive or synergistic effect)

1. Calculation of expected value

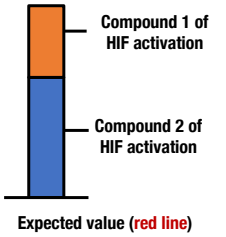

2. Comparison with an experimental value

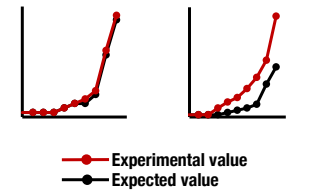

3. Measurement of a ratio of 50-fold luciferase activity (b/a)

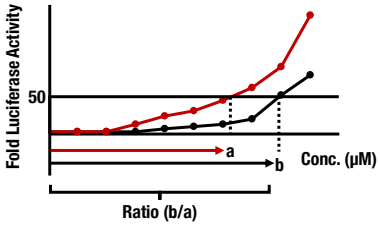

The ratio of 50-fold luciferase activity

$$\frac{\text{b: Expected 50–fold luciferase activity}}{\text{a: Experimental 50–fold luciferase activity}}$$

When 2 chemicals act synergistically, a ratio of 50-fold luciferase activity is bigger.

B

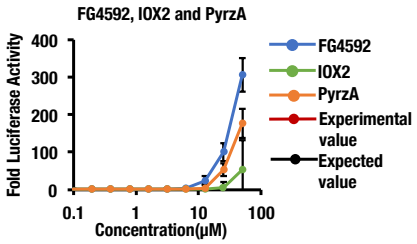

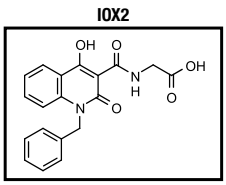

Chemical condition

Chemical	Fixed concentration (μM)	5-fold HIF activity (μM)
FG4592	5	1.87
IOX2	20	3.38
PyrzA	15	13.8

FG4592 and IOX2

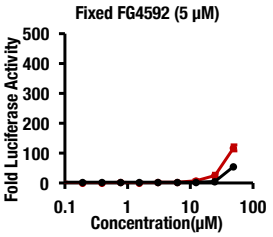

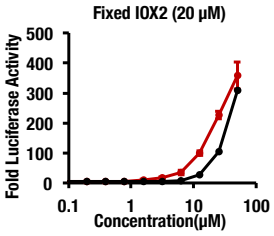

The ratio of 50-fold luciferase activity

Condition	Fixed FG4592	Fixed IOX2
Experimental value (μM)	31.7	7.81
Expected value (μM)	47.8	16.2
Ratio (b/a)	1.50	2.08

FG4592 and PyrzA

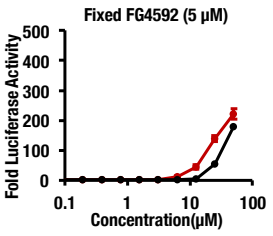

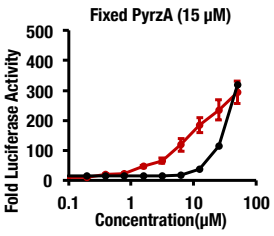

The ratio of 50-fold luciferase activity

Condition	Fixed FG4592	Fixed IOX2
Experimental value (μM)	13.2	1.91
Expected value (μM)	23.6	14.5
Ratio (b/a)	1.79	7.62

C

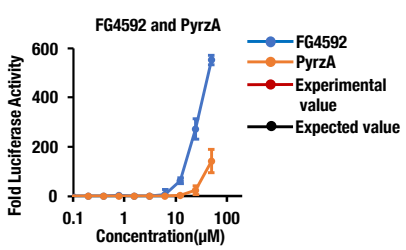

The ratio of 300-fold luciferase activity (high)

Condition	Fixed FG4592	Fixed PyrzA
Experimental value (μM)	3.02	1.86
Expected value (μM)	26.0	18.2
Ratio (b/a)	8.61	9.74

The ratio of 100-fold luciferase activity (middle)

Condition	Fixed FG4592	Fixed PyrzA
Experimental value (μM)	3.15	0.271
Expected value (μM)	27.8	13.3
Ratio (b/a)	8.83	49.1

The ratio of 50-fold luciferase activity (low)

Condition	Fixed FG4592	Fixed PyrzA
Experimental value (μM)	4.62	1.27
Expected value (μM)	29.1	10.8
Ratio (b/a)	6.29	8.48

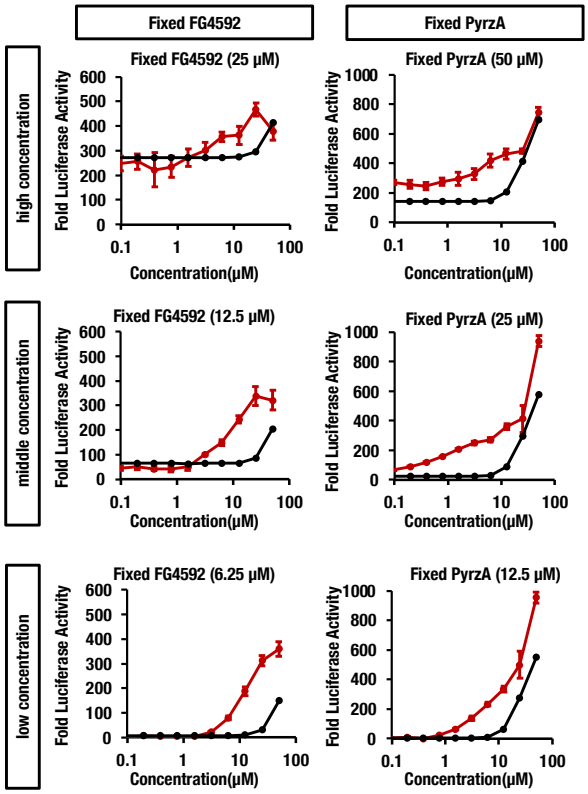

Figure 2-9. HIF-α transcriptional activity treated with both FG4592 and PyrzA can activate higher than expected. (A) Illustrations of an expected value and a ratio of 50-fold luciferase activity. When this ratio is high, two chemicals may act synergistically. (B) HIF-α transcriptional activity results for both IOX2 and FG4592 and both PyrzA and FG4592. HIF-α transcriptional activity results for FG4592 and PyrzA (both serial diluted IOX2 and fixed FG4592 (5 μM) or both serial diluted FG4592 and fixed IOX2 (20 μM)) or FG4592 and IOX2 (both serial diluted PyrzA and fixed FG4592 (5 μM) or both a serial diluted FG4592 and fixed PyrzA (15 μM)) using SKN:HRE-NLuc for 24 h. (C) HIF-α transcriptional activity results for both serial diluted PyrzA and fixed FG4592 (6.25, 12.5, and 25 μM) and both serial diluted FG4592 and fixed PyrzA high concentration (12.5, 25, and 50 μM). The HRE reporter activities are indicated as fold luciferase activity, based on the value from 1% DMSO-treated cells.

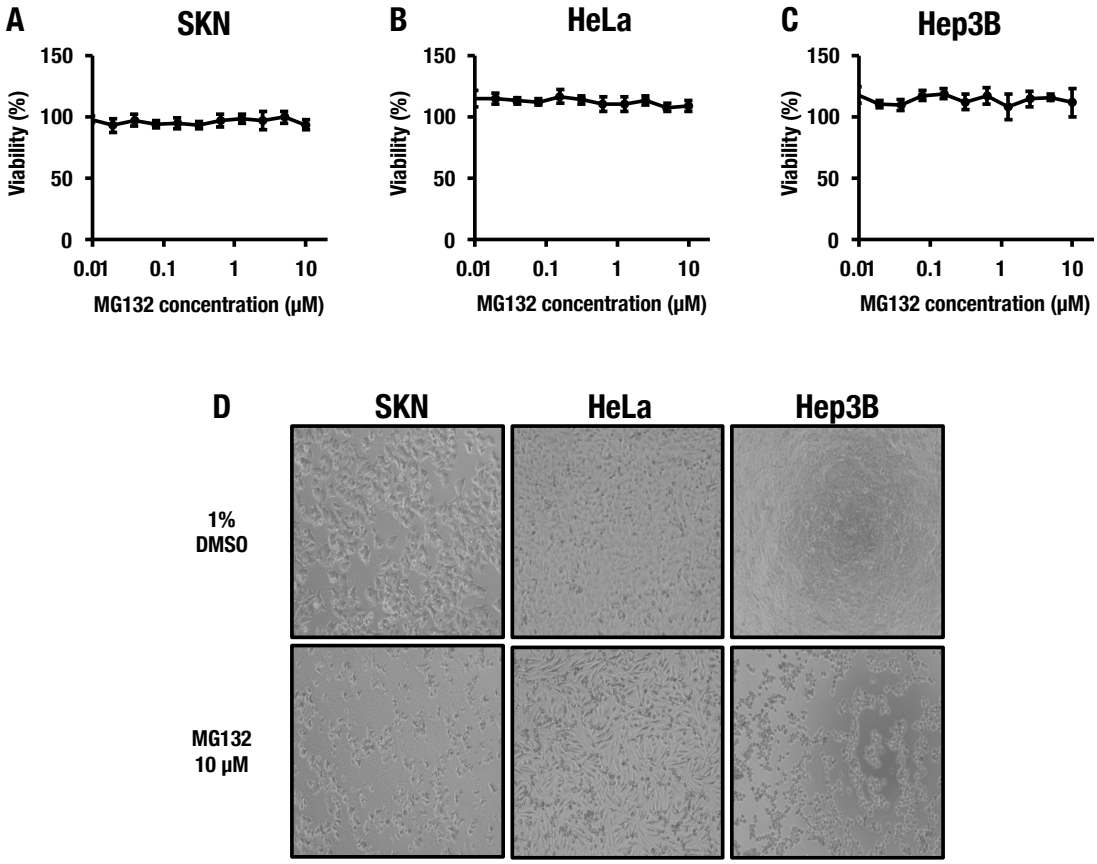

Figure 2-10. Effect of MG132 on various cell lines. (A-C) Cellular viability results for MG132 in SK-N-BE(2)c (A), HeLa (B), and Hep3B (C) cells for 24 h. The cell viability percentile is represented on the value from 1% DMSO treated cells as 100% viability (filled circle and solid line). Error bars represent SEM (n= 4). (D) Representative various cell line images treated with a negative DMSO vehicle control and 10 μM MG132 for 24 h were shown.

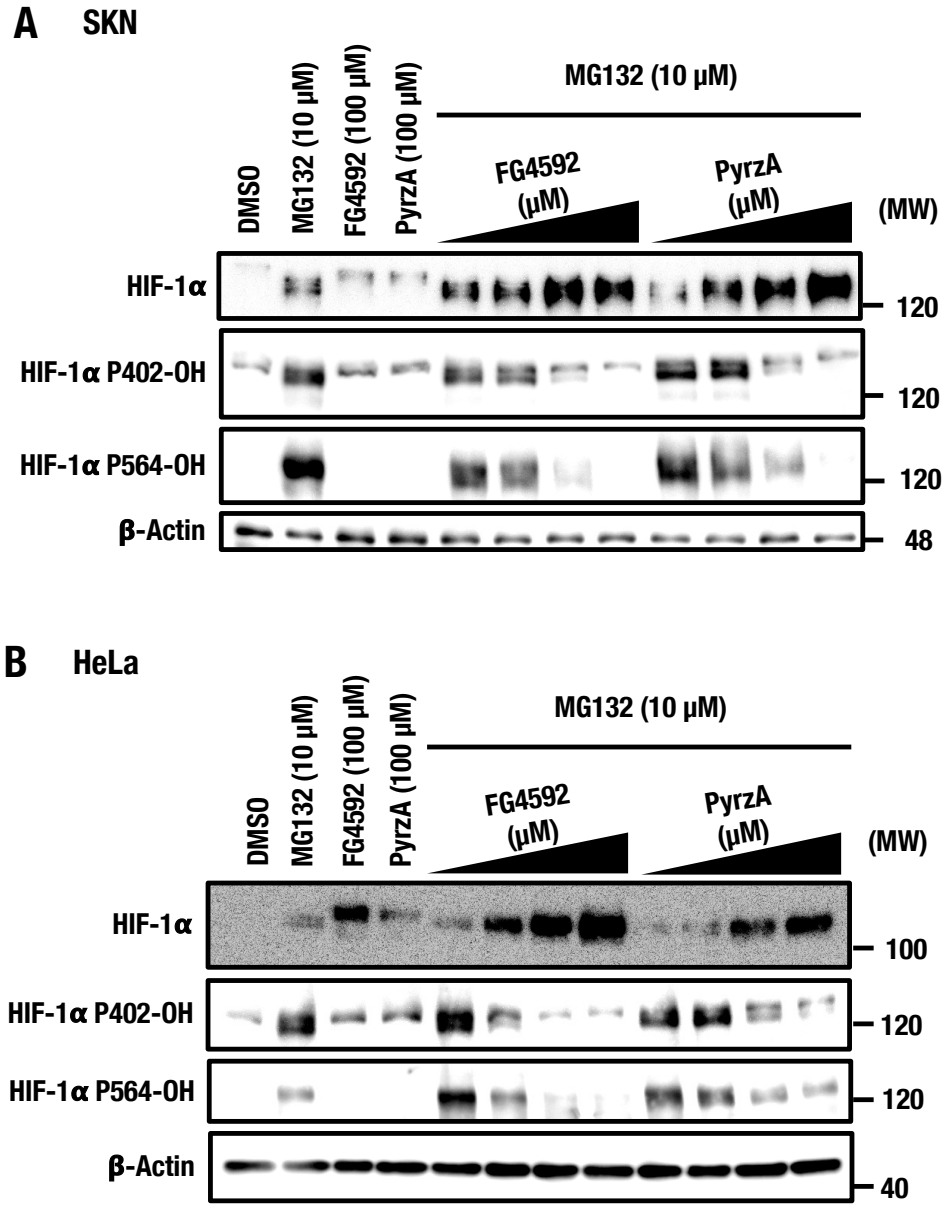

Figure 2-11. PyrzA inhibits HIF-1α prolyl hydroxylation. (A, B) Immunoblot analyses of HIF-α with its hydroxylated prolyl 402 and 564 residues on SK-N-BE(2)c (A) or HeLa (B). Cells were treated with various concentrations (1.0, 5.0, 25, or 100 μM) of PyrzA and FG4592 in the presence of proteasome inhibitor MG132 (10 μM) for 24 h. Simultaneously, cells were independently treated with PyrzA (100 μM), FG4592 (100 μM), or MG132 (10 μM) for 24 h. Equal loading was assessed by probing the blots with antibodies against β-Actin.

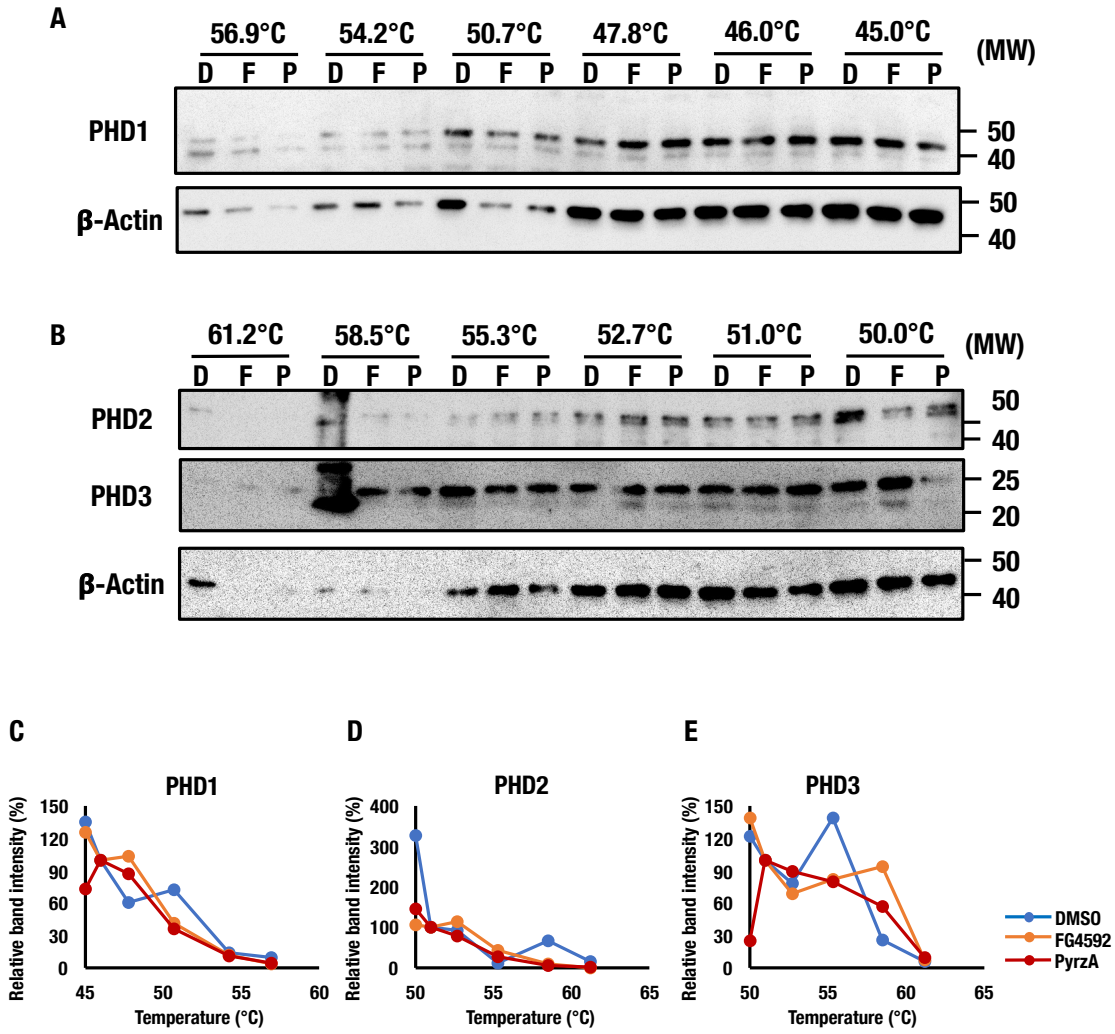

Figure 2-12. Thermodynamic stabilization or destabilization due to the binding of FG4592 or PyrzA to PHDs was compared. (A-E) SK-N-BE(2)c cell lysates were treated with 1% DMSO, FG4592 (F), or PyrzA (P) (100 μM) and then heated at the indicated temperatures for 3 min. After centrifugation, the supernatant was subjected to SDS-PAGE followed by staining with immunoblot for PHD1 (A), PHD2, and PHD3 (B). (C-E) The quantification of PHD1-3 band intensity was shown. The relative band intensity for PHD1-3 was shown with a band ratio of 46.0°C samples (PHD1) or 51.0°C samples (PHD2 and 3) as 1.0.

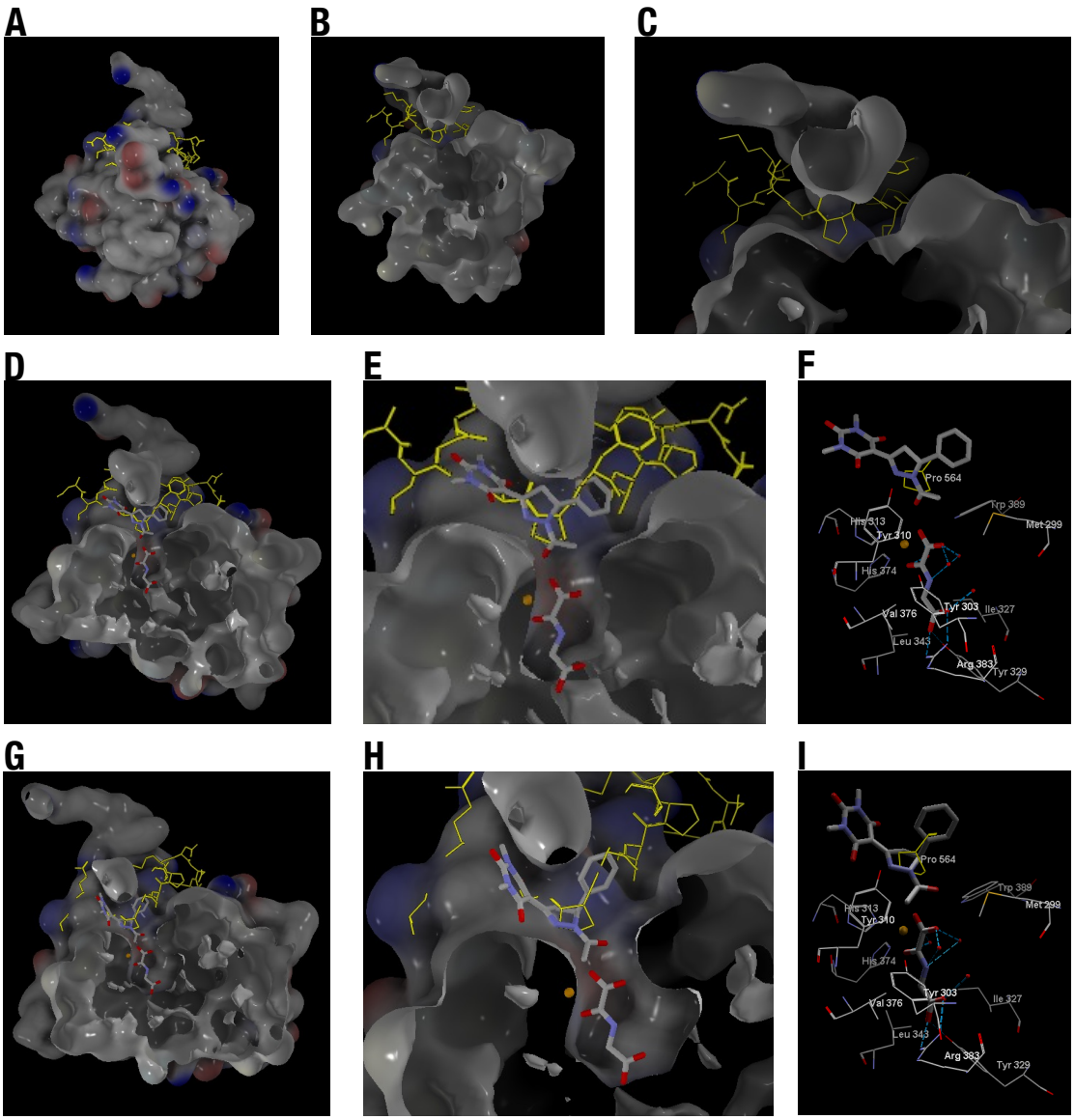

J

Entry	Compound	R/S	Score (MolDock) (kcal/mol)
1	PyrzA	*S*	-99.6763
2	PyrzA	*R*	-89.3412

Figure 2-13. Predicted binding model of PHD2 (PDB ID: 3hqr) within PyrzA. HIF-1α CODD peptide (amino acids number 556−574) (yellow) bound to PHD2; blue corresponds to positive charge and red to negative charge residues. Mn^{2+} (orange) and *N*-oxalylglycine were substitutes for Fe^{2+} and 2-OG, respectively. PyrzA and *N*-oxalylglycine were drawn with carbon in white, oxygen in red, and nitrogen in blue. (A-C) HIF-1α CODD peptide bound to PHD2, (A) overall view, (B) Transverse section of the protein model for visualization of the catalytic site, (C) the magnified image of B. (D-I) (D and G) Overall view. (E and H) Enlarged view of the area around the Pro564 (CODD). (F and I) Enlarged view of the catalytic center of PHD2. These data showed Mn^{2+}, 2-OG, (*S*)−PyrzA, Pro564, and the specified residues of PHD2 (D-F) and Mn^{2+}, 2-OG, (*S*)−PyrzA, Pro564, and the specified residues of PHD2 (G-I). (J) The docking (MolDock) scores of (*S*−or *R*−) PyrzA on PHD2 protein as calculated by Molegro Virtual Docker 7.0.0.

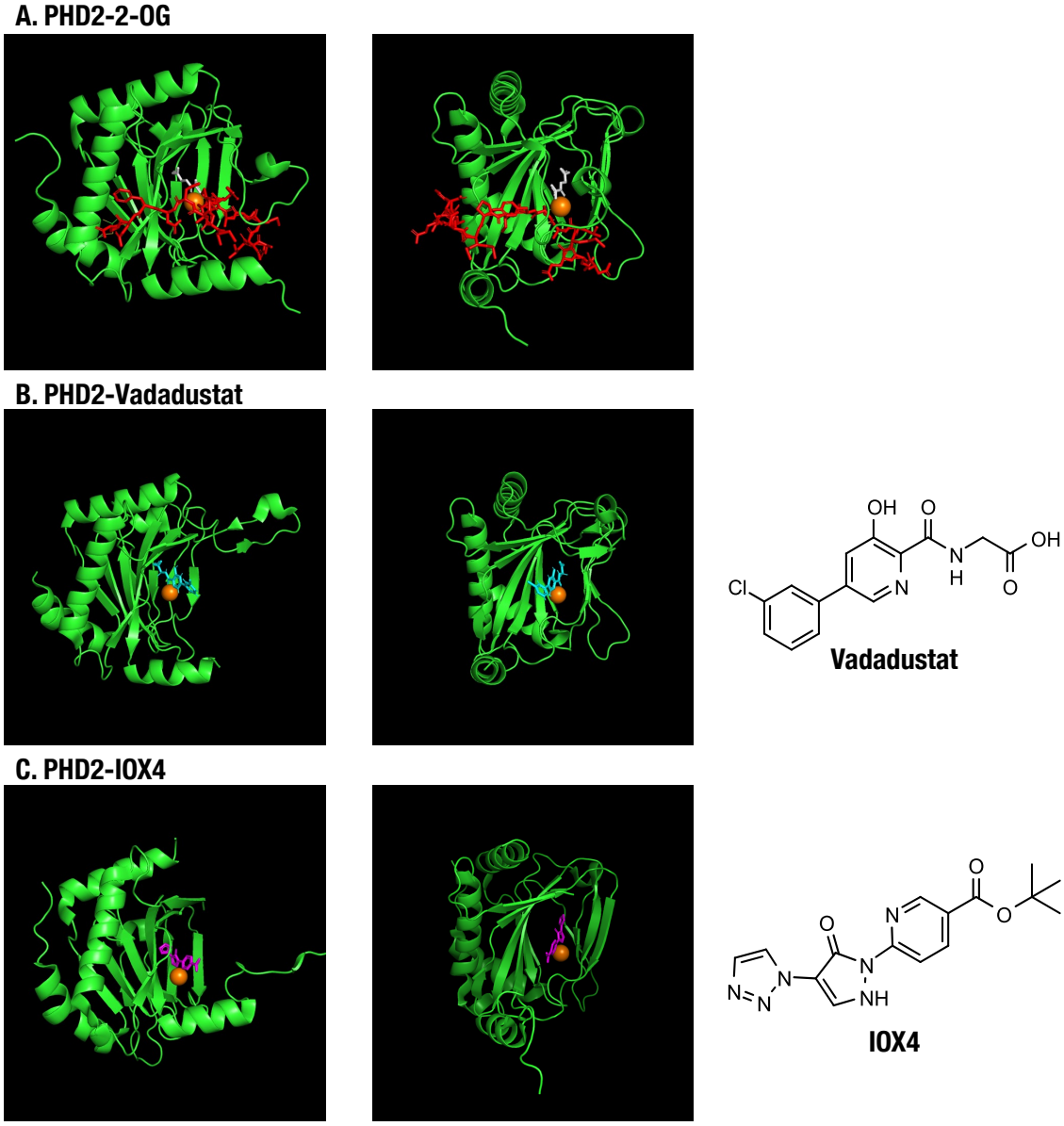

Figure 2-14. PHIs interact with PHD2 at a different site of HIF-1α CODD peptide. (A) Views from HIF-1α CODD peptide (amino acids number 556－574) (red) bound to PHD2; (green) (PDB ID: 3hqr). Mn^{2+} (orange) was substituted for Fe^{2+}. (B) Views from vadadustat (cyan) bound to PHD2 (PDB ID: 5oX6). (C) Views from IOX4 (magenta) bound to PHD2; (green) (PDB ID: 5a3u).

Chapter 3

Selection of higher HIF activity of PyrzA derivative

3-1. Introduction

In a previous chapter, PyrzA was characterized as a novel HIF activator that does not contain the 2-OG scaffold. PyrzA activated HIF target genes to inhibit PHDs. PyrzA also activated HIF signal cascade in mice.

In this chapter, higher HIF activity of PyrzA derivative to improve lipophilicity was selected using HIF activation reporter assay. The structure of PyrzA has a pyrazolidine ring bonded to barbituric acid and acetyl and phenyl groups substituted on the pyrazolidine ring. The general chemical structure of PyrzA derivatives were shown in Figure 3-1 and are compounds in which the phenyl group is replaced by another aryl group (R^1); the N atoms of barbituric acid by an alkyl group (R^2); and the acetyl group by an alkanoyl group (R^3). Then, selected PyrzA derivatives activated HIF cascade in Hep3B cell.

3-2. Experimental section

3-2-1. Reagents

DMSO, FG4592, and PyrzA were obtained as described in 2-2-1. The following PyrzA derivatives were synthesized as described in the literature[121].

3-2-2. Cell culture

All cells were cultured as described in 2-2-3.

3-2-3. Evaluation of HIF activity and cellular viability

Evaluation of HIF activity and cellular viability was performed as described in 2-2-4.

3-2-3. Immunoblot assay

Immunoblot was performed as described in 2-2-7.

3-2-4. RNA isolation and quantitative PCR

Total RNA from the cells was prepared using the Blood/Cultured Cell Total RNA Mini Kit following the manufacturer's instructions. The total RNA was reverse transcribed to cDNA using the FastGene cDNA Synthesis Reagent (Nippon Genetics). The resulting cDNA was used as a template for quantitative PCR (qPCR) using the KAPA SYBR FAST qPCR Master Mix (2×) Kit with Mx3005P qPCR system. 18S rRNA expression levels were used as internal controls. The primer sequences used were as follows: human carbonic anhydrase 9 (*CA9*): (forward) 5′–CCT TTG CCA GAG TTG ACG AG–3′ and (reverse) 5′–GAC AGC AAC TGC TCA TAG GC–3′; human erythropoietin (*EPO*): (forward) 5′–TCA TCT GTG ACA GCC GAG TC–3′ and (reverse) 5′–CAA GCT GCA GTG TTC AGC AC–3′; human *18S rRNA*: (forward) 5′–GTA ACC CGT TGA ACC CCA TT–3′ and (reverse) 5′–CCA TCC AAT CGG TAG TAG CG–3′.

3-2-5. Docking simulation

Docking simulation for PHD2 and **2c** was performed using Molegro Virtual Docker 7.0.0. The crystal structure data for PHD2 (PDB ID: 3hqr[20]) was obtained from the Protein Data Bank (https://pdbj.org). The docking simulations were performed as described in 2-2-10.

3-3. Result

3-3-1. HIF reporter activities and cellular toxicities of PyrzA derivatives

PyrzA derivatives are divided into 2 types: (1) derivatives with modified R^1 and R^3 substituents, (2) derivatives with modified R^2 and R^3 substituents (Figure 3-1). (1) R^1: the phenyl group is replaced by 10 types of aryl group (**1b**-**1k** and **1q**) or R^3: the acetyl group is replaced by 5 types of alkanoyl group (propanoyl, *n*-butanoyl, isobutanoyl, *n*-hexanoyl, and *n*-decanoyl groups) (**1l**-**lq**) (Figure 3-1B and D). (2) R^2: the N atoms of barbituric acid of methyl moiety are replaced by cyclohexyl group and R^3: the acetyl group is replaced by 5 types of alkanoyl group (**2a**-**2f**) (Figure 3-1C and D). PyrzA derivatives with modified R^2 were aimed to improve the high lipid solubility. The HIF transcriptional activities and cellular viabilities of PyrzA (**1a**) and its derivatives (**1b**–**1q**, **2a**–**2f**) were evaluated using SKN:HRE-NLuc cells. While NMR analysis confirmed that **1k**: the phenyl group is replaced by cyclohexyl group was not >95% pure, **1k** was excluded from PyrzA derivatives.

The reporter cells were stimulated using 100 μM to 98 nM PyrzA derivatives (**1a**-**1q**, **2a**-**2f**) for 24 h. After the stimulation, the HIF activities were measured using NLuc activities. Cellular viabilities were also measured using CCK-8. The HIF activity was presented as the intensity of the luciferase activity, with that of the vehicle-treated cells (1% DMSO) set as 1. Cell viability was presented as a percentage, with that of the vehicle-treated cells (1% DMSO) set as 100%.

Graphs of the HIF-α transcriptional activity at various concentrations of the compounds and the cell viability corresponding to each were shown in Figure 3-2. The HIF activities were evaluated at concentrations when the NLuc activities were 5 times the concentrations of the compounds. More effective PyrzA derivatives worked at lower

concentrations. The evaluation of the compounds by luciferase assay in this study was based on 5-fold activity concentration instead of evaluation as EC_{50} analysis because the maximum HIF activity varies among various PyrzA derivatives and some PyrzA derivatives have weak cytotoxicity that reduces HIF activity.

Table 3-1 summarizes 5-fold concentration, LC_{50} and ClogP value (calculated logarithm of the octanol/water partition coefficient), a factor of its lipophilicity, of **1a** and its derivatives **1b-1i**, **1k-1q** and **2a-2f**. Among **1b-1q**, all derivatives with long alkyl chains substituent at R^3 (**1l-1q**) showed higher activities than **1a**. Next, the correlation coefficients were obtained from a scatter plot of the ClogP values and HIF transcriptional activities (Figure 3-3). Subsequently, the correlation coefficient |R| was found to be 0.47, indicating a correlation between ClogP and activity. Therefore, the HIF activities of the more lipophilic PyrzA derivatives **2a-2f** were measured and the transcriptional activity of HIF showed good values when ClogP was less than 4 (**2a-2d**). In terms of cytotoxicity, the SKN:HRE-NLuc cell count was measured using CCK-8 via a colorimetric assay. LC_{50} values of all derivatives were more than 100 μM. For compounds **1a**–**1q**, no decrease in the cell count was observed, indicating no cytotoxicity. In contrast, when compounds **2a** and **2b** were applied to the cells at high concentrations, the cell count decreased, although not up to 50%. The addition of compounds **2c** and **2d** to the cells at higher concentrations did not decrease the cell count. Therefore, compounds **2c** and **2d** were selected from the 22 PyrzA derivatives as compounds with high HIF transcriptional activities and no cytotoxicity. Of these, compound **2c** (PyrzA-50: 5-(1-*n*-Butyryl-5-phenylpyrazolidin-3-ylidene)-1,3-dicyclohexyl-pyrimidine-2,4,6(1*H*,3*H*,5*H*)-trione) (Figure 3-4) was selected for further evaluation.

3-3-2. Stabilization of HIF-α proteins treated with 2c

Next, HIF-α stabilization was confirmed using immunoblot analysis in Hep3B cells. These were evaluated via immunoblot analysis of Hep3B cells using antibodies for HIF-1α and HIF-2α. Hep3B cells were employed for **1a**, **2c**, and FG4592 at concentrations up to 100 μM for 24 h, which led to a dose-dependent stabilization of both HIF-1α and HIF-2α in Hep3B cells (Figure 3-5A). Importantly, **2c** stabilized both HIF-1α and HIF-2α at concentrations as low as 1 μM. Moreover, the stabilization of HIF-α proteins by **2c** reached a plateau from 1 μM to 100 μM. Therefore, HIF-α stabilization at low concentrations of compound **2c** was further evaluated. Hep3B cells were employed with **2c** at concentrations from 16 nM to 1 μM for 24 h (Figure 3-5B). The results suggest that **2c** stabilized both HIF-α proteins dose-dependently at low concentrations. Therefore, **2c** has strong potential to stabilize both the HIF-α proteins compared to first hit **1a** or FG4592.

3-3-3. Effects of HIF target genes treated with 2c

Upregulation of HIF target genes was confirmed using RT-PCR in Hep3B cells. *CA9* and *EPO* were used as HIF target genes. Hep3B cells were employed with **1a** (100 μM) or **2c** (10, 30, and 100 μM) for 24 h, and the negative control vehicle, 1% DMSO. Both selected genes were induced by **2c** (Figure 3-6). Especially, the expression of *EPO* after treatment with **2c** responded significantly at low concentrations (10–30 μM). The results suggest that lead compound **2c** drives the HIF pathway more efficiently than initial hit compound **1a**.

3-3-4. The docking simulation between PHD2 and 2c

Finally, to predict the binding sites of PHD and **2c**, the docking simulation was performed as described in 2-2-12. The human PHD2:Mn^{2+}:*N*-oxalylglycine:HIF-α substrate complex (PDB ID: 3hqr[20]) was selected as a template structure. The coordinates of the five-membered ring structure of only (*S*)-**2c**, but (*R*)-**2c**, were found to overlap with the coordinates of Pro564 in HIF-1α CODD. (Figure 3-7A-F). Thus, (*S*)-**2c** had the potential to interrupt the binding of PHD2 and HIF-1α CODD. Their docking (MolDoc) scores of (*S*)- or (*R*)-**2c** were -112.64 and -83.2863 (kcal/mol), respectively (Figure 3-7G). While the docking score of (*R*)-**2c** was poorer than that of (*R*)-PyrzA, that of (*S*)-**2c** was more potent than that of (*S*)-PyrzA. The docking results indicate that (*S*)-**2c** is more potent than PyrzA and has potentially increased selectivity over inhibitors of 2-OG analogs.

3-4. Discussion

The derivatives of PyrzA, a molecule that activates HIF, were selected to improve its activity, and their structure-activity correlations were discussed. In the selection section, the synthetic route for PyrzA derivatives by introducing the various substituents at R^1, R^2, and R^3 were shown in Table 3-1. In contrast, the precursor compounds of PyrzA derivatives, for which the no alkanoyl group at the N atom of pyrazolidine, showed no HIF transcriptional activity.

Substitution of R^1 introducing *p*-chlorophenyl, and *p*-methoxyphenyl groups, among others, followed Topliss Tress[122]. However, because HIF activation was uncorrelated with Topliss Tress and all derivatives with long alkyl chains substituents at R^3 (**1l-1q**) showed higher activities than **1a**, the lipophilicities of PyrzA derivatives were examined. Figure 3-3 showed a correlation between the lipophilicities of the compounds and their activities

among **1b**-**1i** and **1k**-**1q**. It also was recently reported that some esterified FG4592 derivatives with enhanced lipophilicities improved cell membrane permeability, cell absorption, and therapeutic efficacy[123]. Importantly, increasing lipophilicities of compounds not only improves intracellular uptake but also decreases excretion via urine.

Substitution of R^2 (**2a**-**2f**) replacing the N atoms of barbituric acid by cyclohexyl group become more lipophilicity. The transcriptional activity of HIF showed good values when ClogP was less than 4 (Compounds **2a**-**2d**). However, at higher lipophilicities, such as those of compounds **2e** and **2f**, the cell membrane permeability decreased, which may have resulted in transcriptional activities of HIF. Since the experimentally measured logP value of 1a (1.10 ± 0.09) is reportedly higher than its calculated value (-0.91)[58], the reduced activity of compounds **2e** and **2f** is a reasonable result, considering "Lipinski's rule of five"[124,125]. Moreover, the aspect of poor solubility of **2e** and **2f**, it is difficult to develop higher lipophilic PyrzA derivatives than **2a**-**2d**[126]. For cytotoxicity, LC_{50} values of all derivatives were more than 100 μM. However, when compounds **2a** and **2b** were applied to the cells at high concentrations, the cell count decreased, although not up to 50%. Since Singh *et al*. also reported that PHIs induced autophagy at high concentrations[113], **2a** and **2b** might cause apoptosis to increase HIF activation. The isomers **2c** and **2d** showed high HIF transcriptional activities and no cytotoxicity. Of these, compound **2c** (PyrzA-50: 5-(1-*n*-butyryl-5-phenylpyrazolidin-3-ylidene)-1,3-dicyclohexylpyrimidine-2,4,6 (1*H*,3*H*,5*H*)-trione) (Figure 3-4B) was selected for further evaluation.

1o and **1q** which harbor long alkyl chains also showed high HIF-α transcriptional activities. However, because long alkyl chains may have adverse effects on cell membranes, PyrzA derivative to improve lipophilicity was substituted for another method.

Moreover, PyrzA and some PyrzA derivatives such as **1g**, **1n** and **1o** increased cellular viability. The reason is that the HIF signaling cascade has an effect on cell growth and survival[1,10].

2c showed 30-fold more active for HIF transcription than PyrzA via luciferase assay. Furthermore, **2c** more potently stabilized both HIF-1α and HIF-2α proteins at low concentrations and upregulated HIF target genes than PyrzA in Hep3B cells. Interestingly, **2c** reached a plateau at high concentrations in stabilizing HIF-α proteins and upregulating HIF target genes. On the other hand, **2c** stabilized both HIF-α proteins dose-dependently from 100 nM to1 μM.

Binding site prediction for PHD2 and **2c** showed that the coordinates of the five-membered ring structure of only (*S*)-**2c** were found to overlap the coordinates of Pro564 in HIF-1α CODD as well (*S*)- and (*R*)-PyrzA. Their docking (Moldock) score of (*S*)-**2c** was better than (*R*)-**2c**. The docking results indicate that (*S*)-**2c** is more potent than PyrzA and has potentially increased selectivity over inhibitors of 2-OG analogs and PyrzA derivatives are needed to separate racemic derivatives. In the future, the substitution of R^1 introducing hydrogen to become not racemic derivatives is also being considered.

In conclusion (*S*)-**2c** indicates its potential as a next-generation HIF activator.

A

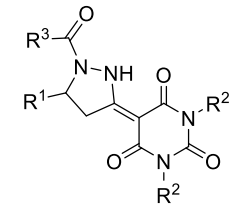

R^1 = Ar, R^2 = Me or Cy, R^3 = Alkyl
1a-q, 2a-f

B

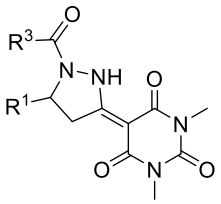

R^1 = Ar, R^2 = Me R^3 = Alkyl
1a-q

C

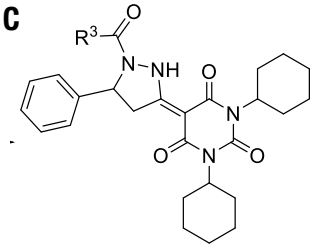

R^1 = Ph, R^2 = Cy, R^3 = Alkyl
2a-f

D

Entry	R^1	R^2	R^3	Product
1	Phenyl	Me	Me	1a
2	*p*-Biphenyl	Me	Me	1b
3	*p*-Fluorophenyl	Me	Me	1c
4	*p*-Chlorophenyl	Me	Me	1d
5	*p*-Methylphenyl	Me	Me	1e
6	*p*-Methoxyphenyl	Me	Me	1f
7	*p*-Phenoxyphenyl	Me	Me	1g
8	*p*-^{n}Octylphenyl	Me	Me	1h
9	*p*-Naphthyl	Me	Me	1i
10	Cyclohexyl	Me	Me	1j
11	2-chrolo-3-metoxyphenyl	Me	Me	1k
12	Phenyl	Me	Et	1l
13	Phenyl	Me	^{n}Pr	1m
14	Phenyl	Me	^{i}Pr	1n
15	Phenyl	Me	^{n}Pen	1o
16	Phenyl	Me	^{n}Non	1p
17	*p*-Biphenyl	Me	Et	1q
18	Phenyl	Cyclohexyl	Me	2a
19	Phenyl	Cyclohexyl	Et	2b
20	Phenyl	Cyclohexyl	^{n}Pr	2c
21	Phenyl	Cyclohexyl	^{i}Pr	2d
22	Phenyl	Cyclohexyl	^{n}Pen	2e
23	Phenyl	Cyclohexyl	^{n}Non	2f

Figure 3-1. The chemical structure of 22 types of PyrzA derivatives. (A-C) The general structures of PyrzA derivatives (A) and its derivatives (**1a**-**1q**, **2a**-**2f**) (B and C). (D) The structural modification of PyrzA (**1a**) and its derivatives (**1b**-**1q**, **2a**-**2f**).

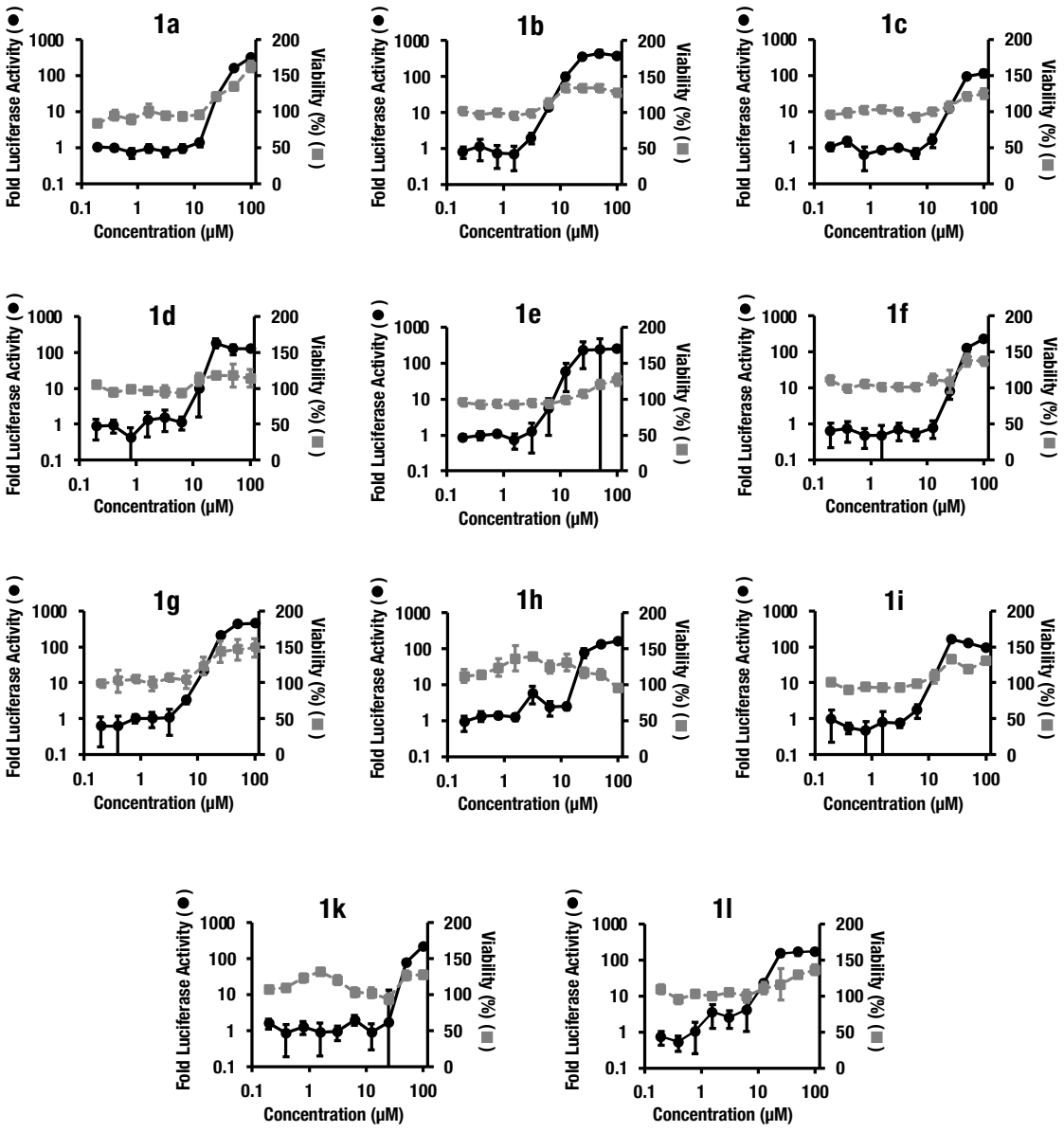
1a
1b
1c
1d
1e
1f
1g
1h
1i
1k
1l
Fold Luciferase Activity (●)
Viability (%) (■)
Concentration (μM)
1000
100
10
1
0.1
200
150
100
50
0
0.1
1
10
100

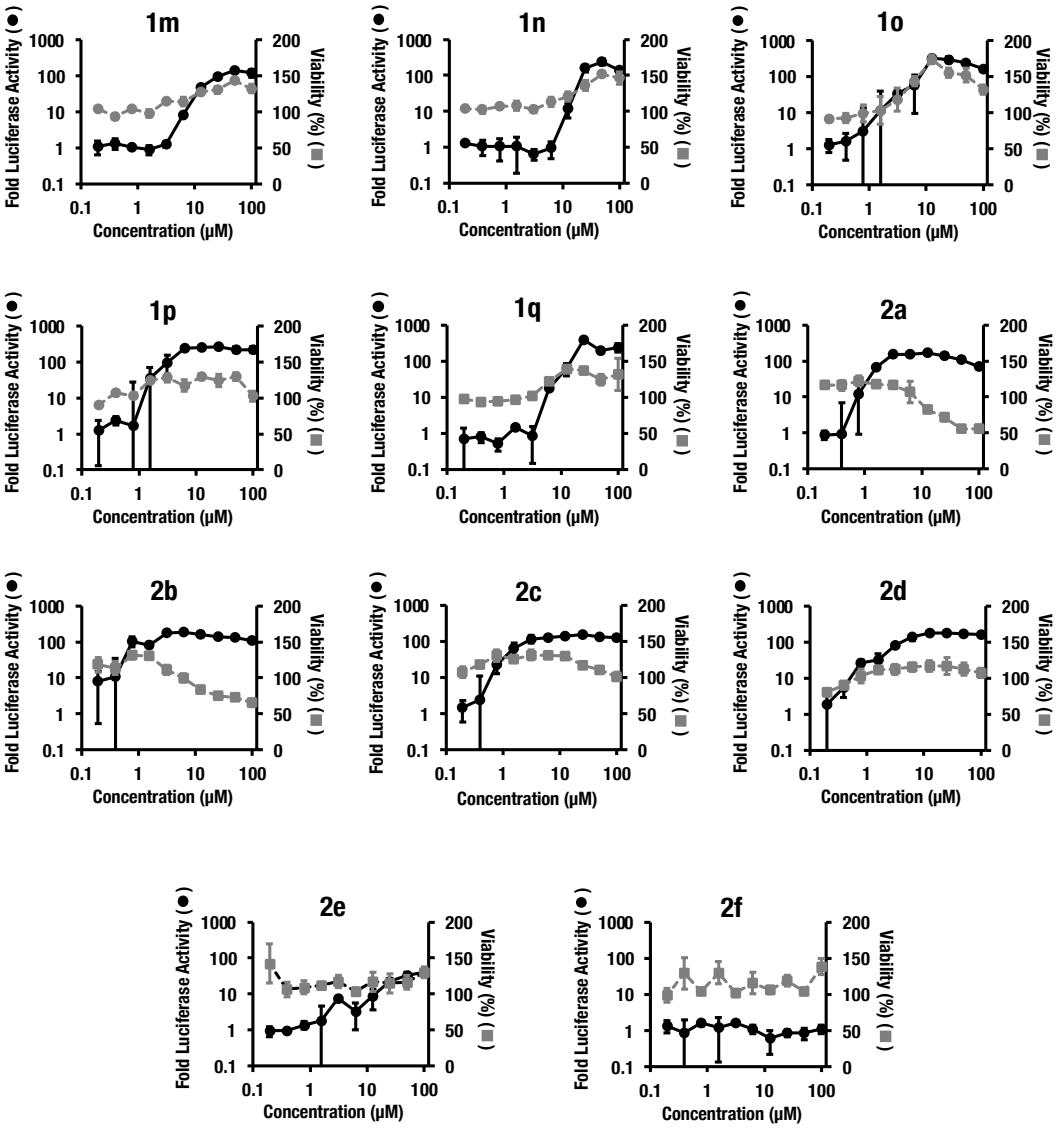
1m
1n
1o
1p
1q
2a
2b
2c
2d
2e
2f
Fold Luciferase Activity (●)
Viability (%) (■)
Concentration (μM)
1000
100
10
1
0.1
200
150
100
50
0
0.1
1
10
100

Figure 3-2. Validation of the PyrzA derivatives **1a**-**1q**, **2a**-**2f**. Those graphs showed HIF-α transcriptional activity and cellular viability for PyrzA derivatives. SKN:HRE-NLuc cells (7.0×10^3 cells/well) were seeded into each well of a 384-well plate and stimulated with various concentrations for 24 h. The luciferase activity and the cell counting kit-8 (CCK-8) using WST-8 (2-(2-methoxy-4-nitrophenyl)-3-(4-nitrophenyl)-5-(2,4-disulfophenyl)-2H-tetrazolium) were measured. HIF-α transcriptional activity is presented as fold luciferase activity, with the value from 1% DMSO stimulated cells set as 1 (filled circle and solid line). The cellular viability percentile is presented on the value from 1% DMSO stimulated cells set as 100% (filled square and dashed line). Error bars represent SEM (n= 4). These experiments were done more than three times, and the results were reproducible. Representative results are presented.

Table 3-1. HIF transcriptional activities of **1a-1q**, **2a-2f**

Entry	Product	5-Fold concentration (μM)	LC_{50} (μM)	cLogP
1	1a	14.3	>100	-0.91
2	1b	3.88	>100	-0.42
3	1c	16.5	>100	-0.77
4	1d	9.10	>100	-0.35
5	1e	5.84	>100	-0.75
6	1f	19.5	>100	-1.03
7	1g	6.82	>100	0.63
8	1h	12.9	>100	2.50
9	1i	7.67	>100	0.09
10	1k	26.1	>100	-0.48
11	1l	6.53	>100	-0.25
12	1m	4.85	>100	0.16
13	1n	8.55	>100	0.31
14	1o	0.960	>100	1.00
15	1p	0.153	>100	2.67
16	1q	3.87	>100	1.42
17	2a	0.533	>100	2.19
18	2b	0.126	>100	2.84
19	2c	0.441	>100	3.26
20	2d	0.364	>100	3.41
21	2e	2.41	>100	4.09
22	2f	>100	>100	5.76

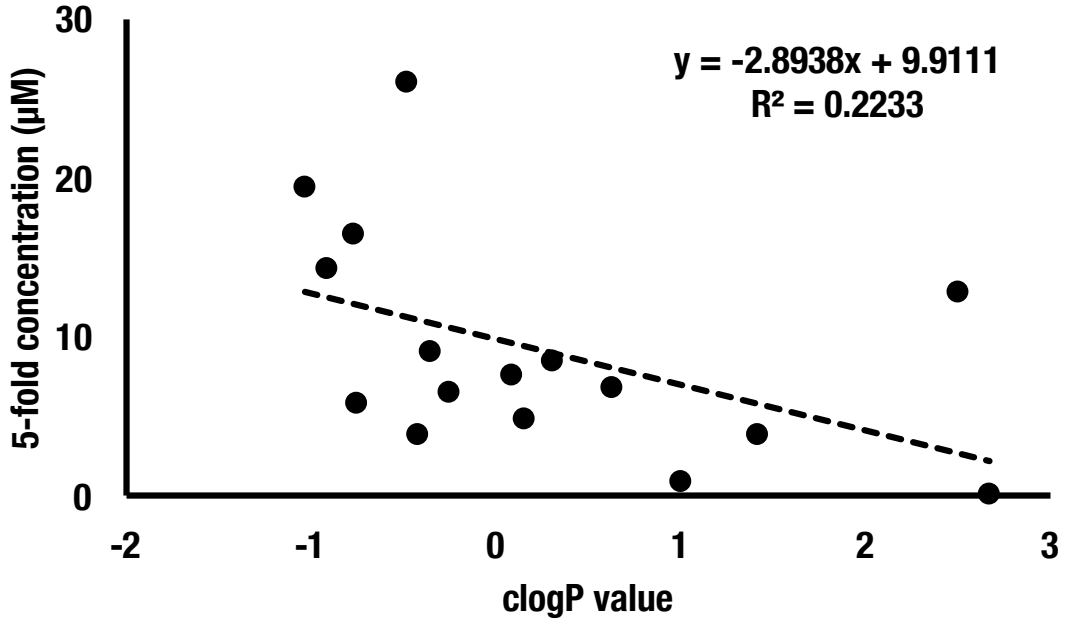

Figure 3-3. Correlation plot between HIF transcriptional activity and lipophilicity of compound **1a**-**1p**. HIF activities were evaluated at concentrations when NLuc activities were 5-fold concentration. Lipophilicity was evaluated at the ClogP values (calculated using Chemdraw). |R| value is 0.47 by calculation from the plots, suggesting that there is a correlation between HIF transcriptional activity and lipophilicity.

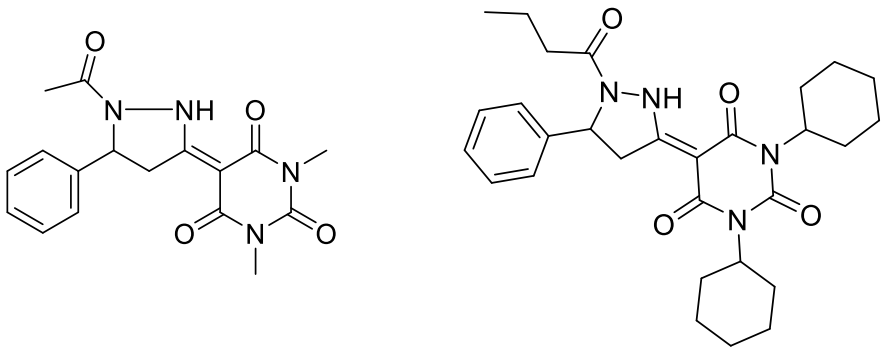

1a, PyrzA **2c, PyrzA-50**

Figure 3-4. The chemical structure of **1a** (PyrzA) and **2c** (PyrzA-50): 5-(1-*n*-Butyryl-5-phenylpyrazolidin-3-ylidene)-1,3-dicyclohexylpyr- imidine-2,4,6(1*H*,3*H*,5*H*)-trione.

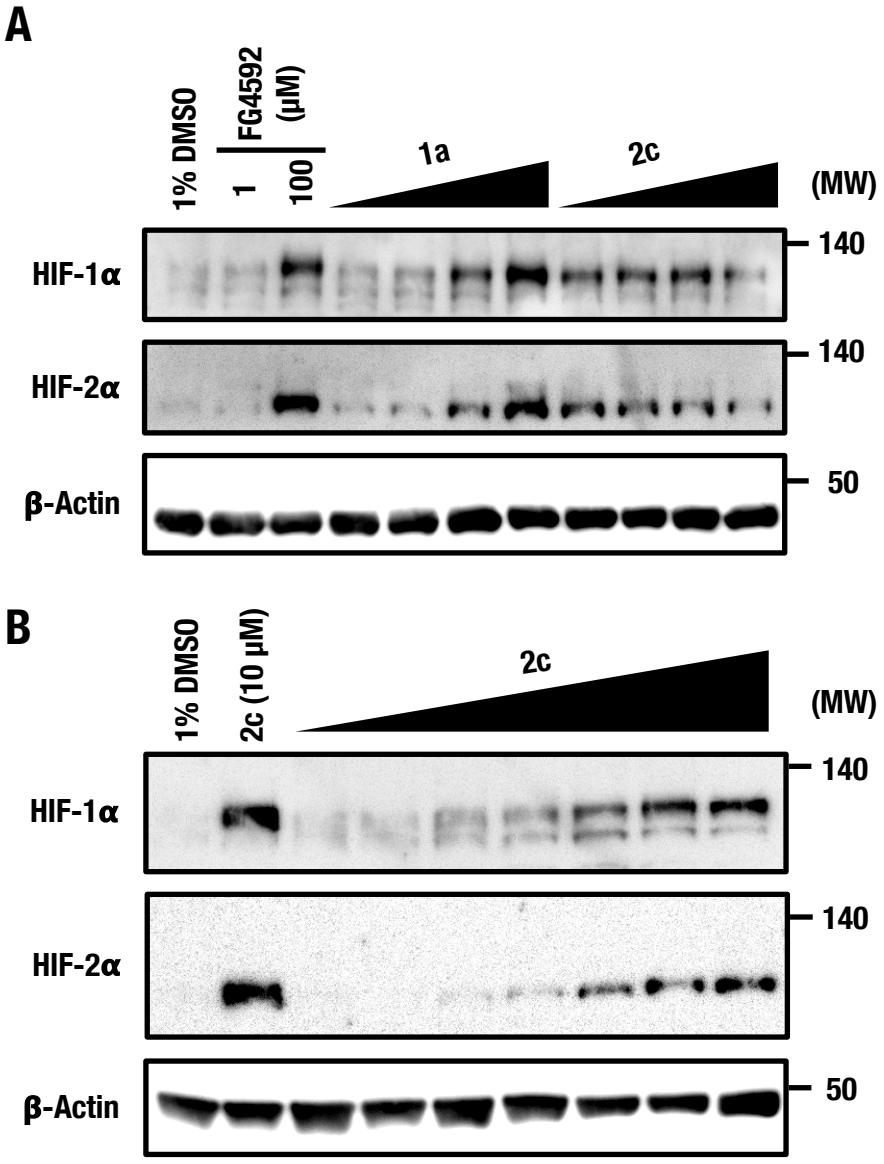

Figure 3-5. Validation of the HIF-α stabilization of the lead compound, **2c**. (A) Immunoblot analyses of HIF-α for various concentrations (1.0, 5.0, 25, and 100 μM) of **2c** and **1a** in Hep3B. Meanwhile, the cells were independently treated with target positive control, FG4592 (100 μM). (B) Immunoblot analyses of HIF-α at low concentrations (15.6, 31.3, 62.5, 125, 250, 500, and 1000 nM) of **2c**. The cells were independently treated with **2c** (10 μM). These experiments were done more than three times, and the results were reproducible. Representative results are presented.

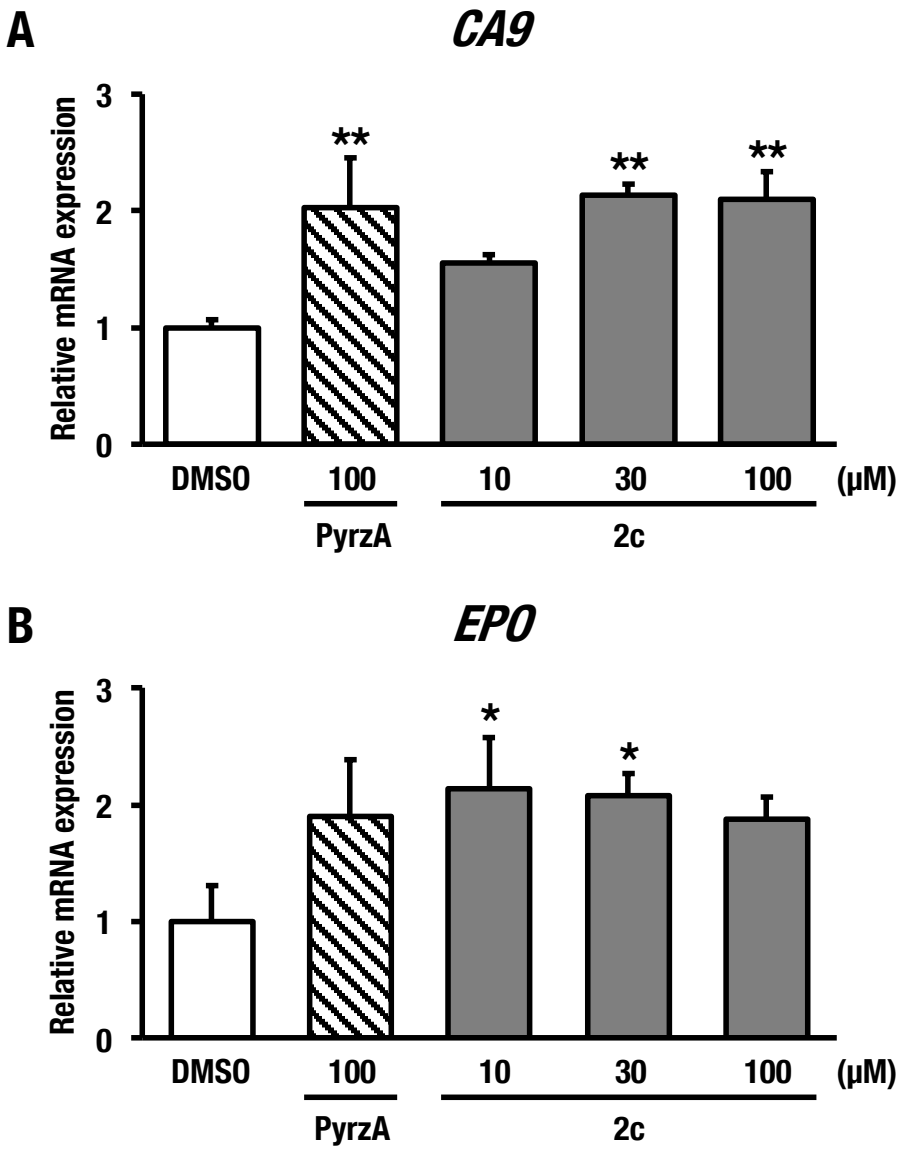

Figure 3-6. Effect of **2c** on HIF target gene regulation. (A, B) The mRNA expression levels of *CA9* and *EPO* were analyzed by RT-qPCR after treatment with **1a** 100 μM or **2c** (10, 30, and 100 μM) for 24 h in Hep3B. 18S rRNA was used as an internal control. Experiments were performed in triplicates. The expression levels in 1% DMSO-treated cells were set as 1.0. *$P < 0.05$, **$P < 0.01$ compared with 1% DMSO (one-way ANOVA with Dunnett's test). All data are expressed as mean ± SEM (n = 3 for each group).

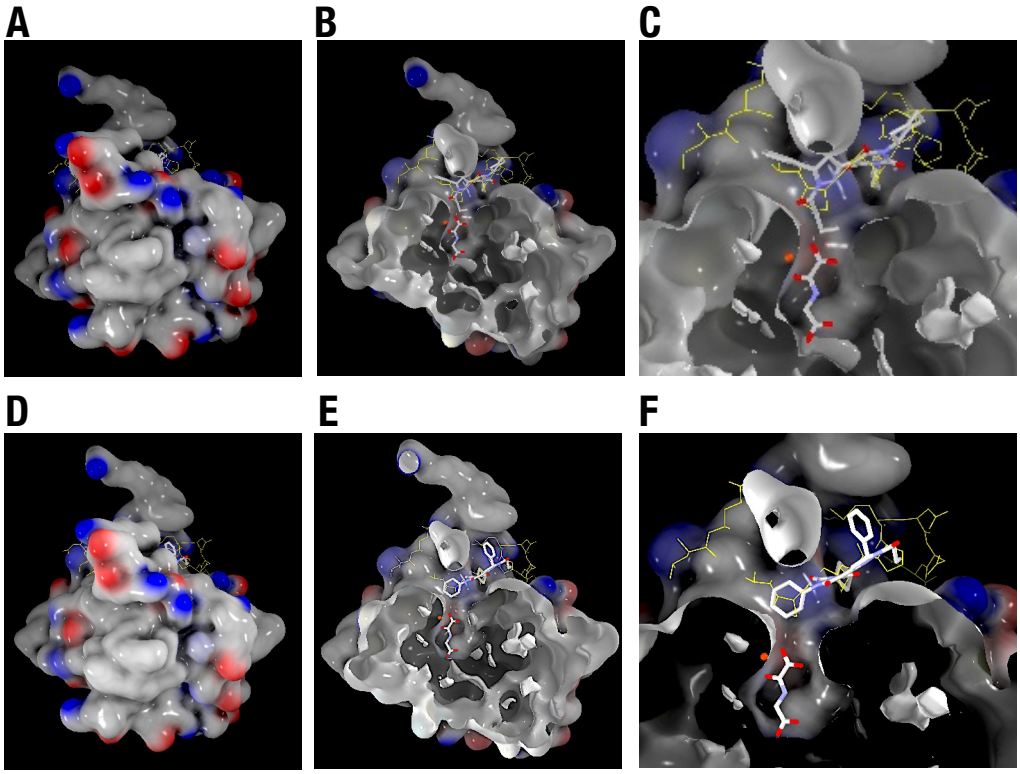

G

Entry	Compound	R/S	Score (MolDock) (kcal/mol)
1	2c	*S*	-112.64
2	2c	*R*	-83.2863

Figure 3-7. Predicted binding model of PHD2 (PDB ID: 3hqr) within **2c**. (A-F) HIF-1α CODD peptide (amino acids number 556–574) (yellow) bound to PHD2; blue corresponds to positive charge and red to negative charge residues. Mn^{2+} (orange) and *N*-oxalylglycine were substitutes for Fe^{2+} and 2-OG, respectively. **2c** and *N*-oxalylglycine were drawn with carbon in white, oxygen in red, and nitrogen in blue. Overall view (A and D). Transverse section of the protein model for visualization of the catalytic site (B and E). Enlarged view of the area around the Pro564 (C and F). Mn^{2+}, 2-OG, (*S*)–**2c**, Pro564, and the specified residues of PHD2 (A-C) and Mn^{2+}, 2-OG, (*R*)–**2c**, Pro564, and the specified residues of PHD2 (D-F). (J) The docking (MolDock) scores of (*S*–or *R*–) **2c** on PHD2 protein as calculated by Molegro Virtual Docker 7.0.0.

Chapter 4

Expression of PHD1 and PHD2 Proteins

4-1. Introduction

In chapter 2, decreasing prolyl-hydroxylated HIF-1α proteins and the docking simulation between PHD2 and PyrzA showed that PyrzA inhibited PHDs. However, how PyrzA inhibits the function of PHDs is unclear. In addition, in terms of that PyrzA mimicked hydroxylation on HIF-α and that PHDs specificity depends on amino acid sequence around the proline reside of HIF-α[127,128], PyrzA derivatives may have specificity for PHD isoforms. It has already been reported that PHD3 hydroxylated CODD but not NODD sequences[128,129].

Furthermore, HIF-α isoforms (HIF-1α and HIF-2α) have the regulation of other HIF target genes. As the result, the expression of HIF-α isoforms has different functions. For example, HIF-1α regulates glucose consumption and glycolysis, while HIF-2α regulates fatty acid storage[10]. However, because most HIF activators are targeted to PHDs, they cannot have HIF isoform specificity. Therefore, the development of HIF-1α or HIF-2α specific activator is required.

In this chapter, to identify the mechanism of PHDs inhibition of PyrzA and discover PyrzA derivatives with PHD isoform specificity, recombinant PHDs proteins produced in *E. coli*., SF21 insect cells or silkworms.

4-2. Experimental section

4-2-1. Reagents

DTT, *o*-phenylenediamine (OPD), catalase, 2-OG, sodium hydroxide, and imidazole were obtained from Fujifilm Wako. Petroleum ether and ferrous chloride were obtained from Katayama chemical (Osaka, Japan). Tris(hydroxymethyl)aminomethane and hydrochloric acid were obtained from Nacalai Tesque. Peptides HIF-1α CODD 17mer was obtained from Thermo Ficher Scientific (Waltham, MA, US). The following antibodies were used. PHD1: anti-HIF Prolyl Hydroxylase 1 (NB100-310) rabbit pAb (Novus Biologicals), PHD2: anti-HIF Prolyl Hydroxylase 2 (NB100-2219) rabbit pAb (Novus Biologicals) PHD3: Rb pAb to PHD3 (ab30782) (Abcam, Cambridge, UK), and β-Actin: Anti β-Actin (PTG9395) mouse mAb (Fujifilm Wako). His: His-Tag (D3I1O) XP rabbit mAb (Cell Signaling Technology) and Anti 6 × Histidine (9C11) mouse mAb (Fujifilm-Wako).

4-2-2. Cell culture

SHuffle Competent *Escherichia coli* (*E. coli*) cells were obtained from New England Biolabs (Ipswich, MA, USA). SF21 cells were obtained from Thermo Ficher Scientific. SHuffle Competent *E. coli* was cultured in LB medium (Nacalai Tesque) containing 30 μg/mL carbenicillin (Nacalai Tesque) at 30°C with shaking. SF21 cells were cultured in Sf-900 II Serum Free Medium (Thermo Ficher Scientific) at 27°C.

4-2-3. Expression of recombinant PHDs proteins in *Escherichia coli* (*E. coli*)

The PHD (1, 2-short, 2-full, 3) fragment cloned into pCold II DNA (Takara Bio, Shiga, Japan) had already been produced. These plasmids were transformed into SHuffle

Competent *E. coli* cells and selected using an ampicillin-resistant gene marker. Expression of recombinant proteins was done using protocol by pCold II DNA. A single colony was grown at 30°C. for 200 rpm till OD_{600} reached 0.4-0.5. At this point, induction of PHDs was done by using 100 μM IPTG and changing the incubation temperature from 37°C to 16°C, and cells were cultured overnight. After incubation, cells were harvested by centrifugation at 4,000 × g for 20 min at 4°C. These pellets were lysed in lysis buffer (50 mM Tris-HCl, pH 8.0, 300 mM sodium chloride, 10 mM imidazole), sonicated and centrifuged at 10,000 × g for 30 min at 4°C. After centrifugation, samples were divided into supernatant samples (Sup.) and precipitate samples (Ppt.) and purified Ni-NTA resin (Qiagen, Hilden, Germany) using following the manufacturer's instructions. Finally, samples were subjected to immunoblot analyses with anti-His antibodies.

4-2-4. Expression of recombinant PHDs proteins in SF21

The PHD1-3 fragment cloned into pFastBac1 (Thermo Ficher Scientific) had already been produced. These vectors were transformed into *E. coli* DH10Bac competent cells (Thermo Ficher Scientific) to generate recombinant bacmids selected using gentamicin-, kanamycin-, and tetracycline-resistant gene maker and LacZ gene maker. After selection, the insertion of the target genes was confirmed using PCR. Several 1 μg of validated bacmids were transfected into Sf21 cells (1.6×10^6 cells/well) seeded into a 6-well plate (Corning) using transfection regent (uniFECTOR, B-Bridge International, Santa Clara, CA, USA). 3 days post-transfection, those cell medium were harvested, which were defined as the first passage1 (P1) of recombinant baculoviruses, and cell debris was subjected to immunoblot analyses with anti-His antibodies.

4-2-5. Expression of recombinant PHDs proteins in *Bombyx mori* (silkworm)

The codon-optimized PHD1 and 2 for silkworms were designed and inserted into pBV-6 × His/recombinant PHD1 or 2. Those vectors were obtained from Vectorbuilder (Chicago, IL, USA). These vectors were transformed into *E. coli* BmDH10Bac competent cells (originally made by Dr. Katsumi Maenaka, Hokkaido University Japan, obtained from Tadato Ban, Kurume University, Japan) to generate recombinant bacmids. Selection and confirmation of bacmids were performed as described in 4-2-4. Several 1 μg/worm of validated bacmids were transfected into silkworm (*B. mori*) (15 larvae) at the fifth larval instar using transfection regent (DMRIE-C, Thermo Ficher Scientific). 6 days post-transfection, their fat bodies were harvested, homogenized, sonicated, and centrifuged at 500 × g for 10 min at 4°C. After removing fat and pellet, supernatant lysis samples (T: total) were also centrifuged at 15,000 × g for 60 min at 4°C. After centrifuged, supernatant samples (Sup.) and precipitate samples (Ppt.) were harvested. Those samples were subjected to immunoblot analyses with anti-His, anti-PHD1, and anti-PHD2 antibodies.

4-2-6. Immunoblot assay

Immunoblot was performed as described in 2-2-7.

4-2-7. PHD enzyme assay

PHD enzyme assay was performed in the previous paper[130]. OPD was recrystallized from petroleum ether before this assay. The assay of 2-OG concentration was carried out by mixing 1 mM DTT, 0.6 mg/ml catalase, various 2-OG concentrations,60 μM peptides HIF-1α CODD, and 50 mM Tris/HCl, pH 7.5, to a final volume of 44 μL and incubation at 37°C for 5 min. Concurrently, ferrous chloride was mixed at room temperature for 3min.

(In the future, recombinant PHDs protein was also mixed). The PHD enzyme reaction was initiated by the addition of 6 μL of enzyme mixture to 44 μL of the substrate mixture. The enzyme reaction was stopped after 5 min by the addition of 100 μL 0.5 M hydrochloric acid. Then, samples were added 50 μL of 10 mg/mL OPD in 0.5 M hydrochloric acid heated at 95°C for 10 min to create the fluoresce derivative. After centrifugation for 5 min, 50 μL of the supernatant was mixed with 30 μL of 1.25 M sodium hydroxide to increase fluorescence intensity. The fluorescence was measured by SpectraMax i3x (Molecular Devices) with the excitation filter at 340 nm and the emission filter at 420 nm.

4-3. Result

4-3-1. *E. coli* expression system was not fit to produce recombinant PHDs proteins

Recombinant PHD1-3 proteins expression was attempted in SHuffle *Escherichia coli* instead of BL21. First, pCold II DNA cloned human PHD 1, short PHD2, full PHD2, and PHD3 genes were transformed into SHuffle Competent *Escherichia coli*. After colony selection, cells were cultured, and expression samples (S) were only induced by IPTG and incubation at low temperature. The negative control samples (NC) were cultured without any stimulation. After harvested and centrifuged, cells were divided into supernatant samples (Sup.) and precipitate samples (Ppt.).

Because those recombinant PHD proteins have N-terminal 6 × Histidine (His) tag, the expression was confirmed using immunoblot analysis. These were evaluated via immunoblot analysis using antibodies for His tag (Figure 4-1). Importantly, the bands of His tag were observed from the precipitate samples of the negative control. In addition, while the designed recombinant PHD1 and full PHD2 protein were observed at the

molecular weight of 48 K and 43 K, respectively. Their bands were existed smaller than expected. Those results suggested that detected bands were non-specific bands and recombinant PHD1-3 proteins failed to express in SHuffle *Escherichia coli*.

4-3-2. Recombinant PHDs proteins could expressed in insect cell expression system

The expression of recombinant PHD1-3 proteins was attempted in the baculovirus system in SF21. Validated PHD2 and PHD3 bacmids were transfected into Sf21 cells. Three days post-transfection, cell debris was harvested. PHD1 bacmid was produced but not validated. Because those recombinant PHD proteins have N-terminal His tags, the expression was confirmed using immunoblot analysis. The results showed recombinant PHD2 not PHD3 protein was expressed in SF21 cells (Figure 4-2). The supernatant of transfected Sf21 cells was harvested and stocked at the virus stock of the first passage1 (P1).

4-3-3. Recombinant PHDs proteins could expressed in silkworms

The expression of recombinant PHD1 and PHD2 proteins was attempted in the baculovirus system in silkworms. Validated PHD1 and PHD2 bacmids were transfected into the fifth larval instar. 6 days post-transfection, their fat bodies were harvested. After centrifuged, supernatant samples (Sup.) and precipitate samples (Ppt.) were harvested. The expression was confirmed using immunoblot analysis with His tag, PHD1 and PHD2 antibodies. The results showed recombinant PHD1 and PHD2 proteins expressed in the supernatant samples of silkworms (Figure 4-3). Furthermore, since recombinant PHD1

and PHD2 proteins in silkworms produced a lot, the purification of PHD1 and PHD2 will use these samples.

4-3-4. Establish the PHD enzyme assay system

PHD enzyme assays have been reported in several ways: tracking the concentration of 2-OG, CO_2, or succinate (production of PHD reaction), detecting hydroxylated HIF-α, or using *in vitro* HIF-PHD2 assay[131,132]. However, most assays require complex methods or equipment such as mass spectrometry, radioactive experimental, or *in vitro* HIF-PHD2 assay. Therefore, *in vitr*o hydroxylation assay of the chemical derivatization of 2-OG by *o*-phenylenediamine (OPD) to generate a fluorescent derivative was performed[129–131]. The reaction between OPD and 2OG obtained the fluorescent product 3-(2-carboxyethyl)-2(1*H*)-quinoxalinone (**1**) (Figure 4-4A). Before PHD enzyme assay, fluorescence with several 2-OG concentrations was linear up to 600 μM (Figure 4-4B). As a next step, pacificated recombinant PHD1 and PHD2 will be analyzed for their properties like K_m values.

4-4. Discussion

Recombinant PHDs proteins were expressed in several manners. The expression of those proteins was validated by immunoblot assay. As a result, recombinant PHDs proteins production in SHuffle *E. coli*. was difficult. On the other hand, the baculovirus system enables PHDs protein production. Among the baculoviruses, more proteins were expressed by silkworms than by insect cells when comparing expression in insect cells and silkworms. As the next step, a high yield purification method will be conducted in silkworms. Codon-optimized genes for silkworms were used for the expression of

recombinant proteins in silkworms. In the future, recombinant PHDs proteins in baculovirus will be used for PHD enzyme assay and crystal structure analysis of PHDs and PyrzA.

PHD enzyme assay generating **1** showed that 2-OG concentration in the reaction solution could be monitored. On the other hand, other PHD enzyme assay methods require complex methods or equipment. For example, detecting consuming CO_2 or producing succinate assay needs ^{14}C, which was used for a radiolabeled 2-OG[131]. Detecting prolyl-hydroxylated HIF-α needs a liquid chromatography mass spectrometry (LC/MS)[131]. *In vitro* HIF-PHD2 assay needs to produce VHL complex[131,133]. Recently, a colorimetric 2-OG detecting method was developed by Wong, S. J. *et al*[132]. However, since spectrofluorimetric assays are more sensitive than colorimetric assays, PHD enzyme assay generating **1** was performed.

In the future, this assay will be used several experiments: (1) confirmation of activity of recombinant PHDs proteins, (2) enzyme kinetics of PHDs, (3) development of PyrzA derivatives which have a specificity of PHD isoforms, (4) confirmation of activity of other 2-OG oxygenases. Especially with regard to (4), since this PHD enzyme assay monitors 2-OG concentration, it can be applied to other 2-OG oxygenases.

Furthermore, after the expression and purification of PHDs proteins, PyrzA can be analyzed as follows. (1) Identification of the inhibition mechanism of PHDs by PyrzA using X-ray crystallographic analysis. PyrzA has the potential to bind PHD at non-catalytic sites, and crystallographic data can demonstrate this view. As an alternative the interaction between PHDs and PyrzA such as hydrogen bonds of Fe^{2+} or PHD amin acid residue be analyzed using NMR or ESR. (2) Development of PHD isoform specific inhibitors or HIF-α isoform specific activators. The reasons for this are main PHIs cannot

distinguish the specificity for PHDs or HIF-α isoforms. In addition, the efficacy of inhibition of isoform specificity of them are proposed in the treatment of various diseases. In this study will plan to synthesize its derivatives and evaluate PHDs or HIF-α isoform specificity using docking simulation based on crystallographic analysis and PHD enzyme assay. Those data will provide insight into the concept a novel mechanism of PHD inhibitor which does not mimic 2-OG.

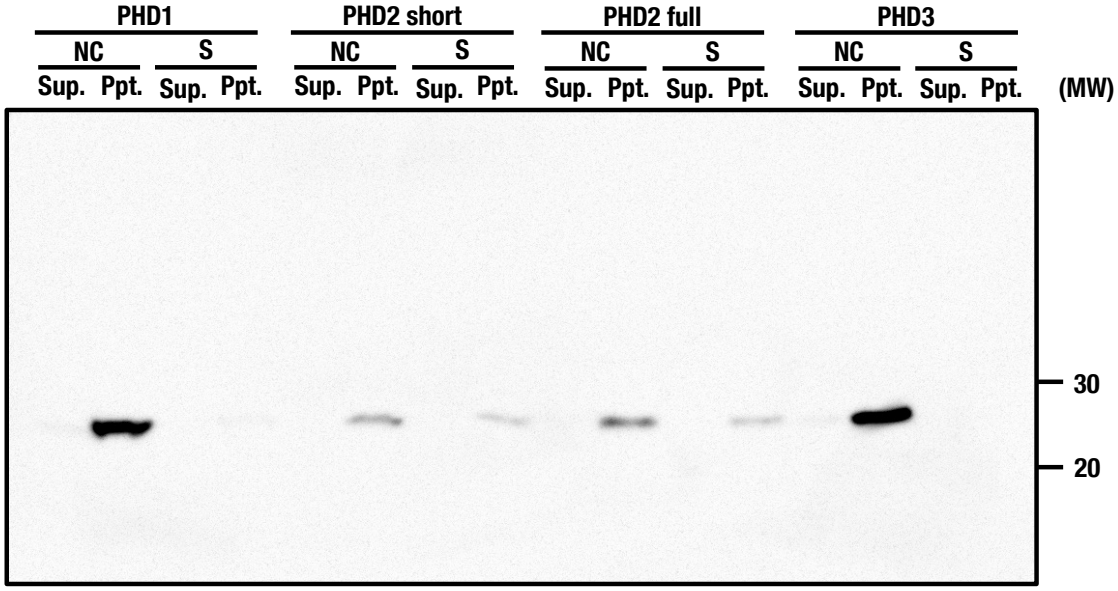

Figure 4-1. Recombinant PHD1-3 proteins were not produced in *E. coli*. *E. coli* was cultured in LB buffer and only samples (S) were changed incubation temperatures to induce the target proteins. Negative control (NC) was cultured at the same temperature. Then, these cells were lysed and sonicated. Sonicated samples were divided into supernatant samples (Sup.) and precipitate samples (Ppt.). Samples were subjected to immunoblot analyses with anti-His antibodies. Bands of PHD1 and full PHD2 are seen at ~50 K and short PHD2 and PHD3 are seen at ~30 K.

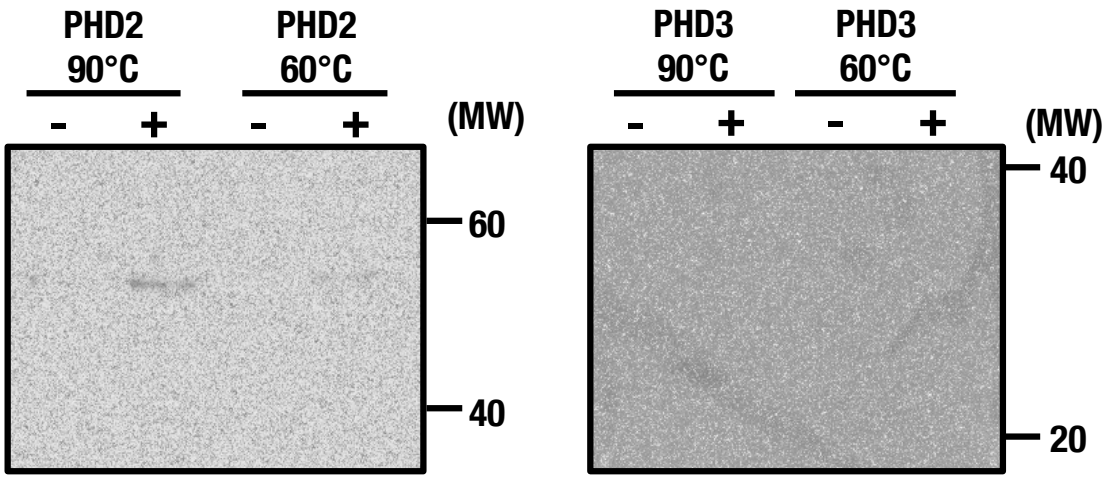

Figure 4-2. Recombinant PHD2 protein was expressed in SF21 cells. Recombinant PHD1 and 2 bacmids were transfected into SF21 cells and transfected SF21 cells were incubated at 72 h. 72 h after their supernatant was obtained the P1 viral stocks and cells were lysed. Cell lysis samples were subjected to immunoblot analyses with anti-His antibodies. Bands of PHD2 and PHD3 are seen at ~48 K and ~27 K, respectively.

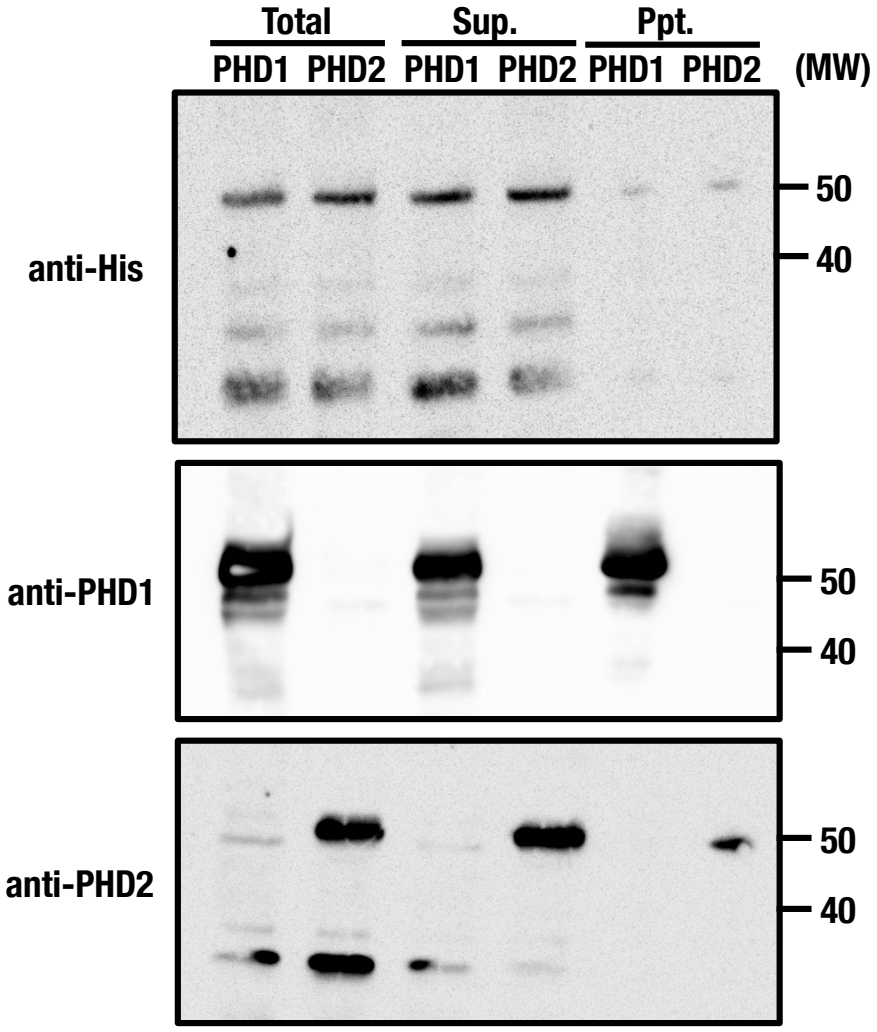

Figure 4-3. Recombinant PHD1 and 2 proteins were expressed in silkworms. 6 days after inoculation of recombinant PHD1 and 2 bacmids into silkworms, silkworm larvae were harvested in fat bodies, homogenized, and centrifuged at 500 × g for 10 min at 4°C. Supernatant lysis samples (Total) were also centrifuged at 15,000 × g for 60 min at 4°C. After centrifuged, supernatant samples (Sup.) and precipitate samples (Ppt.) were harvested. Those samples were subjected to immunoblot analyses with anti-His, anti-PHD1, and anti-PHD2 antibodies. Odd numbers' lanes and even numbers' lanes showed PHD1 and PHD2 protein, respectively.

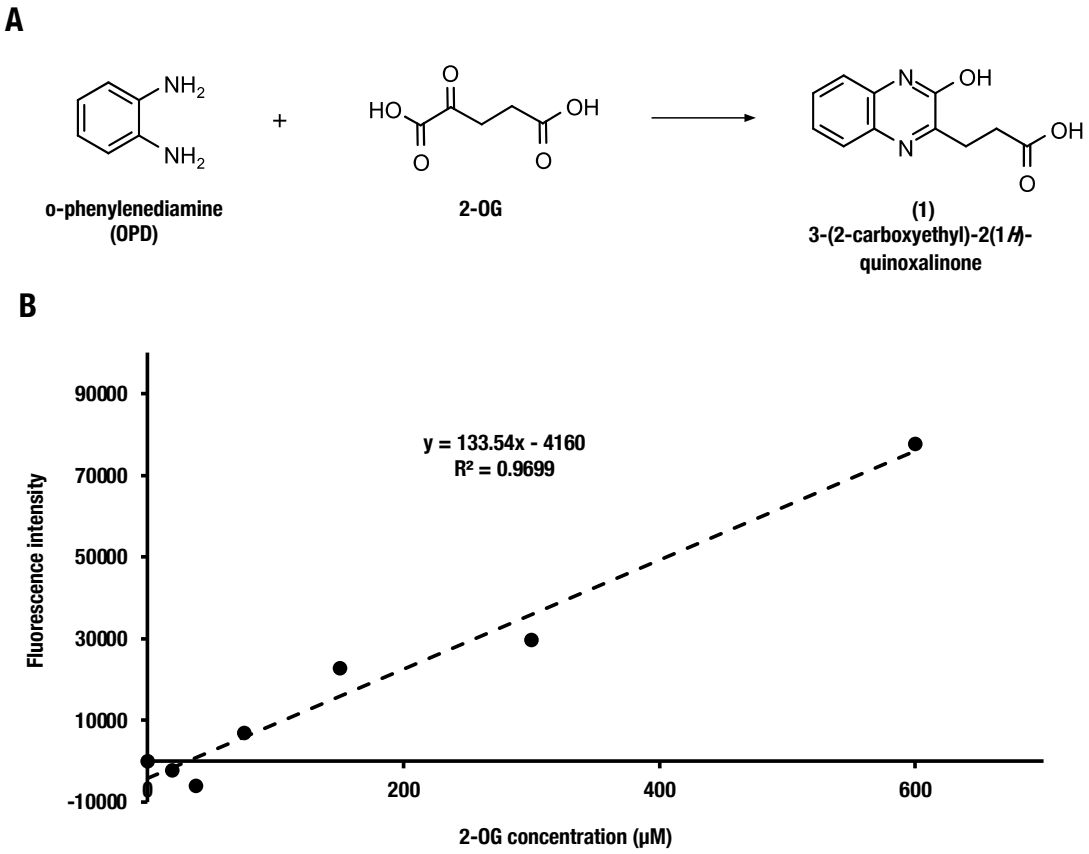

Figure 4-4. The reaction of OPD with varying 2-OG concentrations showed linearity of response. (A) Reaction of OPD with 2OG to form 3-(2-carboxyethyl)-2(1*H*)-quinoxalinone (**1**). (B) Reaction of various concentrations of 2-OG with 10 mg/mL OPD. After the reaction, fluorescence intensity (**1**) was measured.

Chapter 5

General Discussion

PHIs have been developed as therapeutic compounds for renal anemia associated with CKD. Although several papers reported that PHIs or PHD deletion was organ-protective effect[105–107], PHIs have not been approved for the treatment of the ischemic injury. One of the problems is that the upregulation of HIF-α induces inflammation and inhibits organ protection in myeloid and monocyte cells during ischemic tissue injury[134,135]. However, another problem is that PHIs focus on only increasing plasma EPO concentration. Increasing EPO and hemoglobin level has a risk for thromboembolic events which cause stroke, myocardial infarction, and pulmonary embolism[136–138]. Therefore, the development of HIF activators which have the specificity of the organ has been needed. HIF activators also require the high specificity of other enzymes. 2-OG analogs are concerned about side effects on other 2-OG oxygenases such as FIH or JMJD family histone demethylases. Therefore, a novel HIF activator which does not harbor a 2-OG scaffold and have the high specificity for other proteins require.

In this thesis, the biochemical and biophysics properties of a novel PHD inhibitor, PyrzA, which does not harbor a 2-OG scaffold have been investigated and its derivatives with more potent HIF activity have been developed. Their important results are concluded as follows:

Chapter 2 described the effects of administering PyrzA under normoxic condition. The efficacy of PyrzA as a HIF-α transcriptional activity was comparable to that of DMOG and cytotoxicity was low using HIF reporter cells. PyrzA not only stabilized HIF-1α and HIF-2α proteins in several cells but also upregulated HIF target genes including *EPO* and

CA9 in Hep3B cells. PyrzA also upregulated HIF target genes in kidney or liver of six-week-old female C57B6 mice. Those results showed PyrzA activated HIF signaling cascade *in vitro* and *in vivo*. In the future, highly active PyrzA derivatives will be synthesized by examining the effects of PyrzA absorption and metabolism. In addition, the effects such as brain or heart on other organs need to be examined considering the treatment of ischemic diseases.

Chapter 2 also described PyrzA inhibited the prolyl hydroxylation of HIF-1α in SK-N-BE(2)c and HeLa cells. PyrzA mimicked hydroxylation on HIF-α prolyl residues instead of 2-OG using docking simulation between PHD2. Those results showed that PyrzA was inhibited PHDs non-competitively. PHIs which are targeted by a 2-OG scaffold was hardly reported while novel types of HIF activators are required. These results suggest that PyrzA binds to PHDs simultaneously with 2-OG analog and that cooperative binding of PyrzA and 2-OG analog may synergically inhibit PHDs. In this study, it is important to develop PyrzA derivatives with high molecular selectivity and few side effects.

Chapter 3 described the selection of potent HIF activity from a total of 22 PyrzA derivatives. HIF transcriptional activities and cellular viabilities were evaluated from 22 PyrzA derivatives which belong to group A: 16 derivatives with replaced phenyl and acetyl groups and group B: 6 derivatives with replaced acetyl and methyl groups. Lipophilic PyrzA derivatives especially group B were more HIF-α transcriptional activity than PyrzA. Finally, **2c**, which is approximately 30-fold more potent than PyrzA, and has lower cytotoxicity, was found. **2c** also stabilized HIF-α proteins and upregulated *CA9* and *EPO* at lower concentrations than PyrzA in Hep3B. Since **2c** improves cellular absorption, the next step is to examine the effects of **2c** *in vivo*.

Chapter 4 described PHDs recombinant proteins in baculovirus produced and PHDs enzyme assay was prepared. Recombinant PHD 1 and PHD2 proteins were expressed in silkworms and were confirmed using immunoblot analysis. In the future, this study aims to identify the inhibition mechanism of PHDs by PyrzA using X-ray crystallographic analysis and develop PHD isoform specific inhibitors or HIF-α isoform specific activators. Crystallographic analysis data will help us to understand the interaction between PHDs and PyrzA as well as to design novel PyrzA derivatives to improve HIF activity or to have PHDs or HIF-α isoform specificity using docking simulations.

In this way, this thesis clarified the biochemical characterization of PyrzA and demonstrated the finding of **2c**, which was a more potent PyrzA derivative. The author believes that the present study will contribute to understanding under hypoxia condition.

Acknowledgment

I would like to express my deepest gratitude to Shin-ich Kawaguchi and Tadayuki Tsujita for their kind guidance and helpful discussion.

I would like to appreciate Masaharu Komatsu also for his helpful discussion and suggestions.

I would like to appreciate Susumu Mitsutake and Kozue Sakao also for reviewing this thesis.

I am grateful to Shin-ich Kawaguchi and his research member and Tadato Ban and his research group members for providing me with experimental materials and kind guidance.

I would like to genuinely thank the members in Laboratory of Biochemistry, and Center for Education and Research in Agricultural Innovation, Faculty of Agriculture, Saga University.

Finally, I would also like to express my thanks to my family for their understanding and warm support.

Reference

(1) Semenza, G. L. Oxygen Sensing, Homeostasis, and Disease. *N. Engl. J. Med.* **2011**, *365* (6), 537–547. https://doi.org/10.1056/NEJMra1011165

(2) Fraisl, P.; Aragonés, J.; Carmeliet, P. Inhibition of Oxygen Sensors as a Therapeutic Strategy for Ischaemic and Inflammatory Disease. *Nat. Rev. Drug Discov.* **2009**, *8* (2), 139–152. https://doi.org/10.1038/nrd2761

(3) Venkatachalam, M. A.; Griffin, K. A.; Lan, R.; Geng, H.; Saikumar, P.; Bidani, A. K. Acute Kidney Injury: A Springboard for Progression in Chronic Kidney Disease. *Am. J. Physiol. - Ren. Physiol.* **2010**, *298* (5), 1078–1094. https://doi.org/10.1152/ajprenal.00017.2010

(4) Semenza, G. L.; Wang, G. L. A Nuclear Factor Induced by Hypoxia via de Novo Protein Synthesis Binds to the Human Erythropoietin Gene Enhancer at a Site Required for Transcriptional Activation. *Mol. Cell. Biol.* **1992**, *12* (12), 5447–5454. https://doi.org/10.1128/mcb.12.12.5447-5454.1992

(5) Wang, G. L.; Semenza, G. L. General Involvement of Hypoxia-Inducible Factor 1 in Transcriptional Response to Hypoxia. *Proc. Natl. Acad. Sci. U. S. A.* **1993**, *90* (9), 4304–4308. https://doi.org/10.1073/pnas.90.9.4304

(6) Weidemann, A.; Johnson, R. S. Biology of HIF-1α. *Cell Death Differ.* **2008**, *15* (4), 621–627. https://doi.org/10.1038/cdd.2008.12

(7) Wang, G. L.; Jiang, B. H.; Rue, E. A.; Semenza, G. L. Hypoxia-Inducible Factor 1 Is a Basic-Helix-Loop-Helix-PAS Heterodimer Regulated by Cellular O2 Tension. *Proc. Natl. Acad. Sci. U. S. A.* **1995**, *92* (12), 5510–5514. https://doi.org/10.1073/pnas.92.12.5510

(8) Wang, G. L.; Semenza, G. L. Purification and Characterization of Hypoxia-

Inducible Factor 1. *J. Biol. Chem.* **1995**, *270* (3), 1230–1237. https://doi.org/10.1074/jbc.270.3.1230

(9) Kimura, H.; Weisz, A.; Ogura, T.; Hitomi, Y.; Kurashima, Y.; Hashimoto, K.; D'Acquisto, F.; Makuuchi, M.; Esumi, H. Identification of Hypoxia-Inducible Factor 1 Ancillary Sequence and Its Function in Vascular Endothelial Growth Factor Gene Induction by Hypoxia and Nitric Oxide. *J. Biol. Chem.* **2001**, *276* (3), 2292–2298. https://doi.org/10.1074/jbc.M008398200

(10) Majmundar, A. J.; Wong, W. J.; Simon, M. C. Hypoxia-Inducible Factors and the Response to Hypoxic Stress. *Mol. Cell* **2010**, *40* (2), 294–309. https://doi.org/10.1016/j.molcel.2010.09.022

(11) Shweiki, D.; Itin, A.; Soffer, D.; Keshet, E. Vascular Endothelial Growth Factor Induced by Hypoxia May Mediate Hypoxia-Induced Angiogenesis. *Nature* **1992**, *359*, 843–845. https://doi.org/10.1038/359843a0

(12) Carmeliet, P.; Dor, Y.; Herber, J. M.; Fukumura, D.; Brusselmans, K.; Dewerchin, M.; Neeman, M.; Bono, F.; Abramovitch, R.; Maxwell, P.; Koch, C. J.; Ratcliffe, P.; Moons, L.; Jain, R. K.; Collen, D.; Keshet, E. Role of HIF-1α in Hypoxia-Mediated Apoptosis, Cell Proliferation and Tumour Angiogenesis. *Nature* **1998**, *394*, 485–490. https://doi.org/10.1038/28867

(13) Matsumoto, M.; Makino, Y.; Tanaka, T.; Tanaka, H.; Ishizaka, N.; Noiri, E.; Fujita, T.; Nangaku, M. Induction of Renoprotective Gene Expression by Cobalt Ameliorates Ischemic Injury of the Kidney in Rats. *J. Am. Soc. Nephrol.* **2003**, *14* (7), 1825–1832. https://doi.org/10.1097/01.ASN.0000074239.22357.06

(14) Kamba, T.; McDonald, D. M. Mechanisms of Adverse Effects of Anti-VEGF Therapy for Cancer. *Br. J. Cancer* **2007**, *96* (12), 1788–1795. https://doi.org/

10.1038/sj.bjc.6603813

(15) Kaelin, W. G.; Ratcliffe, P. J. Oxygen Sensing by Metazoans: The Central Role of the HIF Hydroxylase Pathway. *Mol. Cell* **2008**, *30* (4), 393–402. https://doi.org/10.1016/j.molcel.2008.04.009

(16) Bruick, R. K. Oxygen Sensing in the Hypoxic Response Pathway: Regulation of the Hypoxia-Inducible Transcription Factor. *Genes Dev.* **2003**, *17* (21), 2614–2623. https://doi.org/10.1101/gad.1145503

(17) Berra, E.; Benizri, E.; Ginouvès, A.; Volmat, V.; Roux, D.; Pouysségur, J. HIF Prolyl-Hydroxylase 2 Is the Key Oxygen Sensor Setting Low Steady-State Levels of HIF-1α in Normoxia. *EMBO J.* **2003**, *22* (16), 4082–4090. https://doi.org/10.1093/emboj/cdg392

(18) McDonough, M. A.; Li, V.; Flashman, E.; Chowdhury, R.; Mohr, C.; Liénard, B. M. R.; Zondlo, J.; Oldham, N. J.; Clifton, I. J.; Lewis, J.; McNeill, L. A.; Kurzeja, R. J. M.; Hewitson, K. S.; Yang, E.; Jordan, S.; Syed, R. S.; Schofield, C. J. Cellular Oxygen Sensing: Crystal Structure of Hypoxia-Inducible Factor Prolyl Hydroxylase (PHD2). *Proc. Natl. Acad. Sci. U. S. A.* **2006**, *103* (26), 9814–9819. https://doi.org/10.1073/pnas.0601283103

(19) Fong, G. H.; Takeda, K. Role and Regulation of Prolyl Hydroxylase Domain Proteins. *Cell Death Differ.* **2008**, *15* (4), 635–641. https://doi.org/10.1038/cdd.2008.10

(20) Chowdhury, R.; McDonough, M. A.; Mecinović, J.; Loenarz, C.; Flashman, E.; Hewitson, K. S.; Domene, C.; Schofield, C. J. Structural Basis for Binding of Hypoxia-Inducible Factor to the Oxygen-Sensing Prolyl Hydroxylases. *Structure* **2009**, *17* (7), 981–989. https://doi.org/10.1016/j.str.2009.06.002

(21) Rabinowitz, M. H. Inhibition of Hypoxia-Inducible Factor Prolyl Hydroxylase Domain Oxygen Sensors: Tricking the Body into Mounting Orchestrated Survival and Repair Responses. *J. Med. Chem.* **2013**, *56* (23), 9369–9402. https://doi.org/10.1021/jm400386j

(22) Koury, M. J.; Haase, V. H. Anaemia in Kidney Disease: Harnessing Hypoxia Responses for Therapy. *Nat. Rev. Nephrol.* **2015**, *11* (7), 394–410. https://doi.org/10.1038/nrneph.2015.82

(23) Chan, M. C.; Holt-Martyn, J. P.; Schofield, C. J.; Ratcliffe, P. J. Pharmacological Targeting of the HIF Hydroxylases - A New Field in Medicine Development. *Mol. Aspects Med.* **2016**, *47–48*, 54–75. https://doi.org/10.1016/j.mam.2016.01.001

(24) Yeh, T. L.; Leissing, T. M.; Abboud, M. I.; Thinnes, C. C.; Atasoylu, O.; Holt-Martyn, J. P.; Zhang, D.; Tumber, A.; Lippl, K.; Lohans, C. T.; Leung, I. K. H.; Morcrette, H.; Clifton, I. J.; Claridge, T. D. W.; Kawamura, A.; Flashman, E.; Lu, X.; Ratcliffe, P. J.; Chowdhury, R.; Pugh, C. W.; Schofield, C. J. Molecular and Cellular Mechanisms of HIF Prolyl Hydroxylase Inhibitors in Clinical Trials. *Chem. Sci.* **2017**, *8* (11), 7651–7668. https://doi.org/10.1039/c7sc02103h

(25) Rose, N. R.; McDonough, M. A.; King, O. N. F.; Kawamura, A.; Schofield, C. J. Inhibition of 2-Oxoglutarate Dependent Oxygenases. *Chem. Soc. Rev.* **2011**, *40* (8), 4364–4397. https://doi.org/10.1039/c0cs00203h

(26) Rankin, E. B.; Rha, J.; Unger, T. L.; Wu, C. H.; Shutt, H. P.; Johnson, R. S.; Simon, M. C.; Keith, B.; Haase, V. H. Hypoxia-Inducible Factor-2 Regulates Vascular Tumorigenesis in Mice. *Oncogene* **2008**, *27* (40), 5354–5358. https://doi.org/10.1038/onc.2008.160

(27) Minamishima, Y. A.; Moslehi, J.; Bardeesy, N.; Cullen, D.; Bronson, R. T.; Kaelin,

W. G. Somatic Inactivation of the PHD2 Prolyl Hydroxylase Causes Polycythemia and Congestive Heart Failure. *Blood* **2008**, *111* (6), 3236–3244. https://doi.org/10.1182/blood-2007-10-117812

(28) Gordan, J. D.; Lal, P.; Dondeti, V. R.; Letrero, R.; Parekh, K. N.; Oquendo, C. E.; Greenberg, R. A.; Flaherty, K. T.; Rathmell, W. K.; Keith, B.; Simon, M. C.; Nathanson, K. L. HIF-α Effects on c-Myc Distinguish Two Subtypes of Sporadic VHL-Deficient Clear Cell Renal Carcinoma. *Cancer Cell* **2008**, *14* (6), 435–446. https://doi.org/10.1016/j.ccr.2008.10.016

(29) Takeda, K.; Ho, V. C.; Takeda, H.; Duan, L. J.; Nagy, A.; Fong, G. H. Placental but Not Heart Defects Are Associated with Elevated Hypoxia-Inducible Factor α Levels in Mice Lacking Prolyl Hydroxylase Domain Protein 2. *Mol. Cell. Biol.* **2006**, *26* (22), 8336–8346. https://doi.org/10.1128/mcb.00425-06

(30) Tojo, Y.; Sekine, H.; Hirano, I.; Pan, X.; Souma, T.; Tsujita, T.; Kawaguchi, S-i.; Takeda, N.; Takeda, K.; Fong, G. H.; Dan, T.; Ichinose, M.; Miyata, T.; Yamamoto, M.; Suzuki, N. Hypoxia Signaling Cascade for Erythropoietin Production in Hepatocytes. *Mol. Cell. Biol.* **2015**, *35* (15), 2658–2672. https://doi.org/10.1128/mcb.00161-15

(31) Souma, T.; Nezu, M.; Nakano, D.; Yamazaki, S.; Hirano, I.; Sekine, H.; Dan, T.; Takeda, K.; Fong, G. H.; Nishiyama, A.; Ito, S.; Miyata, T.; Yamamoto, M.; Suzuki, N. Erythropoietin Synthesis in Renal Myofibroblasts Is Restored by Activation of Hypoxia Signaling. *J. Am. Soc. Nephrol.* **2016**, *27* (2), 428–438. https://doi.org/10.1681/ASN.2014121184

(32) Köditz, J.; Nesper, J.; Wottawa, M.; Stiehl, D. P.; Camenisch, G.; Franke, C.; Myllyharju, J.; Wenger, R. H.; Katschinski, D. M. Oxygen-Dependent ATF-4

Stability Is Mediated by the PHD3 Oxygen Sensor. *Blood* **2007**, *110* (10), 3610–3617. https://doi.org/10.1182/blood-2007-06-094441

(33) Ullah, K.; Rosendahl, A. H.; Izzi, V.; Bergmann, U.; Pihlajaniemi, T.; Mäki, J. M.; Myllyharju, J. Hypoxia-Inducible Factor Prolyl-4-Hydroxylase-1 Is a Convergent Point in the Reciprocal Negative Regulation of NF-KB and P53 Signaling Pathways. *Sci. Rep.* **2017**, *7*, 17220. https://doi.org/10.1038/s41598-017-17376-0

(34) Hiwatashi, Y.; Kanno, K.; Takasaki, C.; Goryo, K.; Sato, T.; Torii, S.; Sogawa, K.; Yasumoto, K-i. PHD1 Interacts with ATF4 and Negatively Regulates Its Transcriptional Activity without Prolyl Hydroxylation. *Exp. Cell Res.* **2011**, *317* (20), 2789–2799. https://doi.org/10.1016/j.yexcr.2011.09.005

(35) Deschoemaeker, S.; Di Conza, G.; Lilla, S.; Martín-Pérez, R.; Mennerich, D.; Boon, L.; Hendrikx, S.; Maddocks, O. D.; Marx, C.; Radhakrishnan, P.; Prenen, H.; Schneider, M.; Myllyharju, J.; Kietzmann, T.; Vousden, K. H.; Zanivan, S.; Mazzone, M. PHD 1 Regulates P53-mediated Colorectal Cancer Chemoresistance. *EMBO Mol. Med.* **2015**, *7* (10), 1350–1365. https://doi.org/10.15252/emmm.201505492

(36) Xie, L.; Pi, X.; Townley-Tilson, W. H. D.; Li, N.; Wehrens, X. H. T.; Entman, M. L.; Taffet, G. E.; Mishra, A.; Peng, J.; Schisler, J. C.; Meissner, G.; Patterson, C. PHD2/3-Dependent Hydroxylation Tunes Cardiac Response to β-Adrenergic Stress via Phospholamban. *J. Clin. Invest.* **2015**, *125* (7), 2759–2771. https://doi.org/10.1172/JCI80369

(37) Rodriguez, J.; Herrero, A.; Li, S.; Rauch, N.; Quintanilla, A.; Wynne, K.; Krstic, A.; Acosta, J. C.; Taylor, C.; Schlisio, S.; von Kriegsheim, A. PHD3 Regulates P53 Protein Stability by Hydroxylating Proline 359. *Cell Rep.* **2018**, *24* (5), 1316–1329.

https://doi.org/10.1016/j.celrep.2018.06.108

(38) Heir, P.; Srikumar, T.; Bikopoulos, G.; Bunda, S.; Poon, B. P.; Lee, J. E.; Raught, B.; Ohh, M. Oxygen-Dependent Regulation of Erythropoietin Receptor Turnover and Signaling. *J. Biol. Chem.* **2016**, *291* (14), 7357–7372. https://doi.org/10.1074/jbc.M115.694562

(39) Kennel, K. B.; Burmeister, J.; Schneider, M.; Taylor, C. T. The PHD1 Oxygen Sensor in Health and Disease. *J. Physiol.* **2018**, *596* (17), 3899–3913. https://doi.org/10.1113/JP275327

(40) Strowitzki, M. J.; Cummins, E. P.; Taylor, C. T. Protein Hydroxylation by Hypoxia-Inducible Factor (HIF) Hydroxylases: Unique or Ubiquitous? *Cells* **2019**, *8* (5), 384. https://doi.org/10.3390/cells8050384

(41) Cockman, M. E.; Lippl, K.; Tian, Y. M.; Pegg, H. B.; Figg, W. D.; Abboud, M. I.; Heilig, R.; Fischer, R.; Myllyharju, J.; Schofield, C. J.; Ratcliffe, P. J. Lack of Activity of Recombinant HIF Prolyl Hydroxylases (PHDs) on Reported Non-HIF Substrates. *eLife* **2019**, *8*, e46490. https://doi.org/10.7554/eLife.46490

(42) Ogoshi, Y.; Matsui, T.; Mitani, I.; Yokota, M.; Terashita, M.; Motoda, D.; Ueyama, K.; Hotta, T.; Ito, T.; Hase, Y.; Fukui, K.; Deai, K.; Yoshiuchi, H.; Ito, S.; Abe, H. Discovery of JTZ-951: A HIF Prolyl Hydroxylase Inhibitor for the Treatment of Renal Anemia. *ACS Med. Chem. Lett.* **2017**, *8* (12), 1320–1325. https://doi.org/10.1021/acsmedchemlett.7b00404

(43) Duffy, K. J.; Fitch, D. M.; Jin, J.; Liu, R.; Shaw, A. N.; Wiggall, K. Prolyl Hydroxylase Inhibitors. PCT Int. Appl. WO2007/150011, 2007.

(44) Thevis, M.; Milosovich, S.; Licea-Perez, H.; Knecht, D.; Cavalier, T.; Schänzer, W. Mass Spectrometric Characterization of a Prolyl Hydroxylase Inhibitor

GSK1278863, Its Bishydroxylated Metabolite, and Its Implementation into Routine Doping Controls. *Drug Test. Anal.* **2016**, *8* (8), 858–863. https://doi.org/10.1002/dta.1870

(45) Beck, H.; Jeske, M.; Thede, K.; Stoll, F.; Flamme, I.; Akbaba, M.; Ergüden, J. K.; Karig, G.; Keldenich, J.; Oehme, F.; Militzer, H. C.; Hartung, I. V.; Thuss, U. Discovery of Molidustat (BAY 85-3934): A Small-Molecule Oral HIF-Prolyl Hydroxylase (HIF-PH) Inhibitor for the Treatment of Renal Anemia. *ChemMedChem* **2018**, *13* (10), 988–1003. https://doi.org/10.1002/cmdc.201700783

(46) Desai, R. C.; Pandya, V.; Patel, P. R. Novel Quinolone Derivatives. PCT Int. Appl. WO2014/102818, 2014.

(47) Dhillon, S. Roxadustat: First Global Approval. *Drugs* **2019**, *79* (5), 563–572. https://doi.org/10.1007/s40265-019-01077-1

(48) Arend, M. P.; Flippin, L. A.; Guenzler-pukall, V.; Ho, W. B.; Turtle, E. D.; Du, X. Nitrogen-Containing Heteroaryl Compounds and Their Use in Increasing Endogenous Erythropoietin. PCT Int. Appl. WO2004/108681, 2004.

(49) Loenarz, C.; Schofield, C. J. Physiological and Biochemical Aspects of Hydroxylations and Demethylations Catalyzed by Human 2-Oxoglutarate Oxygenases. *Trends Biochem. Sci.* **2011**, *36* (1), 7–18. https://doi.org/10.1016/j.tibs.2010.07.002

(50) Molle, I. V; Thomann, A.; Buckley, D. L.; So, E. C.; Lang, S.; Crews, C. M.; Ciulli, A. Dissecting Fragment-Based Lead Discovery at the von Hippel-Lindau Protein:Hypoxia Inducible Factor 1α Protein-Protein Interface. *Chem. Biol.* **2012**, *19* (10), 1300–1312. https://doi.org/10.1016/j.chembiol.2012.08.015

(51) Frost, J.; Galdeano, C.; Soares, P.; Gadd, M. S.; Grzes, K. M.; Ellis, L.; Epemolu, O.; Shimamura, S.; Bantscheff, M.; Grandi, P.; Read, K. D.; Cantrell, D. A.; Rocha, S.; Ciulli, A. Potent and Selective Chemical Probe of Hypoxic Signalling Downstream of HIF-α Hydroxylation via VHL Inhibition. *Nat. Commun.* **2016**, *7*, 13312. https://doi.org/10.1038/ncomms13312

(52) Banerji, B.; Conejo-Garcia, A.; McNeill, L. A.; McDonough, M. A.; Buck, M. R. G.; Hewitson, K. S.; Oldham, N. J.; Schofield, C. J. The Inhibition of Factor Inhibiting Hypoxia-Inducible Factor (FIH) by β-Oxocarboxylic Acids. *Chem. Commun.* **2005**, *43*, 5438–5440. https://doi.org/10.1039/b510707e

(53) McDonough, M. A.; McNeill, L. A.; Tilliet, M.; Papamicaël, C. A.; Chen, Q. Y.; Banerji, B.; Hewitson, K. S.; Schofield, C. J. Selective Inhibition of Factor Inhibiting Hypoxia-Inducible Factor. *J. Am. Chem. Soc.* **2005**, *127* (21), 7680–7681. https://doi.org/10.1021/ja050841b

(54) Conejo-Garcia, A.; McDonough, M. A.; Loenarz, C.; McNeill, L. A.; Hewitson, K. S.; Ge, W.; Liénard, B. M.; Schofield, C. J.; Clifton, I. J. Structural Basis for Binding of Cyclic 2-Oxoglutarate Analogues to Factor-Inhibiting Hypoxia-Inducible Factor. *Bioorganic Med. Chem. Lett.* **2010**, *20* (20), 6125–6128. https://doi.org/10.1016/j.bmcl.2010.08.032

(55) Chan, M. C.; Ilott, N. E.; Schödel, J.; Sims, D.; Tumber, A.; Lippl, K.; Mole, D. R.; Pugh, C. W.; Ratcliffe, P. J.; Ponting, C. P.; Schofield, C. J. Tuning the Transcriptional Response to Hypoxia by Inhibiting Hypoxia-Inducible Factor (HIF) Prolyl and Asparaginyl Hydroxylases. *J. Biol. Chem.* **2016**, *291* (39), 20661–20673. https://doi.org/10.1074/jbc.M116.749291

(56) Kawaguchi, S-i.; Gonda, Y.; Yamamoto, T.; Sato, Y.; Shinohara, H.; Kobiki, Y.;

Ichimura, A.; Dan, T.; Sonoda, M.; Miyata, T.; Ogawa, A.; Tsujita, T. Furan- and Thiophene-2-Carbonyl Amino Acid Derivatives Activate Hypoxia-Inducible Factor via Inhibition of Factor Inhibiting Hypoxia-Inducible Factor-1. *Molecules* **2018**, *23* (4), 885. https://doi.org/10.3390/molecules23040885

(57) Tsujita, T.; Kawaguchi, S-i.; Dan, T.; Baird, L.; Miyata, T.; Yamamoto, M. Hypoxia-Sensitive Reporter System for High-Throughput Screening. *Tohoku J. Exp. Med.* **2015**, *235* (2), 151–159. https://doi.org/10.1620/tjem.235.151

(58) Sonoda, K.; Bogahawaththa, S.; Katayama, A.; Ujike, S.; Kuroki, S.; Kitagawa, N.; Hirotsuru, K.; Suzuki, N.; Miyata, T.; Kawaguchi, S-i.; Tsujita, T. Prolyl Hydroxylase Domain Protein Inhibitor Not Harboring a 2-Oxoglutarate Scaffold Protects against Hypoxic Stress. *ACS Pharmacol. Transl. Sci.* **2022**, *5* (5), 362–372. https://doi.org/10.1021/acsptsci.2c00002

(59) Kawaguchi, S-i.; Tsujita, T. Novel nitrogen-containing cyclic compounds and their applications. Japan Patent JP2021/6904528, 2021.

(60) Chowdhury, R.; Leung, I. K. H.; Tian, Y. M.; Abboud, M. I.; Ge, W.; Domene, C.; Cantrelle, F. X.; Landrieu, I.; Hardy, A. P.; Pugh, C. W.; Ratcliffe, P. J.; Claridge, T. D. W.; Schofield, C. J. Structural Basis for Oxygen Degradation Domain Selectivity of the HIF Prolyl Hydroxylases. *Nat. Commun.* **2016**, *7*. 13312. https://doi.org/10.1038/ncomms12673

(61) Majamaa, K.; Günzler, V.; Hanauske-Abel, H. M.; Myllylä, R.; Kivirikko, K. I. Partial Identity of the 2-Oxoglutarate and Ascorbate Binding Sites of Prolyl 4-Hydroxylase. *J. Biol. Chem.* **1986**, *261* (17), 7819–7823. https://doi.org/10.1016/S0021-9258(19)57475-0

(62) Davis, C. K.; Jain, S. A.; Bae, O. N.; Majid, A.; Rajanikant, G. K. Hypoxia Mimetic

Agents for Ischemic Stroke. *Front. Cell Dev. Biol.* **2019**, *6*, 175. https://doi.org/10.3389/fcell.2018.00175

(63) Smirnova, N. A.; Rakhman, I.; Moroz, N.; Basso, M.; Payappilly, J.; Kazakov, S.; Hernandez-Guzman, F.; Gaisina, I. N.; Kozikowski, A. P.; Ratan, R. R.; Gazaryan, I. G. Utilization of an In Vivo Reporter for High Throughput Identification of Branched Small Molecule Regulators of Hypoxic Adaptation. *Chem. Biol.* **2010**, *17* (4), 380–391. https://doi.org/10.1016/j.chembiol.2010.03.008

(64) Neitemeier, S.; Dolga, A. M.; Honrath, B.; Karuppagounder, S. S.; Alim, I.; Ratan, R. R.; Culmsee, C. Inhibition of HIF-Prolyl-4-Hydroxylases Prevents Mitochondrial Impairment and Cell Death in a Model of Neuronal Oxytosis. *Cell Death Dis.* **2016**, *7* (5), e2214. https://doi.org/10.1038/cddis.2016.107

(65) Baell, J. B.; Holloway, G. A. New Substructure Filters for Removal of Pan Assay Interference Compounds (PAINS) from Screening Libraries and for Their Exclusion in Bioassays. *J. Med. Chem.* **2010**, *53* (7), 2719–2740. https://doi.org/10.1021/jm901137j

(66) Daina, A.; Michielin, O.; Zoete, V. SwissADME: A Free Web Tool to Evaluate Pharmacokinetics, Drug-Likeness and Medicinal Chemistry Friendliness of Small Molecules. *Sci. Rep.* **2017**, *7*, 42717. https://doi.org/10.1038/srep42717

(67) Gorovoy, A. S.; Guyader, D.; Lejon, T. Highly Efficient Synthesis of Trioxopyrimidine-Based Chalconoids Under Solvent-Free Conditions. *Synth. Commun.* **2014**, *44* (9), 1296–1300. https://doi.org/10.1080/00397911.2013.853801

(68) Thomsen, R.; Christensen, M. H. MolDock: A New Technique for High-Accuracy Molecular Docking. *J. Med. Chem.* **2006**, *49* (11), 3315–3321. https://doi.org/

10.1021/jm051197e

(69) Downes, N. L.; Laham-Karam, N.; Kaikkonen, M. U.; Ylä-Herttuala, S. Differential but Complementary HIF1α and HIF2α Transcriptional Regulation. *Mol. Ther.* **2018**, *26* (7), 1735–1745. https://doi.org/10.1016/j.ymthe.2018.05.004

(70) Smythies, J. A.; Sun, M.; Masson, N.; Salama, R.; Simpson, P. D.; Murray, E.; Neumann, V.; Cockman, M. E.; Choudhry, H.; Ratcliffe, P. J.; Mole, D. R. Inherent DNA-binding Specificities of the HIF-1α and HIF-2α Transcription Factors in Chromatin. *EMBO Rep.* **2019**, *20*, e46401. https://doi.org/10.15252/embr.201846401

(71) Rodríguez, F. A.; Ventura, J. L.; Casas, M.; Casas, H.; Pagés, T.; Rama, R.; Ricart, A.; Palacios, L.; Viscor, G. Erythropoietin Acute Reaction and Haematological Adaptations to Short, Intermittent Hypobaric Hypoxia. *Eur. J. Appl. Physiol.* **2000**, *82* (3), 170–177. https://doi.org/10.1007/s004210050669

(72) Del Balzo, U.; Signore, P. E.; Walkinshaw, G.; Seeley, T. W.; Brenner, M. C.; Wang, Q.; Guo, G.; Arend, M. P.; Flippin, L. A.; Chow, F. A.; Gervasi, D. C.; Kjaergaard, C. H.; Langsetmo, I.; Guenzler, V.; Liu, D. Y.; Klaus, S. J.; Lin, A.; Neff, T. B. Nonclinical Characterization of the Hypoxia-Inducible Factor Prolyl Hydroxylase Inhibitor Roxadustat, a Novel Treatment of Anemia of Chronic Kidney Disease. *J. Pharmacol. Exp. Ther.* **2020**, *374* (2), 342–353. https://doi.org/10.1124/jpet.120.265181

(73) Hoppe, G.; Yoon, S.; Gopalan, B.; Savage, A. R.; Brown, R.; Case, K.; Vasanji, A.; Chan, E. R.; Silver, R. B.; Sears, J. E. Comparative Systems Pharmacology of HIF Stabilization in the Prevention of Retinopathy of Prematurity. *Proc. Natl. Acad. Sci. U. S. A.* **2016**, *113* (18), E2516–E2525. https://doi.org/10.1073/pnas.1523005113

(74) Masson, N.; Willam, C.; Maxwell, P. H.; Pugh, C. W.; Ratcliffe, P. J. Independent Function of Two Destruction Domains in Hypoxia-Inducible Factor-α Chains Activated by Prolyl Hydroxylation. *EMBO J.* **2001**, *20* (18), 5197–5206. https://doi.org/10.1093/emboj/20.18.5197

(75) Tian, Y. M.; Yeoh, K. K.; Lee, M. K.; Eriksson, T.; Kessler, B. M.; Kramer, H. B.; Edelmann, M. J.; Willam, C.; Pugh, C. W.; Schofield, C. J.; Ratcliffe, P. J. Differential Sensitivity of Hypoxia Inducible Factor Hydroxylation Sites to Hypoxia and Hydroxylase Inhibitors. *J. Biol. Chem.* **2011**, *286* (15), 13041–13051. https://doi.org/10.1074/jbc.M110.211110

(76) Chowdhury, R.; Candela-Lena, J. I.; Chan, M. C.; Greenald, D. J.; Yeoh, K. K.; Tian, Y. M.; McDonough, M. A.; Tumber, A.; Rose, N. R.; Conejo-Garcia, A.; Demetriades, M.; Mathavan, S.; Kawamura, A.; Lee, M. K.; Van Eeden, F.; Pugh, C. W.; Ratcliffe, P. J.; Schofield., C. J. Selective Small Molecule Probes for the Hypoxia Inducible Factor (HIF) Prolyl Hydroxylases. *ACS Chem. Biol.* **2013**, *8* (7), 1488–1496. https://doi.org/10.1021/cb400088q

(77) Molina, D. M.; Jafari, R.; Ignatushchenko, M.; Seki, T.; Larsson, E. A.; Dan, C.; Sreekumar, L.; Cao, Y.; Nordlund, P. Monitoring Drug Target Engagement in Cells and Tissues Using the Cellular Thermal Shift Assay. *Science* **2013**, *341* (6141), 84–87. https://doi.org/10.1126/science.1233606

(78) Nagasawa, I.; Muroi, M.; Kawatani, M.; Ohishi, T.; Ohba, S-i; Kawada, M.; Osada, H. Identification of a Small Compound Targeting PKM2-Regulated Signaling Using 2D Gel Electrophoresis-Based Proteome-Wide CETSA. *Cell Chem. Biol.* **2020**, *27* (2), 186-196. https://doi.org/10.1016/j.chembiol.2019.11.010

(79) Nelson, K. M.; Dahlin, J. L.; Bisson, J.; Graham, J.; Pauli, G. F.; Walters, M. A.

The Essential Medicinal Chemistry of Curcumin. *J. Med. Chem.* **2017**, *60* (5), 1620–1637. https://doi.org/10.1021/acs.jmedchem.6b00975

(80) Percy, G. C.; Thornton, D. A. N-Aryl Salicylaldimine Complexes: Infrared and PMR Spectra of the Ligands and Vibrational Frequencies of Their Metal(II) Chelates. *J. Inorg. Nucl. Chem.* **1972**, *34* (11), 3357–3367. https://doi.org/10.1016/0022-1902(72)80230-6

(81) Sundararajan, M. L.; Jeyakumar, T.; Anandakumaran, J.; Selvan, B. K. Synthesis of Metal Complexes Involving Schiff Base Ligand with Methylenedioxy Moiety: Spectral, Thermal, XRD and Antimicrobial Studies. *Spectrochim. Acta - Part A Mol. Biomol. Spectrosc.* **2014**, *131*, 82–93. https://doi.org/10.1016/j.saa.2014.04.055

(82) Wongsuwan, S.; Chatwichien, J.; Pinchaipat, B.; Kumphune, S.; Harding, D. J.; Harding, P.; Boonmak, J.; Youngme, S.; Chotima, R. Synthesis, Characterization and Anticancer Activity of Fe(II) and Fe(III) Complexes Containing N-(8-Quinolyl)Salicylaldimine Schiff Base Ligands. *J. Biol. Inorg. Chem.* **2021**, *26* (2–3), 327–339. https://doi.org/10.1007/s00775-021-01857-9

(83) Wilkins, S. E.; Islam, S.; Gannon, J. M.; Markolovic, S.; Hopkinson, R. J.; Ge, W.; Schofield, C. J.; Chowdhury, R. JMJD5 Is a Human Arginyl C-3 Hydroxylase. *Nat. Commun.* **2018**, *9*, 1180. https://doi.org/10.1038/s41467-018-03410-w

(84) Mahon, P. C.; Hirota, K.; Semenza, G. L. FIH-1: A Novel Protein That Interacts with HIF-1α and VHL to Mediate Repression of HIF-1 Transcriptional Activity. *Genes Dev.* **2001**, *15* (20), 2675–2686. https://doi.org/10.1101/gad.924501

(85) Lando, D.; Peet, D. J.; Whelan, D. A.; Gorman, J. J.; Whitelaw, M. L. Asparagine Hydroxylation of the HIF Transactivation Domain: A Hypoxic Switch. *Science*

2002, *295* (5556), 858–861. https://doi.org/10.1126/science.1068592

(86) Hewitson, K. S.; McNeill, L. A.; Riordan, M. V.; Tian, Y. M.; Bullock, A. N.; Welford, R. W.; Elkins, J. M.; Oldham, N. J.; Bhattacharya, S.; Gleadle, J. M.; Ratcliffe, P. J.; Pugh, C. W.; Schofield, C. J. Hypoxia-Inducible Factor (HIF) Asparagine Hydroxylase Is Identical to Factor Inhibiting HIF (FIH) and Is Related to the Cupin Structural Family. *J. Biol. Chem.* **2002**, *277* (29), 26351–26355. https://doi.org/10.1074/jbc.C200273200

(87) Stolze, I. P.; Tian, Y. M.; Appelhoff, R. J.; Turley, H.; Wykoff, C. C.; Gleadle, J. M.; Ratcliffe, P. J. Genetic Analysis of the Role of the Asparaginyl Hydroxylase Factor Inhibiting Hypoxia-Inducible Factor (HIF) in Regulating HIF Transcriptional Target Genes. *J. Biol. Chem.* **2004**, *279* (41), 42719–42725. https://doi.org/10.1074/jbc.M406713200

(88) Takeuchi, T.; Watanabe, Y.; Takano-Shimizu, T.; Kondo, S. Roles of Jumonji and Jumonji Family Genes in Chromatin Regulation and Development. *Dev. Dyn.* **2006**, *235* (9), 2449–2459. https://doi.org/10.1002/dvdy.20851

(89) Markolovic, S.; Leissing, T. M.; Chowdhury, R.; Wilkins, S. E.; Lu, X.; Schofield, C. J. Structure–Function Relationships of Human JmjC Oxygenases—Demethylases versus Hydroxylases. *Curr. Opin. Struct. Biol.* **2016**, *41*, 62–72. https://doi.org/10.1016/j.sbi.2016.05.013

(90) Tian, H.; McKnight, S. L.; Russell, D. W. Endothelial PAS Domain Protein 1 (EPAS1), a Transcription Factor Selectively Expressed in Endothelial Cells. *Genes Dev.* **1997**, *11* (1), 72–82. https://doi.org/10.1101/gad.11.1.72

(91) Ema, M.; Taya, S.; Yokotani, N.; Sogawa, K.; Matsuda, Y.; Fujii-Kuriyama, Y. A Novel BHLH-PAS Factor with Close Sequence Similarity to Hypoxia-Inducible

Factor 1α Regulates the VEGF Expression and Is Potentially Involved in Lung and Vascular Development. *Proc. Natl. Acad. Sci. U. S. A.* **1997**, *94* (9), 4273–4278. https://doi.org/10.1073/pnas.94.9.4273

(92) Flamme, I.; Fröhlich, T.; von Reutern, M.; Kappel, A.; Damert, A.; Risau, W. HRF, a Putative Basic Helix-Loop-Helix-PAS-Domain Transcription Factor Is Closely Related to Hypoxia-Inducible Factor-1α and Developmentally Expressed in Blood Vessels. *Mech. Dev.* **1997**, *63* (1), 51–60. https://doi.org/10.1016/S0925-4773(97)00674-6

(93) Holmquist-Mengelbier, L.; Fredlund, E.; Löfstedt, T.; Noguera, R.; Navarro, S.; Nilsson, H.; Pietras, A.; Vallon-Christersson, J.; Borg, Å.; Gradin, K.; Poellinger, L.; Påhlman, S. Recruitment of HIF-1α and HIF-2α to Common Target Genes Is Differentially Regulated in Neuroblastoma: HIF-2α Promotes an Aggressive Phenotype. *Cancer Cell* **2006**, *10* (5), 413–423. https://doi.org/10.1016/j.ccr.2006.08.026

(94) Koh, M. Y.; Lemos, R.; Liu, X.; Powis, G. The Hypoxia-Associated Factor Switches Cells from HIF-1α- to HIF-2α-Dependent Signaling Promoting Stem Cell Characteristics, Aggressive Tumor Growth and Invasion. *Cancer Res.* **2011**, *71* (11), 4015–4027. https://doi.org/10.1158/0008-5472.CAN-10-4142

(95) Florczyk, U.; Czauderna, S.; Stachurska, A.; Tertil, M.; Nowak, W.; Kozakowska, M.; Poellinger, L.; Jozkowicz, A.; Loboda, A.; Dulak, J. Opposite Effects of HIF-1α and HIF-2α on the Regulation of IL-8 Expression in Endothelial Cells. *Free Radic. Biol. Med.* **2011**, *51* (10), 1882–1892. https://doi.org/10.1016/j.freeradbiomed.2011.08.023

(96) Hamidian, A.; von Stedingk, K.; Thorén, M. M.; Mohlin, S.; Påhlman, S.

Differential Regulation of HIF-1α and HIF-2α in Neuroblastoma: Estrogen-Related Receptor Alpha (ERRα) Regulates HIF2A Transcription and Correlates to Poor Outcome. *Biochem. Biophys. Res. Commun.* **2015**, *461* (3), 560–567. https://doi.org/10.1016/j.bbrc.2015.04.083

(97) Koshiji, M.; Kageyama, Y.; Pete, E. A.; Horikawa, I.; Barrett, J. C.; Huang, L. E. HIF-1α Induces Cell Cycle Arrest by Functionally Counteracting Myc. *EMBO J.* **2004**, *23* (9), 1949–1956. https://doi.org/10.1038/sj.emboj.7600196

(98) Koshiji, M.; To, K. K. W.; Hammer, S.; Kumamoto, K.; Harris, A. L.; Modrich, P.; Huang, L. E. HIF-1α Induces Genetic Instability by Transcriptionally Downregulating MutSα Expression. *Mol. Cell* **2005**, *17* (6), 793–803. https://doi.org/10.1016/j.molcel.2005.02.015

(99) Das, B.; Bayat-Mokhtari, R.; Tsui, M.; Lotfi, S.; Tsuchida, R.; Felsher, D. W.; Yeger, H. HIF-2α Suppresses P53 to Enhance the Stemness and Regenerative Potential of Human Embryonic Stem Cells. *Stem Cells* **2012**, *30* (8), 1685–1695. https://doi.org/10.1002/stem.1142

(100) Suzuki, M.; Ohneda, K.; Hosoya-Ohmura, S.; Tsukamoto, S.; Ohneda, O.; Philipsen, S.; Yamamoto, M. Real-Time Monitoring of Stress Erythropoiesis in Vivo Using Gata1 and β-Globin LCR Luciferase Transgenic Mice. *Blood* **2006**, *108* (2), 726–733. https://doi.org/10.1182/blood-2005-10-4064

(101) Jelkmann, W. Regulation of Erythropoietin Production. *J. Physiol.* **2011**, *589* (6), 1251–1258. https://doi.org/10.1113/jphysiol.2010.195057

(102) Obara, N.; Suzuki, N.; Kim, K.; Nagasawa, T.; Imagawa, S.; Yamamoto, M. Repression via the GATA Box Is Essential for Tissue-Specific Erythropoietin Gene Expression. *Blood* **2008**, *111* (10), 5223–5232. https://doi.org/10.1182/blood-

2007-10-115857

(103) Goi, T.; Nakajima, T.; Komatsu, Y.; Kawata, A.; Yamakoshi, S.; Okada, O.; Sugahara, M.; Umeda, A.; Takada, Y.; Murakami, J.; Ohashi, R.; Watanabe, T.; Fukase, K. Pyrazolo[4,3- d]Pyrimidine Derivatives as a Novel Hypoxia-Inducible Factor Prolyl Hydroxylase Domain Inhibitor for the Treatment of Anemia. *ACS Med. Chem. Lett.* **2020**, *11* (7), 1416–1420. https://doi.org/10.1021/acsmedchemlett.0c00108

(104) Wei, H.; Gou, W.; Gao, J.; Ning, H.; Song, Y.; Li, D.; Qin, Y.; Hou, W.; Li, Y. Novel PHD2/HDACs Hybrid Inhibitors Protect against Cisplatin-Induced Acute Kidney Injury. *Eur. J. Med. Chem.* **2022**, *230*, 114115. https://doi.org/10.1016/j.ejmech.2022.114115

(105) Quaegebeur, A.; Segura, I.; Schmieder, R.; Verdegem, D.; Decimo, I.; Bifari, F.; Dresselaers, T.; Eelen, G.; Ghosh, D.; Davidson, S. M.; Schoors, S.; Broekaert, D.; Cruys, B.; Govaerts, K.; De Legher, C.; Bouché, A.; Schoonjans, L.; Ramer, M. S.; Hung, G.; Bossaert, G.; Cleveland, D. W.; Himmelreich, U.; Voets, T.; Lemmens, R.; Bennett, C. F.; Robberecht, W.; De Bock, K.; Dewerchin, M.; Ghesquière, B.; Fendt, S. M.; Carmeliet, P. Deletion or Inhibition of the Oxygen Sensor PHD1 Protects against Ischemic Stroke via Reprogramming of Neuronal Metabolism. *Cell Metab.* **2016**, *23* (2), 280–291. https://doi.org/10.1016/j.cmet.2015.12.007

(106) Cai, Z.; Zhong, H.; Bosch-Marce, M.; Fox-Talbot, K.; Wang, L.; Wei, C.; Trush, M. A.; Semenza, G. L. Complete Loss of Ischaemic Preconditioning-Induced Cardioprotection in Mice with Partial Deficiency of HIF-1α. *Cardiovasc. Res.* **2008**, *77* (3), 463–470. https://doi.org/10.1093/cvr/cvm035

(107) Koeppen, M.; Lee, J. W.; Seo, S. W.; Brodsky, K. S.; Kreth, S.; Yang, I. V.; Buttrick,

P. M.; Eckle, T.; Eltzschig, H. K. Hypoxia-Inducible Factor 2-Alpha-Dependent Induction of Amphiregulin Dampens Myocardial Ischemia-Reperfusion Injury. *Nat. Commun.* **2018**, *9*, 816. https://doi.org/10.1038/s41467-018-03105-2

(108) Minamishima, Y. A.; Moslehi, J.; Padera, R. F.; Bronson, R. T.; Liao, R.; Kaelin, W. G. A Feedback Loop Involving the Phd3 Prolyl Hydroxylase Tunes the Mammalian Hypoxic Response In Vivo. *Mol. Cell. Biol.* **2009**, *29* (21), 5729–5741. https://doi.org/10.1128/mcb.00331-09

(109) Horak, P.; Crawford, A. R.; Vadysirisack, D. D.; Nash, Z. M.; DeYoung, M. P.; Sgroi, D.; Ellisen, L. W. Negative Feedback Control of HIF-1 through REDD1-Regulated ROS Suppresses Tumorigenesis. *Proc. Natl. Acad. Sci. U. S. A.* **2010**, *107* (10), 4675–4680. https://doi.org/10.1073/pnas.0907705107

(110) Foxler, D. E.; Bridge, K. S.; Foster, J. G.; Grevitt, P.; Curry, S.; Shah, K. M.; Davidson, K. M.; Nagano, A.; Gadaleta, E.; Rhys, H. I.; Kennedy, P. T.; Hermida, M. A.; Chang, T. Y.; Shaw, P. E.; Reynolds, L. E.; McKay, T. R.; Wang, H. W.; Ribeiro, P. S.; Plevin, M. J.; Lagos, D.; Lemoine, N. R.; Rajan, P.; Graham, T. A.; Chelala, C.; Hodivala-Dilke, K. M.; Spendlove, I.; Sharp, T. V. A HIF–LIMD 1 Negative Feedback Mechanism Mitigates the Pro-tumorigenic Effects of Hypoxia. *EMBO Mol. Med.* **2018**, *10* (8), e8304. https://doi.org/10.15252/emmm.201708304

(111) Goldoni, M.; Johansson, C. A Mathematical Approach to Study Combined Effects of Toxicants in Vitro: Evaluation of the Bliss Independence Criterion and the Loewe Additivity Model. *Toxicol. Vitr.* **2007**, *21* (5), 759–769. https://doi.org/10.1016/j.tiv.2007.03.003

(112) Tallarida, R. J. Interactions between Drugs and Occupied Receptors. *Pharmacol.*

Ther. **2007**, *113* (1), 197–209. https://doi.org/10.1016/j.pharmthera.2006.08.002

(113) Singh, A.; Wilson, J. W.; Schofield, C. J.; Chen, R. Hypoxia-Inducible Factor (HIF) Prolyl Hydroxylase Inhibitors Induce Autophagy and Have a Protective Effect in an in-Vitro Ischaemia Model. *Sci. Rep.* **2020**, *10*, 1597. https://doi.org/10.1038/s41598-020-58482-w

(114) Beyett, T. S.; To, C.; Heppner, D. E.; Rana, J. K.; Schmoker, A. M.; Jang, J.; De Clercq, D. J. H.; Gomez, G.; Scott, D. A.; Gray, N. S.; Jänne, P. A.; Eck, M. J. Molecular Basis for Cooperative Binding and Synergy of ATP-Site and Allosteric EGFR Inhibitors. *Nat. Commun.* **2022**, 2530. https://doi.org/10.1038/s41467-022-30258-y

(115) Frost, J.; Rocha, S.; Ciulli, A. Von Hippel-Lindau (VHL) Small-Molecule Inhibitor Binding Increases Stability and Intracellular Levels of VHL Protein. *J. Biol. Chem.* **2021**, *297* (2), 100910. https://doi.org/10.1016/j.jbc.2021.100910

(116) Xue, X.; Kang, J. B.; Yang, X.; Li, N.; Chang, L.; Ji, J.; Meng, X. K.; Zhang, H. Q.; Zhong, Y.; Yu, S. P.; Wu, W. Y.; Wang, X. L.; Li, N. G.; Sun, S. L. An Efficient Strategy for Digging Protein-Protein Interactions for Rational Drug Design - A Case Study with HIF-1α/VHL. *Eur. J. Med. Chem.* **2022**, *227*, 113871. https://doi.org/10.1016/j.ejmech.2021.113871

(117) Salminen, A.; Kauppinen, A.; Kaarniranta, K. 2-Oxoglutarate-Dependent Dioxygenases Are Sensors of Energy Metabolism, Oxygen Availability, and Iron Homeostasis: Potential Role in the Regulation of Aging Process. *Cell. Mol. Life Sci.* **2015**, *72* (20), 3897–3914. https://doi.org/10.1007/s00018-015-1978-z

(118) Kivirikko, K. I.; Prockop, D. J. Enzymatic Hydroxylation of Proline and Lysine in Protocollagen. *Proc. Natl. Acad. Sci.* **1967**, *57* (3), 782–789. https://doi.org/

10.1073/pnas.57.3.782

(119) Figg, W. D.; McDonough, M. A.; Chowdhury, R.; Nakashima, Y.; Zhang, Z.; Holt-Martyn, J. P.; Krajnc, A.; Schofield, C. J. Structural Basis of Prolyl Hydroxylase Domain Inhibition by Molidustat. *ChemMedChem* **2021**, *16* (13), 2082–2088. https://doi.org/10.1002/cmdc.202100133

(120) Chan, M. C.; Atasoylu, O.; Hodson, E.; Tumber, A.; Leung, I. K. H.; Chowdhury, R.; Gómez-Pérez, V.; Demetriades, M.; Rydzik, A. M.; Holt-Martyn, J.; Tian, Y. M.; Bishop, T.; Claridge, T. D. W.; Kawamura, A.; Pugh, C. W.; Ratcliffe, P. J.; Schofield, C. J. Potent and Selective Triazole-Based Inhibitors of the Hypoxia-Inducible Factor Prolyl-Hydroxylases with Activity in the Murine Brain. *PLoS One* **2015**, *10* (7), e0132004. https://doi.org/10.1371/journal.pone.0132004

(121) Sonoda, K.; Ujike, S.; Katayama, A.; Suzuki, N.; Kawaguchi, S-i.; Tsujita, T. Improving Lipophilicity of 5-(1-Acetyl-5-Phenylpyrazolidin-3-Ylidene)-1,3-Dimethylbarbituric Acid Increases Its Efficacy to Activate Hypoxia-Inducible Factors. *Bioorganic Med. Chem.* **2022**, *73*, 117039. https://doi.org/10.1016/j.bmc.2022.117039

(122) Topliss, J. G. Utilization of Operational Schemes for Analog Synthesis in Drug Design. *J. Med. Chem.* **1972**, *15* (10), 1006–1011. https://doi.org/10.1021/jm00280a002

(123) Nakai, T.; Saigusa, D.; Iwamura, Y.; Matsumoto, Y.; Umeda, K.; Kato, K.; Yamaki, H.; Tomioka, Y.; Hirano, I.; Koshiba, S.; Yamamoto, M.; Suzuki, N. Esterification Promotes the Intracellular Accumulation of Roxadustat, an Activator of Hypoxia-Inducible Factors, to Extend Its Effective Duration. *Biochem. Pharmacol.* **2022**, *197*, 114939. https://doi.org/10.1016/j.bcp.2022.114939

(124) Lipinski, C. A.; Lombardo, F.; Dominy, B. W.; Feeney, P. J. Experimental and Computational Approaches to Estimate Solubility and Permeability in Drug Discovery and Development Settings. *Adv. Drug Deliv. Rev.* **2012**, *64*, 4–17. https://doi.org/10.1016/j.addr.2012.09.019

(125) Mignani, S.; Rodrigues, J.; Tomas, H.; Jalal, R.; Singh, P. P.; Majoral, J. P.; Vishwakarma, R. A. Present Drug-Likeness Filters in Medicinal Chemistry during the Hit and Lead Optimization Process: How Far Can They Be Simplified? *Drug Discov. Today* **2018**, *23* (3), 605–615. https://doi.org/10.1016/j.drudis.2018.01.010

(126) Jornada, D. H.; dos Santos Fernandes, G. F.; Chiba, D. E.; de Melo, T. R. F.; dos Santos, J. L.; Chung, M. C. The Prodrug Approach: A Successful Tool for Improving Drug Solubility. *Molecules* **2016**, *21* (1). 42 https://doi.org/10.3390/molecules21010042

(127) Landázuri, M. O.; Vara-Vega, A.; Vitón, M.; Cuevas, Y.; del Peso, L. Analysis of HIF-Prolyl Hydroxylases Binding to Substrates. *Biochem. Biophys. Res. Commun.* **2006**, *351* (2), 313–320. https://doi.org/10.1016/j.bbrc.2006.09.170

(128) Smirnova, N. A.; Hushpulian, D. M.; Speer, R. E.; Gaisina, I. N.; Ratan, R. R.; Gazaryan, I. G. Catalytic Mechanism and Substrate Specificity of HIF Prolyl Hydroxylases. *Biochem. (Mosc.)* **2012**, *77* (10), 1108–1119. https://doi.org/10.1134/S0006297912100033

(129) Hirsilä, M.; Koivunen, P.; Günzler, V.; Kivirikko, K. I.; Myllyharju, J. Characterization of the Human Prolyl 4-Hydroxylases That Modify the Hypoxia-Inducible Factor. *J. Biol. Chem.* **2003**, *278* (33), 30772–30780. https://doi.org/10.1074/jbc.M304982200

(130) McNeill, L. A.; Bethge, L.; Hewitson, K. S.; Schofield, C. J. A Fluorescence-Based

Assay for 2-Oxoglutarate-Dependent Oxygenases. *Anal. Biochem.* **2005**, *336* (1), 125–131. https://doi.org/10.1016/j.ab.2004.09.019

(131) Hewitson, K. S.; Schofield, C. J.; Ratcliffe, P. J. Hypoxia-Inducible Factor Prolyl-Hydroxylase: Purification and Assays of PHD2. *Methods Enzymol.* **2007**, *435* (07), 25–42. https://doi.org/10.1016/S0076-6879(07)35002-7

(132) Wong, S. J.; Ringel, A. E.; Yuan, W.; Paulo, J. A.; Yoon, H.; Currie, M. A.; Haigis, M. C. Development of a Colorimetric α-Ketoglutarate Detection Assay for Prolyl Hydroxylase Domain (PHD) Proteins. *J. Biol. Chem.* **2021**, *296*, 100397. https://doi.org/10.1016/j.jbc.2021.100397

(133) Vachal, P.; Miao, S.; Pierce, J. M.; Guiadeen, D.; Colandrea, V. J.; Wyvratt, M. J.; Salowe, S. P.; Sonatore, L. M.; Milligan, J. A.; Hajdu, R.; Gollapudi, A.; Keohane, C. A.; Lingham, R. B.; Mandala, S. M.; DeMartino, J. A.; Tong, X.; Wolff, M.; Steinhuebel, D.; Kieczykowski, G. R.; Fleitz, F. J.; Chapman, K.; Athanasopoulos, J.; Adam, G.; Akyuz, C. D.; Jena, D. K.; Lusen, J. W.; Meng, J.; Stein, B. D.; Xia, L.; Sherer, E. C.; Hale, J. J. 1,3,8-Triazaspiro[4.5]Decane-2,4-Diones as Efficacious Pan-Inhibitors of Hypoxia-Inducible Factor Prolyl Hydroxylase 1-3 (HIF PHD1-3) for the Treatment of Anemia. *J. Med. Chem.* **2012**, *55* (7), 2945–2959. https://doi.org/10.1021/jm201542d

(134) Codo, A. C.; Davanzo, G. G.; Monteiro, L. de B.; de Souza, G. F.; Muraro, S. P.; Virgilio-da-Silva, J. V.; Prodonoff, J. S.; Carregari, V. C.; de Biagi Junior, C. A. O.; Crunfli, F.; Jimenez Restrepo, J. L.; Vendramini, P. H.; Reis-de-Oliveira, G.; Bispo dos Santos, K.; Toledo-Teixeira, D. A.; Parise, P. L.; Martini, M. C.; Marques, R. E.; Carmo, H. R.; Borin, A.; Coimbra, L. D.; Boldrini, V. O.; Brunetti, N. S.; Vieira, A. S.; Mansour, E.; Ulaf, R. G.; Bernardes, A. F.; Nunes, T. A.; Ribeiro, L. C.;

Palma, A. C.; Agrela, M. V.; Moretti, M. L.; Sposito, A. C.; Pereira, F. B.; Velloso, L. A.; Vinolo, M. A. R.; Damasio, A.; Proença-Módena, J. L.; Carvalho, R. F.; Mori, M. A.; Martins-de-Souza, D.; Nakaya, H. I.; Farias, A. S.; Moraes-Vieira, P. M. Elevated Glucose Levels Favor SARS-CoV-2 Infection and Monocyte Response through a HIF-1α/Glycolysis-Dependent Axis. *Cell Metab.* **2020**, *32* (3), 437-446. https://doi.org/10.1016/j.cmet.2020.07.007

(135) DeBerge, M.; Lantz, C.; Dehn, S.; Sullivan, D. P.; van der Laan, A. M.; Niessen, H. W. M.; Flanagan, M. E.; Brat, D. J.; Feinstein, M. J.; Kaushal, S.; Wilsbacher, L. D.; Thorp, E. B. Hypoxia-Inducible Factors Individually Facilitate Inflammatory Myeloid Metabolism and Inefficient Cardiac Repair. *J. Exp. Med.* **2021**, *218* (9), e20200667. https://doi.org/10.1084/jem.20200667

(136) Besarab, A.; Bolton, W. K.; Browne, J. K.; Egrie, J. C.; Nissenson, A. R.; Okamoto, D. M.; Schwab, S. J.; Goodkin, D. A. The Effects of Normal as Compared with Low Hematocrit Values in Patients with Cardiac Disease Who Are Receiving Hemodialysis and Epoetin. *N. Engl. J. Med.* **1998**, *339* (9), 584–590. https://doi.org/10.1056/nejm199808273390903

(137) Singh, A. K.; Szczech, L.; Tang, K. L.; Barnhart, H.; Sapp, S.; Wolfson, M.; Reddan, D. Correction of Anemia with Epoetin Alfa in Chronic Kidney Disease. *N. Engl. J. Med.* **2006**, 355 (20), 2085–2098. https://doi.org/10.1056/nejmoa065485

(138) Pfeffer, M. A.; Burdmann, E. A.; Chen, C. Y.; Cooper, M. E.; de Zeeuw, D.; Eckardt, K. U.; Feyzi, J. M.; Ivanovich, P.; Kewalramani, R.; Levey, A. S.; Lewis, E. F.; McGill, J. B.; McMurray, J. J. V.; Parfrey, P.; Parving, H. H.; Remuzzi, G.; Singh, A. K.; Solomon, S. D.; Toto, R. A Trial of Darbepoetin Alfa in Type 2 Diabetes and

Chronic Kidney Disease. *N. Engl. J. Med.* **2009**, *361* (21), 2019–2032